University of Kentucky
UKnowledge

Theses and Dissertations--Plant and Soil Sciences

Plant and Soil Sciences

2018

EXPLORING SPATIAL AND TEMPORAL VARIABILITY OF SOIL AND CROP PROCESSES FOR IRRIGATION MANAGEMENT

Javier Reyes
University of Kentucky, jareyes05@gmail.com
Author ORCID Identifier:
https://orcid.org/0000-0002-4088-4475
Digital Object Identifier: https://doi.org/10.13023/etd.2018.316

Right click to open a feedback form in a new tab to let us know how this document benefits you.

Recommended Citation

Reyes, Javier, "EXPLORING SPATIAL AND TEMPORAL VARIABILITY OF SOIL AND CROP PROCESSES FOR IRRIGATION MANAGEMENT" (2018). *Theses and Dissertations--Plant and Soil Sciences*. 107.
https://uknowledge.uky.edu/pss_etds/107

This Doctoral Dissertation is brought to you for free and open access by the Plant and Soil Sciences at UKnowledge. It has been accepted for inclusion in Theses and Dissertations--Plant and Soil Sciences by an authorized administrator of UKnowledge. For more information, please contact UKnowledge@lsv.uky.edu.

STUDENT AGREEMENT:

I represent that my thesis or dissertation and abstract are my original work. Proper attribution has been given to all outside sources. I understand that I am solely responsible for obtaining any needed copyright permissions. I have obtained needed written permission statement(s) from the owner(s) of each third-party copyrighted matter to be included in my work, allowing electronic distribution (if such use is not permitted by the fair use doctrine) which will be submitted to UKnowledge as Additional File.

I hereby grant to The University of Kentucky and its agents the irrevocable, non-exclusive, and royalty-free license to archive and make accessible my work in whole or in part in all forms of media, now or hereafter known. I agree that the document mentioned above may be made available immediately for worldwide access unless an embargo applies.

I retain all other ownership rights to the copyright of my work. I also retain the right to use in future works (such as articles or books) all or part of my work. I understand that I am free to register the copyright to my work.

REVIEW, APPROVAL AND ACCEPTANCE

The document mentioned above has been reviewed and accepted by the student's advisor, on behalf of the advisory committee, and by the Director of Graduate Studies (DGS), on behalf of the program; we verify that this is the final, approved version of the student's thesis including all changes required by the advisory committee. The undersigned agree to abide by the statements above.

Javier Reyes, Student

Dr. Ole Wendroth, Major Professor

Dr. Mark Coyne, Director of Graduate Studies

EXPLORING SPATIAL AND TEMPORAL VARIABILITY OF SOIL AND CROP PROCESSES FOR IRRIGATION MANAGEMENT

DISSERTATION

A dissertation submitted in partial fulfillment of the
requirements for the degree of Doctor of Philosophy in the
College of Agriculture, Food and Environment
at the University of Kentucky

By
Javier Reyes

Lexington, Kentucky

Director: Dr. Ole Wendroth, Professor of Soil Physics

Lexington, Kentucky

2018

Copyright © Javier Reyes 2018

ABSTRACT OF DISSERTATION

EXPLORING SPATIAL AND TEMPORAL VARIABILITY OF SOIL AND CROP PROCESSES FOR IRRIGATION MANAGEMENT

Irrigation needs to be applied to soils in relatively humid regions such as western Kentucky to supply water for crop uptake to optimize and stabilize yields. Characterization of soil and crop variability at the field scale is needed to apply site specific management and to optimize water application. The objective of this work is to propose a characterization and modeling of soil and crop processes to improve irrigation management. Through an analysis of spatial and temporal behavior of soil and crop variables the variability in the field was identified. Integrative analysis of soil, crop, proximal and remote sensing data was utilized. A set of direct and indirect measurements that included soil texture, electrical conductivity (EC), soil chemical properties (pH, organic matter, N, P, K, Ca, Mg and Zn), NDVI, topographic variables, were measured in a silty loam soil near Princeton, Kentucky. Maps of measured properties were developed using kriging, and cokriging. Different approaches and two cluster methods (FANNY and CLARA) with selected variables were applied to identify management zones. Optimal scenarios were achieved with dividing the entire field into 2 or 3 areas. Spatial variability in the field is strongly influenced by topography and clay content. Using Root Zone Water Quality Model 2.0 (RZWQM), soil water tension was modeled and predicted at different zones based on the previous delineated zones. Soil water tension was measured at three depths (20, 40 and 60 cm) during different seasons (20016 and 2017) under wheat and corn. Temporal variations in soil water were driven mainly by precipitation but the behavior is different among management zones. The zone with higher clay content tends to dry out faster between rainfall events and reveals higher fluctuations in water tension even at greater depth. The other zones are more stable at the lower depth and share more similarities in their cyclic patterns. The model predictions were satisfactory in the surface layer but the accuracy decreased in deeper layers. A study of clay mineralogy was performed to explore field spatial differences based on the map classification. kaolinite, vermiculite, HIV and smectite are among the identified minerals. The clayey area presents higher quantity of some of the clay minerals. All these results show the ability to identify and characterize the field spatial variability, combining easily obtainable data under realistic farm conditions. This information can be utilized to manage resources more effectively through site specific application.

KEYWORDS: Soil Physics, Soil water Status, Precision Agriculture, Geostatistics, Soil Mineralogy

Javier Reyes
Student's Signature

30/07/2018
Date

EXPLORING SPATIAL AND TEMPORAL VARIABILITY OF SOIL AND CROP PROCESSES FOR IRRIGATION MANAGEMENT

By

Javier Reyes

Ole Wendroth
Director of Dissertation

Mark Coyne
Director of Graduate Studies

30/07/2018
Date

ACKNOWLEDGEMENTS

This work is the culmination of a fruitful and enjoyable stance in Lexington. I want to thank God for this opportunity. Thanks to my family and my parents for their support.

I want to give special thanks to my advisor Dr. Ole Wendroth for sharing his friendship, knowledge and life experience. I'm really grateful for the opportunity of working with a bright and wonderful person. Thanks to Dr. Anastasios Karathanasis, Christopher Matocha, Wei Ren and Junfeng Zhu for serving as committee members and being supportive during these years, and to Dr. Daniel Howe for serving as Outside Examiner. Also I want to thank Dr. Cristopher Matocha for the opportunity to work with him as Teaching Assistant.

Special thanks to Riley Jason Walton, for all his help in the soil physics lab, always willing to help and find a solution. Also I want to thank James Dollarhide, Yvonne Thompson, and Martin Vandiviere for their technical support, all staff members of the Department of Plant and Soil Science and the Director of Graduate School, Dr. Mark Coyne. Thank you to my friends and colleagues Xi Zhang and Saadi Shahadha for their help during my work.

I want to acknowledge the financial support of this PhD project by the Kentucky Small Grain Growers' Association, the Kentucky Corn Growers' Association, the Kentucky Soybean Board, the Southern Soybean Research Program, the SFB 271 Water Quality Program through the College of Agriculture, Food and the Environment, and the Department of Plant & Soil Sciences. Finally, I want to thank the farmer Trevor Gilkey,

Hillview Farms, Princeton, KY for allowing this research to be conducted on his farm.

TABLE OF CONTENTS

ACKNOWLEDGEMENTS……..…….....iii

LIST OF TABLES…….....vii

LIST OF FIGURES ……..……viii

Chapter 1 Introduction……..……1
1.1 Irrigation Management ……...……...1
1.2 Site Specific Management……..2
1.3 Modeling soil water status using Agro-system models……...5
1.4 Objectives of the study……...7

Chapter 2 Reliably Mapping Clay Content Coregionalized with EC……..…10
2.1 Introduction……..……...10
2.2 Material and methods….…….……14
2.2.1 Site description……...14
2.2.2 Soil sampling and EC_a data collection……15
2.2.3 Sampling schemes……..17
2.2.4 Geostatistical interpolation…….....19
2.2.5 Data Validation……...20
2.3 Results and discussion ….……...……22
2.3.1 Semivariograms based on all data …….……24
2.3.2 Kriging and Cokriging predictions using all data……....26
2.3.3 Kriging and Cokriging scenarios……28
2.3.4 Sample Validation……..34
2.3.5 Utilization of EC_a and cokriging……38
2.4 Conclusions ….……...……..……...40

Chapter 3 Delineating site-specific management zones and evaluating soil water temporal dynamics in a farmer's field in Kentucky……...42
3.1 Introduction…….…….....42
3.2 Material and methods….…….……47
3.2.1 Site description and data sampling……..……47
3.2.2 Data analysis……...50
3.3 Results and discussion ….……...……55
3.3.1 Geostatistical interpolation……..……...57
3.3.2 Principal component analysis……57
3.3.3 Potential Management zone delineation……60
3.3.4 Evaluating management zones……...……65

3.4 Conclusions ……..……73

Chapter 4 Evaluating and Predicting Soil Water Status in a Farmer's Field in Western Kentucky…...……..……..……75
4.1 Introduction…...……..……..75
4.2 Material and methods…..……..……77
4.2.1 Site description and data sampling……..77
4.2.2 Model evaluation and calibration……80
4.3 Results and discussion …..……..……82
4.3.1 Soil properties and crop yield……..……82
4.3.2 Predicted and calibrated soil water status……86
4.3.3 Potential use of model predictions……..90
4.4 Conclusions …..……..……91

Chapter 5 Spatial variability of clay mineralogy in a farmer's field in Kentucky……..……..……..…92
5.1 Introduction……..……92
5.2 Material and methods…..……..……94
5.2.1 Site description and data sampling ……94
5.2.2 Mineralogical characterization……...95
5.2.3 Soil properties……96
5.3 Results and discussion …..……..……97
5.3.1 Clay mineralogy…… ……..……...97
5.3.2 Soil properties at each location……104
5.4 Summary …..……..……...105

Chapter 6 Conclusions……..……..……..106

References……..……..……109

Vita……..……...……..132

LIST OF TABLES

Table 2.1. Descriptive statistics of clay samples used in each scenario and the validation set (Clay val.) and the electrical conductivity at a shallow (EC_{as}) and deep (EC_{ad}) depth……23
Table 2.2. Bias and prediction error of clay content (%) in each scenario using Leave-one-out cross validation. ME: mean error, RMSE: Root mean squared error (RMSE), RSR: RMSE-observation standard deviation ratio. ECas was used as secondary variable for cokriging. Notice, the number of predicted points differs between scenarios……..……33
Table 2.3. Bias and prediction error of clay content (%) for unused samples in each scenario. ME: mean error, RMSE: Root mean squared error (RMSE), RSR: RMSE-observation standard deviation ratio. EC_{as} was used as secondary variable for cokriging……34
Table 2.4. Bias and prediction error of clay content (%) using an independent validation data set for which locations are shown in Figure 1. ME: mean error, RMSE: Root mean squared error (RMSE), RSR: RMSE-observation standard deviation ratio. EC_{as} was used as secondary variable for cokriging……..37
Table 2.5. Bias and prediction error of clay content (%) of samples combining validation from LOOCV and unused samples in each scenario. ME: mean error, RMSE: Root mean squared error (RMSE), RSR: RMSE-observation standard deviation ratio. EC_{as} was used as secondary variable for cokriging…….37
Table 3.1. Descriptive statistics of all measured variables. Chemical properties correspond to the surface layer (0-15 cm). Sample size corresponds to the 96 soil samples and the intersected NDVI and topographic attributes for the corresponding locations……...56
Table 3.2. Factor loadings of each variable for the first 3 components. In parenthesis is the percentage of explained variance for each component. Chemical properties correspond to the surface layer (0-15 cm)……60
Table 3.3. Average corn yield among different management zones by using different variables and cluster algorithms……...66
Table 4.1. Soil Properties at different zones and depths……83
Table 4.2. Wheat and corn yield in each field zone……83
Table 4.3. Bias and prediction error of calibrated soil water tension predictions under wheat and corn at each zone……...90
Table 5.1. Quantitative mineralogical composition of the clay fraction using Thermo-gravimetric analysis……98
Table 5.2. Soil properties obtained at different locations and depths……...104

LIST OF FIGURES

Figure 2.1. Study area and sampling locations. Red and yellow bullets denote 96 sampling locations for soil texture while yellow bullets indicate the validation points. Blue bullets reflect the paths for EC_a measurements……15
Figure 2.2. Sampling schemes for each scenario. Number labels in (A) indicate the locations referred to in the 1-dimensional display of results in Figure 2.6……18
Figure 2.3. Classic cross variogram of Log Clay and Log EC_a……..……..……...24
Figure 2.4. Scenario 1 with all data: semivariogram and model for ln-transformed clay content at 0-20 cm used for ordinary kriging (A); semivariograms and linear models of coregionalization for ln-transformed clay content at 0-20 cm (B), ln-transformed electrical conductivity at shallow depth (C) and pseudo cross variogram of ln-transformed clay content and electrical conductivity (D). Maps of clay content for scenario 1 (all measurements) using kriging (E) and cokriging with apparent electrical conductivity at shallow depth (F)……...25
Figure 2.5. Semivariogram and semivariogram model for scenario 1 (A) and kriged map of clay content (B) based on the spherical model……..27
Figure 2.6. Cross validation of predicted clay content at 0-20 cm using kriging (A) and cokriging (B) with all measurements (scenario 1)……28
Figure 2.7. Scenarios 2: semivariogram and model for clay content at 0-20 cm used for ordinary kriging (A); semivariograms and linear models of coregionalization for clay content at 0-20 cm (B), electrical conductivity at shallow depth (C) and pseudo cross variogram of clay content and electrical conductivity (D). Scenario 3: semivariogram and model for clay content at 0-20 cm used for ordinary kriging (E); semivariograms and linear models of coregionalization for clay content at 0-20 cm (F), electrical conductivity at shallow depth (G) and pseudo cross variogram of clay content and electrical conductivity (H)……30
Figure 2.8. Scenario 4: semivariogram and model for clay content at 0-20 cm used for ordinary kriging (A); semivariograms and linear models of coregionalization for clay content at 0-20 cm (B), electrical conductivity at shallow depth (C) and pseudo cross variogram of clay content and electrical conductivity (D). Scenario 5: semivariogram and model for clay content at 0-20 cm used for ordinary kriging (E); semivariograms and linear models of coregionalization for clay content at 0-20 cm (F), electrical conductivity at shallow depth (G) and pseudo cross variogram of clay content and electrical conductivity (H)……31
Figure 2.9. Maps of clay content using kriging (A, C, E and G) and cokriging with apparent electrical conductivity at shallow depth (B, D, F and H) in scenarios 2, 3 (48 points each one), 4 (24 points) and 5 (12 points)……32
Figure 2.10. 1:1 plots of predicted and measured values. CCC: Lin's concordance correlation coefficient. Dashed line shows the concordance line and solid line shows the linear model……35
Figure 2.11. Taylor diagram comparing predictions of scenarios 1-5 by using predictions from LOOCV and unused samples at each scenario. The black arc is representing the measured standard deviation……..38
Figure 3.1. Study area and sampling locations for soil texture and chemical properties as well as for electrical conductivity……48

Figure 3.2. Pearson correlation between measured variables. Colored cells represent significant correlation ($p < 0.01$)……56
Figure 3.3. Maps of spatial distribution of clay content at 0-20 cm (a), and 20-40 cm (b), NDVI June 2015 (c), organic matter (d), total nitrogen (e), extractable phosphorous (f), slope (g), topographic wetness index (h), and apparent electrical conductivity (i) at a shallow depth (0-30 cm). Black dots represent the soil sampling grid……...58
Figure 3.4. Principal component analysis map of variable for: a) PC1vs PC2 and b) PC1 vs PC3……..59
Figure 3.5. Average silhouette width for different number of cluster using FANNY and CLARA……61
Figure 3.6. Maps of delineated management zones. Based on maps of principal components factor scores by using a) FANNY and b) CLARA; based on Clay content at 0-20 cm, Organic matter and Topographic wetness index by using c) FANNY and d) CLARA; based on Clay at 0-20 cm and 20-40 cm, NDVI at June 2015, and Slope by using e) FANNY and f) CLARA……62
Figure 3.7. Elevation profile in a transect from NW to SE of the field……64
Figure 3.8. Management zones obtained from a FANNY analysis by using apparent electrical conductivity at a shallow depth (0-30 cm)……65
Figure 3.9. a) NDVI map of June 2017. b) Delineated zones using FANNY and based on Clay at 0-20 cm and 20-40 cm, Slope and NDVI at June 2017……67
Figure 3.10. Soil water tension and precipitation at different cluster areas……69
Figure 3.11. Continuous wavelet transform at different depths for each cluster zone. Period resolution is 1 hour. Significant differences ($p < 0.05$) against red noise is shown as a thick contour. The light shade represents the area outside of the cone of influence……..70
Figure 3.12. Wavelet Coherence between depths for individual cluster zones. Period resolution is 1 hour. Significant differences ($p < 0.05$) against red noise is shown as a thick contour. The light shade represents the area outside of the cone of influence. Arrows indicate the relative phase relationship: Right: in-phase; Left: anti-phase; Down: first series leading second series by 90°; Up: second series leading first series by 90°……71
Figure 3.13. Wavelet Coherence between cluster zones at different depths. Period resolution is 1 hour. Significant differences ($p < 0.05$) against red noise is shown as a thick contour. The light shade represents the area outside of the cone of influence. Arrows indicate the relative phase relationship: Right: in-phase; Left: anti-phase; Down: first series leading second series by 90°; Up: second series leading first series by 90°……73
Figure 4.1. Study area and sampling locations. Soil measurement were done at both red and yellow bullets……79
Figure 4.2. Topographic model of the delineated zones in the field. The area corresponds to the red rectangle showed on Figure 4.1……..80
Figure 4.3. Soil water tension at 20, 40 and 60 cm depth and daily precipitation under wheat (2016) and corn (2017) crops……...85
Figure 4.4. Predicted and measured soil water tension under wheat crop (2016) at different zones and depths……..87

Figure 4.5. Predicted and measured soil water tension under corn crop (2017) at different zones and depths……..88
Figure 5.1. Study area and soil classification. Red bullets indicate the soil sampling location. The locations are assigned as Nolin (map unit: Np), Crider I (map unit: CrA), Crider II (map unit: CrB2), and Crider III (map unit: CrC3). Map units were obtained from Sol Survey Staff (2017).……95
Figure 5.2. X-ray diffraction patterns of clay fractions for Mg and Mg glycerol treatments at different locations and depths.……..99
Figure 5.3. X-ray diffraction patterns of clay fractions for K 25 °C and K 550 °C treatments at different locations and depths.……100
Figure 5.4. Thermal analysis of clay fractions at different locations and depths……..101
Figure 5.5. Fourier transform infrared (FTIR) spectra of clay fractions at different locations and depths……..103

Chapter 1 Introduction

1.1 Irrigation Management

Irrigation in humid areas has increased in recent years in the United States. The application occurs during short-term periods of drought in summer. Among the reasons, we find that irrigation is used to optimize and stabilize crop yield at times of water shortage during the growing period. Another reason is the relatively high abundance of water for irrigation in these regions. Whether or not irrigation is profitable depends on different aspects such as costs (installation of systems, environmental), crop revenue, and total field area (Boyer et al., 2014). Another aspect to consider is the extensive demands of water resources in agriculture, industry and households for different uses in goods and services. Due to the competition with other demands, the water needs to be managed with better efficiency. One of the concepts most commonly used to discuss about effectiveness is the water use efficiency (WUE), which is referring to a ratio between crop productivity and water applied (Evans and Sadler, 2008), although there is not a unique definition. On the other hand, WUE has been used in a more general context, with a connotation closer to water conservation rather than productivity, although WUE and water conservation should not be used as equals. This is one of the challenges when irrigation is applied, on one side is the objective to increase crop yield, which implies higher water consumption and evapotranspiration (ET), but on the other side it is also required to consume less water to improve its conservation.

One way to optimize irrigation is the site specific irrigation management, also called precision irrigation (Sadler et al., 2005). The concept refers to applying the right amount of water at the right time but also considering the locations in the field. Therefore, a variable-rate water supply should be applied in light of the characteristics of the field. Spatial differences in topography and soil physical and chemical properties can be found on the same field, thus the infiltration and soil water movement also varies when irrigation is applied. In the literature we found examples during different decades (Nielsen et al., 1973, Wendroth et al., 1999) showing the spatial and temporal variability of soil water at field scale. Understanding spatial variation in soil hydraulic properties and its relation with other soil and crop properties can help to make better prediction of soil water dynamics and use it as a base for developing an appropriate site specific irrigation management (Li et al., 2014).

1.2 Site specific management

Precision Agriculture or site specific management is based on the concept of dividing a field in areas that share similar characteristics. Areas with the same characteristics may be managed in the same way, i.e., receive the same or similar input, however, inputs can vary between areas with different characteristics in order to optimize crop production and to obtain environmental benefits. The foundation of site specific management is the characterization of soil and crop properties at the field scale. The resulting maps of variable resource application are influenced by sampling scheme, measurement methods, support, scale, vegetation, local weather, and soil conditions used in the studies.

The spatial variability of soil and crop properties can be obtained from different sources (e.g. NRCS) or generated using field measurements. With the later one, maps can be generated using geostatistical interpolation (e.g. kriging, inverse distance weighting, regression kriging) of a grid sampling. For example, Mueller et al. (2001) mentioned that soil fertility condition maps are commonly generated from coarse sampling grids (100-m or more) and simple interpolation methods, but with concerns about its performance. In general, field scale measurements are cumbersome and infeasible to be performed in all fields of a farm at a resolution that would support a high-quality map. An alternative to increase the resolution and accuracy of field maps is the use of ancillary data, which should be easier to measure and possibly be collected at a finer resolution than the main variable. One example of ancillary data is the apparent electrical conductivity (EC_a) obtained from proximal sensing tools such as electromagnetic induction sensors (EMI) or coulter-electrode contact sensors (e.g. Veris system). This variable has been widely used to predict different variables including soil texture (Moral et al., 2010), soil drainage (Kravchenko et al., 2002), soil organic matter content (Kühn et al., 2009), soil water content (Peralta et al., 2013), cation exchange capacity (Triantafilis et al., 2009), soil water drainage (Dadfar et al., 2011) and soil salinity (Goff et al., 2009).

Soil variables and ancillary data can also be estimated from remote sensing techniques (Viscarra Rossel et al., 2011; Mohanty, 2013). The difference between proximal and remote sensing tools is the proximity with the measured variable; where proximal sensing tools are in direct contact or very close. On the other hand, images from drones and satellite are examples of remote sensing data but they present differences in the level of details and

coverage. While the satellite images can cover large areas they present a low spatial and/or temporal resolution, and atmospheric conditions could affect the image quality.

Remote sensing methods should be validated with field measurements (Ochsner et al., 2013). Remote sensing can complement field work and to observe spatial variation focus on relative spatial differences rather than a previse magnitude of values when the level of details is low. For example, satellite images can be used to monitor crop growth during the growing season and over different seasons by deriving different vegetation indices such as normalized difference vegetation index (NDVI) and leaf area index (LAI).

Different approaches can be applied to delineate management zones. For example, the spatial variation of yield maps from different seasons can be used as criteria to identify areas with differences in crop productivity. Another approach is to use soil physical and chemical and crop variables, or a combination of them. Unsupervised classification algorithms with the field data are often used to divide the field in zones (Zhang et al., 2010). The general idea is that comparing dissimilarities in the data between locations, the optimal number of division can be determined. One challenge about using this method is that the numerical solution should provide a number and delineation of areas that could be used on real farm conditions. Another aspect to consider when performing a delineation is how to select variables to characterize the field. Variables should be representative of the field variation for a specific management and preferably, easy to obtain in a realistic scenario. Consequently, the use of proximal and remote sensing data is recommended to complement field measurements as independent variables or ancillary data.

1.3 Modeling soil water status using Agro-system models

Agro-system models are important tools that are capable to integrate and synthesize information to describe relevant agro-ecological processes, including crop growth, soil water and nutrients balance and dynamics. They can help get better understanding of field conditions and identify adequate management alternatives under different scenarios that otherwise, may require large amount of data from field experiments, which may be not feasible for land managers (James et al., 2017). Several models have been developed to predict soil water balance and dynamics. The prediction of soil water status involves a characterization of several processes, including infiltration of precipitation or irrigation water, water movement and redistribution through the soil profile, and water losses by evapotranspiration and deep drainage.

Among models with a module related with soil water predictions we found RZWQM2 (Ma et al., 2002), SWAP (Jiang et al., 2001), and HYDRUS 1D/2D/3D (Šimůnek et al., 2017). RZWQM2 (Root Zone Water Quality Model version 2), is one dimensional model with emphasis on effects of management on water quantity, water quality, and crop production. It integrates the interactions between weather, soil properties, hydrology, agricultural management practices, crop growth, and chemical transport (Ahuja et al., 2000). The models provide several ways to estimate hydraulic properties. For example, soil water retention curve (SWRC) described by the Brooks–Corey equations (Brooks and Corey, 1964) can be estimated using the soil textural class parameters; saturated hydraulic conductivity can also be estimated based on the textural class and the effective macroporosity (Ma et al., 2012).

Agro system models are potential tools to support management practices including the optimization of water use. However, due to the complexity of modeling processes it requires a large quantity of input parameters, and the quality of the data should also be evaluated. For example, RZWQM2 requires parameters such as soil properties, weather, and management practices. In most of the cases, measuring all the input parameters is not possible, therefore it is needed to obtain data from alternatives such as neural networks, pedotransfer functions or estimations from the model itself. The experimental field data can be used to calibrate and evaluate the model. The model calibration can be performed manually (the most commonly method with RZWQ2) or by using computer-based automatic methods. In manual calibration, a trial-and-error parameter adjustment based on predicted versus measures values. This approach may be time consuming, considering that that several parameters could be modified and the scientist needs to have knowledge about the sensitive of parameters or perform a sensitivity analysis. With the automatic calibration, parameters are adjusted automatically according to a specified search scheme and numerical measures of the goodness-of-fit. On the other hand, an automatic procedure requires the selection of an objective function, a search algorithm, and a criterion by which to terminate the search (Gupta et a., 1999). The calibration is fast, and the confidences of model simulation can be stated. However, the automatic methods may not be transferable to other person due to different criteria to select an objective function, and the optimized parameter could not present physical or biological meanings (Boyle et al., 2000; Ma et al., 2011). How to improve the procedure of obtaining good quality measured and estimated field data, and to optimize the process of model calibration are one of the first steps to get

accurate predictions to be applied on forecasting, and then be used as a decision support tool.

1.4 Objectives of the study

This study has the aim to improve irrigation management through a survey of soil and crop variables in a farmer's field located in Western Kentucky. The specific objectives are a) to perform an integrative analysis of soil, crop and remote sensing variables to define management zones for irrigation; b) Synthesize information and develop processes for understanding soil water status through system models.

In chapter 2 we are presenting a procedure to create a clay content map using EC_a as secondary data. The purpose of the study is to answer questions about optimal sampling density, identify the spatial variability in the field, and the reliability of using ancillary data to increase the accuracy and the map resolution. Clay content is one of the key variables affecting the soil water status in the field, although field measurements are costly and time consuming. We present different scenarios changing the sampling density of clay content while maintaining all the EC_a measurements. The data is coregionalized using cokriging; the models are fitted for each scenario and different validation procedures are presented.

To perform a site specific management is necessary to delineate areas in the fields. In chapter 3, an integrative analysis of soil, proximal and remote sensing data is used to delineate zones. The methodology includes different approaches to select variables: a) using maps derived from a principal component analysis, b) identifying key variables from

the PCA and c) selected variables that are both representative of field variability and easy to obtain. To divide the field a hard and soft cluster algorithms were used. The purpose of using different approaches was to observe how different the result will be when different criteria is used. To validate the field divisions, a comparison of crop yield and soil water dynamics in each area is presented. To compare the temporal variation of soil water dynamics at different zones and depths a wavelet analysis is presented.

After delineating zones in the field in chapter 3, we study the soil water status at different zones and depths in chapter 4. In the chapter we compare differences in soil water tension between zones and study how it is related with other soil properties. We also evaluate the model prediction of soil water tension using the RZWQM2. We use field measurement and model derived parameters as inputs, and perform a calibration after the initial predictions. By predicting the soil water tension at different zones we can determine the right time to perform irrigation and also water amount and irrigation rate scenarios.

Lastly, in chapter 5 we are presenting a complementary study to characterize the clay mineralogy variation in the field. Clay mineralogy is not commonly studied at field scale although it is intrinsically related with other soil properties and can affect the soil management. The purpose of this study was to observe if the clay mineralogy variation is significant at field scales, how it is related to other variables, and if the characteristics have concordance with actual soil classification provided by NRCS. The samples were taken at soil map units based on the NRCS classification. In the field, we found map units from the Crider soil (Alfisol) series and from the Nolin soil series (Inceptisol). Data is compared

with other soil properties and the mineralogical characterization was obtained using a x-ray diffraction, a thermogravimetric analysis and Fourier-Transform-Infrared spectroscopy.

Copyright © Javier Reyes 2018

Chapter 2 Reliably Mapping Clay Content Coregionalized with EC

Reproduced with permission from Reyes, J., O. Wendroth, C. Matocha, J. Zhu, W. Ren, A.D. Karathanasis. 2018. Reliably Mapping Clay Content Coregionalized with Electrical Conductivity. Soil Science Society of America Journal, doi:10.2136/sssaj2017.09.0327. Copyright © Soil Science Society of America 2018

https://dl.sciencesocieties.org/publications/sssaj/abstracts/82/3/578

2.1 Introduction

Efficiency and environmental sustainability of crop production can be improved through precision agriculture that involves site-specific management of planting density, fertilizers and pesticides and recently irrigation (Yao et al., 2014; Peralta et al., 2015; Haghverdi et al., 2016). Knowing the spatial variability of soil textural composition across a farmer's field is important for precision agriculture because of its strong influence on a large number of soil physical and chemical properties and processes. In many regions of the United States, soil texture can exhibit high spatial variability at the field scale, and thus cause spatial differences in crop growth and yield (Burke et al., 1989; Bronson et al., 2005; Sudduth et al., 2005). Special attention has been focused on soil clay content, which is the most active fraction participating in processes such as soil water retention, hydraulic conductivity, soil aggregation, and cation exchange behavior through mineralogy (Schulze, 1989). The clay fraction is important for soil structure and fertility, but an excessive percentage of clay can negatively affect water infiltration and aeration of the soil.

The estimation of soil properties at the field scale is influenced by the measurement method, sampling scheme, scale, i.e., sample size, separation distance, domain size (Blöschl and Sivapalan, 1995), vegetation, and local soil conditions, and magnitude of variance. The appropriate spatial sampling resolution that provides a representative map of a variable remains unknown *a priori*; without any further information, application of the map for agricultural management remains uncertain as well (Frogbrook, 1999). Several geostatistical approaches can be applied to produce maps that represent spatial variation. One of those commonly used is ordinary kriging. Other methods are inverse distance weighting and universal kriging (Liu et al., 2006). For a meaningful map based on kriging it is necessary to obtain semivariogram models that represent the observed spatial structure (Nielsen and Wendroth, 2003; Kravchenko, 2003). On the other hand, interpolation based on inverse distance weighting does not depend on structured variability of observations but on an arbitrarily chosen coefficient that weighs measurements in the vicinity of the estimated location. For this reason, inverse distance interpolation produces less meaningful results than kriging (Kravchenko, 2003). In case of using universal kriging, trends underlying the data are removed and only the residuals are kriged. Then, the trend is added to the kriged residuals (Nielsen and Wendroth, 2003). Compared to univariate kriging, the estimation and map accuracy can be improved through cokriging by adding one or more secondary variables that are spatially associated with the primary variable. Cokriging requires a linear model of coregionalization and positive definiteness (Deutsch and Journel, 1992; Nielsen and Wendroth, 2003). Triantafilis and Lesch (2005) and Weller et al. (2007) gave examples for soil clay content maps derived from univariate ordinary kriging. Cokriging and regression kriging have also been used to estimate clay content with

electrical conductivity as a covariate by, e.g., Triantafilis et al. (2001), Moral et al. (2010), and Heil and Schmidhalter (2012). In addition, Odeh and McBratney (2000), employed satellite images, and Odeh et al. (1994) applied digital elevation models as ancillary data in their multivariate geostatistical predictions of clay content.

Geophysical techniques have increasingly been used to support the prediction of soil properties that are comparably expensive and time consuming to obtain at high spatial resolution (McBratney et al., 2003; Casa et al., 2013). One of the most common variables used to coregionalize soil clay content is apparent electrical conductivity (EC_a) or its reciprocal value, i.e., electrical resistivity (Wendroth et al., 2006). While EC_a has been used to predict clay content and other variables, we have to consider that EC_a varies in time due to its relationship with soil water content (Corwin and Lesch, 2003; Sudduth et al., 2005). Therefore, depending on the time of measurement and the respective variability structure, not every mapping campaign of EC_a may result in a pattern that supports a linear model of coregionalization with soil clay content. EC_a has been intensively studied by using non-invasive electromagnetic induction sensors (EMI) such as EM38 (Geonics limited), GEM-2 (Geophex limited) and DUALEM-21S (DUALEM) (Doolittle and Brevik, 2014). In recent applications, EMI was used as ancillary variable to predict soil organic matter content (Kühn et al., 2009), soil water content (Peralta et al., 2013), cation exchange capacity (Triantafilis et al., 2009), soil water drainage (Dadfar et al., 2011) and soil salinity (Goff et al., 2009). Although not as widely used as EMI sensors, coulter-electrode contact sensors such as the Veris system (Veris technologies, 2016) can also be coregionalized with cation exchange capacity (Bishop and McBratney, 2001), soil drainage (Kravchenko

et al., 2002), and soil texture mapping (Moral et al., 2010). For further information, Corwin and Lesh (2005) and Doolittle and Brevik (2014) have provided comprehensive reviews of EC_a applications.

Several studies that include a secondary variable through cokriging or other interpolation methods present results for only one sampling resolution without quantifying the impact of spatial support. Not much is known about the behavior of coregionalization results obtained for primary data collected at different levels of spatial support (Mueller and Pierce, 2003). While the use of ancillary data has shown improvements in primary variable predictions compared to univariate kriging in general, the behavior of estimation quality for various sampling densities of the primary variable requires further study. Such investigations are of substantial relevance for on-farm conditions where a realistic and affordable density of soil samples for textural analysis is essential while it is relatively easy to obtain EC_a as a secondary variable at a fine resolution. EC_a correlation with different soil properties has been studied in Kentucky (Mueller et al., 2003) but not its use as a secondary variable to develop clay content maps. The objective of this work was to obtain a reliable soil clay content map in a farmer's field in Western Kentucky by using clay content measurements coregionalized with apparent electrical conductivity data acquired from a Veris system. Ordinary kriging and cokriging of soil clay content using EC_a should be employed to compare the map quality under various primary variable sampling support scenarios. Complementary, the effect of spatial clay sampling resolution on the consistency of estimation models and the accuracy of predictions should be examined for identifying how many samples would be needed to produce a clay map with appropriate accuracy. For

this purpose, scenarios with different spatial resolution of clay content measurements should be investigated while spatial density of EC_a data remained the same in all scenarios.

2.2 Material and Methods

2.2.1 Site description

The study was conducted at a field site of Hillview Farms (Figure 2.1) located in Princeton KY, Caldwell County (37° 1'58.02"N, 87°51'33.06"W, 142 m asl). At this location, the annual precipitation is 1312 mm, with a mean annual temperature of 15 °C. The maximum monthly mean temperature is 30°C (June) and the minimum monthly mean temperature is -5 °C (January) (US climate data, 2016).

The soils belong mainly to the Crider series, and are described as Fine-silty, mixed, active, mesic Typic Paleudalfs; these soils are formed in a loess mantle and the underlying residuum from limestone. In some areas we found soils from the Nolin series, which are classified as Fine-silty, mixed, active, mesic Dystric Fluventic Eutrudepts; these soils are formed in alluvium derived from limestones, sandstones, siltstones, shales, and loess (Soil Survey Staff, 1999). The area covered by our measurements was approximately 27 ha. The field was cultivated with corn (*Zea mays* L.) under no till soil management during the growing seasons of 2014 and 2015.

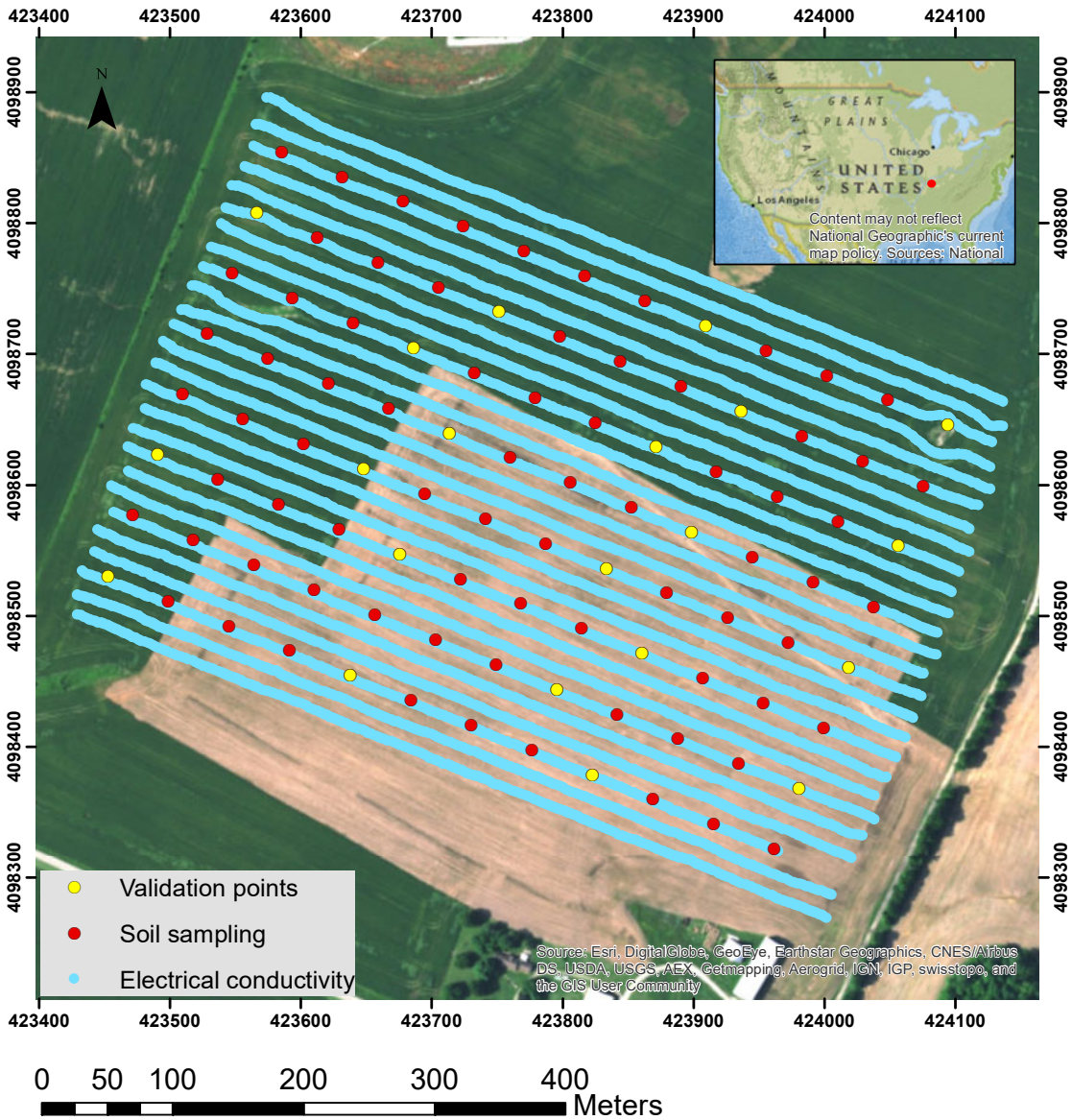

Figure 2.1. Study area and sampling locations. Red and yellow bullets denote 96 sampling locations for soil texture while yellow bullets indicate the validation points. Blue bullets reflect the paths for EC_a measurements.

2.2.2 Soil sampling and EC_a data collection

Soil texture was sampled in a 50 by 50-m-grid of 96 points (Figure 2.1) at five 20-cm-intervals from 0 to 100 cm depth, while only the upper 0-20 cm were considered for the

spatial EC_a-clay content relationship in this study. Sand fractions were separated by sieving, medium and fine silt (0.002-0.005 mm) and clay (< 0.002 mm) were measured with the pipette method (Gee and Or 2002). Coarse silt (0.05-0.02 mm) was calculated as the residual.

Soil EC_a was measured in the spring in April of 2015 using a Veris 3150. This device is a contact sensor that has six rolling coulters-electrodes and a width about 235 cm. On the field, it reach a maximum speed about 25 km h^{-1} (Veris Technologies, 2016). One pair of coulter-electrodes injects current to the soil and other is used to measure the voltage (Sudduth et al., 2005). The electrodes are configured with the Wenner array and we obtained cumulative measurements over a shallow depth (about 0-30 cm) and a deep depth (about 0-90 cm), which we define as EC_{as} and EC_{ad} respectively. EC_a was measured on the day before corn planting when soil conditions were appropriately moist for good coulter-soil contact, but not too moist to prevent soil compaction. Corwin and Scudiero (2016) recommended to run EC_a sensors under sufficient soil moisture (i.e., approximately 2/3 of field capacity) to establish a good contact between the coulters and the soil and to maintain continuous conductance to the depth of measurements (about 90 cm for Veris). EC_a measurements were collected along several transects in the field (Figure 2.1). Transects were spaced approximately about 17 m to have 2 paths in between each grid line, and the spacing between points along each transect was approximately 2 m, generating a database of some 7350 points. To analyze clay content and EC_a correlations and to perform a classic cross semivariogram analysis described in Nielsen and Wendroth (2003), we paired points of clay content with an average value of the nearest EC_a points that were located within a

radius of 2 m around each clay sampling location. EC_a and clay measurements could not be collected at exactly the same coordinates. The average distance between clay and EC_a measurement location was 1.31 m (s.d. = 0.56 m).

2.2.3 Sampling schemes

Five scenarios were created to evaluate the consistency of clay content predictions (Figure 2.2). In four scenarios the number of sampling points available for kriging and cokriging analysis was reduced compared with the original data (scenario 1, Figure 2.2A). In the different scenarios, the number of observations was reduced by 50 %, i.e., 96, 48, 24, and 12 locations were considered. For scenarios 2 and 3 we investigated how two different spatial arrangements with the same number of observations affect the spatial predictions. In scenario 2 (Figure 2.2B), 48 locations were selected with a minimum distance of 70 m, while in scenario 3 (Figure 2.2C), 48 locations were arranged in pairs of points with the original lag distance of 50 m and in account of that, more pairs with lag distances larger than 70 m. In scenarios 4 and 5, grids were designed with equally spaced sampling points covering the entire field. In scenario 4 (Figure 2.2D) we used 24 points in a regular 100-m-grid. For scenario 5 (Figure 2.2E), 12 points were arranged in a regular 150-m-grid.

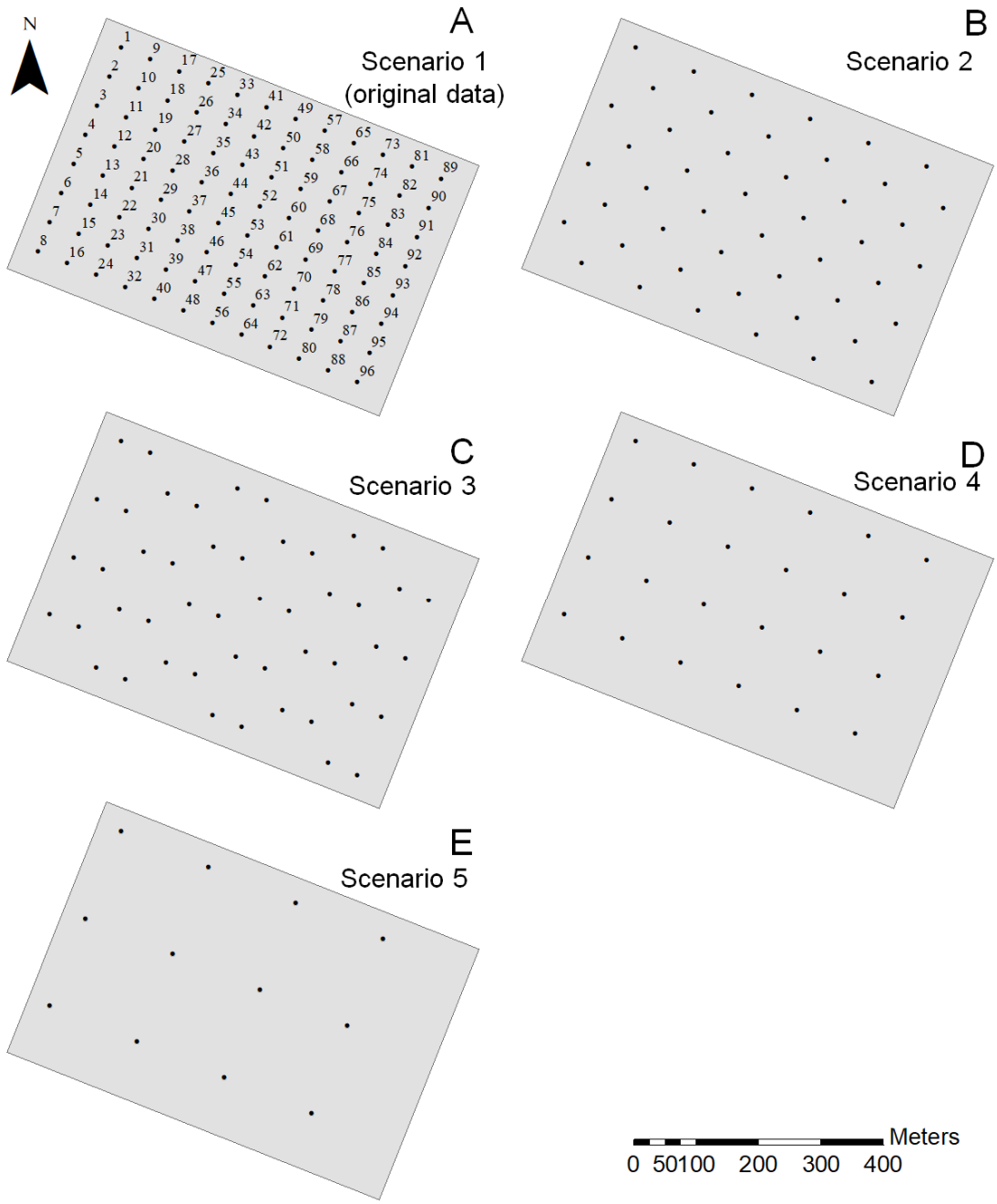

Figure 2.2. Sampling schemes for each scenario. Number labels in (A) indicate the locations referred to in the 1-dimensional display of results in Figure 2.6.

2.2.4 Geostatistical Interpolation

To apply kriging and cokriging as interpolation methods, parameters have to be identified that describe the spatial variance structure in semivariograms. In this study, experimental semivariograms were fitted to Spherical, Gaussian, or Exponential models (Journel and Huijbregts, 1978). Instead of a classical experimental cross semivariogram, the pseudo cross variogram (Myers, 1991) was applied for cokriging that is defined as:

$$g(h) = \frac{1}{2N(h)} \sum_{i=1}^{N(h)} \left(A(x_i) - B(x_i + h)\right)^2 \quad (eq. 2.1)$$

where $g(h)$ is the cross semivariance, $A(x_i)$ is the measured value at location x_i, $A(x_i+h)$ is the measured value at location x_i+h, h represents the lag distance between two locations, and $N(h)$ is the number of paired points that are separated by a lag distance of h, B is the secondary variable value measured at location (x_i+h). The model functions were fitted by a weighting factor ($N_{(h)}/ h_i^2$) of the squared residuals. Despite the fact that experimental pseudo and traditional cross semivariograms are calculated differently, the pseudo cross variogram is used in the same way as the traditional cross semivariogram in the cokriging computation. With the pseudo cross variogram all measurements of the secondary variable are included in the calculations whereas classical cross semivariograms only consider measurements of both variables that are obtained for the same location. The use of pseudo cross variograms has an advantage in cases where many observations for the secondary variable exist while only a limited number of samples for the primary variable are available, and identifying the spatial structure with the traditional cross semivariogram would therefore be difficult. On the other hand, concerns exist regarding the use of pseudo cross

variograms such as the effect of differences in variability or magnitude (different units) between variables (Myers, 1991). Moreover, when there is a large difference in sampling density between primary and secondary variables, the variability of the variable sampled at a higher density may dominate the variability structure.

For each of the scenarios we recalculated the experimental semivariograms and cross semivariogram and their respective models based on the data considered for the particular scenario. To interpolate values at unsampled locations using only one variable ordinary kriging was used. To include a secondary variable in the interpolation, ordinary cokriging was applied. Nested semivariogram models were used in the cokriging analysis that include two empirical models as components and allow a better fit. The procedures and equations used to perform the geostatistical interpolation are explained in Nielsen and Wendroth (2003).

2.2.5 Data Validation

The estimation for each scenario was cross-validated with a leave-one-out approach. This method consists of removing each of the measured clay points one by one and estimate its value with the remaining points. To complement this approach, each scenario was validated with unused samples (48 points for scenarios 2 and 3, 72 points for scenario 4, and 84 points for scenario 5) and Lin's concordance correlation coefficient was computed (Lin, 1989). In addition, an independent validation data set for the same 21 locations (Figure 2.1) was chosen to compare scenarios 2 – 5 directly with each other and results of this comparison were visualized in a Taylor diagram (Taylor, 2001).

The mean error (ME) is a criterion to evaluate the bias of model predictions. To identify the accuracy the root mean squared error (RMSE), and the RMSE-observation standard deviation ratio (RSR) were computed. A paired t-test ($P < 0.05$) allowed to compare mean differences of RMSE between ordinary kriging and cokriging for each scenario, and One-way ANOVA with post-hoc LSD test ($P < 0.05$) was performed for multiple comparison. These indices were calculated according to:

$$ME = \frac{1}{n}\sum_{i=1}^{n}(\mathrm{z}'(\mathrm{i}) - \mathrm{z}(\mathrm{i})) \qquad (eq.\,2.2)$$

$$RMSE = \sqrt{\frac{1}{n}\sum_{i=1}^{n}(\mathrm{z}'(\mathrm{i}) - \mathrm{z}(\mathrm{i}))^2} \qquad (eq.\,2.3)$$

$$RSR = \frac{\sqrt{\frac{1}{n}\sum_{i=1}^{n}(\mathrm{z}'(\mathrm{i}) - \mathrm{z}(\mathrm{i}))^2}}{SD\ z} \qquad (eq.\,2.4)$$

where n is the number of samples, $z(i)$ is the measured value at location i; $z'(i)$ is the predicted value at location i, and $SD\ z$ is the standard deviation of measured data.

Our analysis was centered in the relationship between clay content at the surface layer (0-20 cm) and EC_{as}. Although EC_{ad} can also be used, we have to consider that it is a value that integrates soil properties down to 90 cm depth and it is difficult or even impossible to relate

it to properties in individual layers. Both variables were log-transformed, to normalize their distribution and homogenize their magnitude, the latter being recommended for pseudo cross variogram analysis (Myers, 1991). Shapiro's test showed that log-transformed clay was normally distributed ($P = 0.12$) at a 95% confidence limit. Log-transformed EC_{as} did not reveal a normal distribution ($P < 0.05$), which has to be expected due to the large number of samples considerably narrowing the confidence interval. However, a normal distribution for log-transformed EC_{as} can be assumed considering that quantile-quantile plots showed a pattern of normal distribution and based on randomly subsampling a number of log-EC_{as} observations similar to clay samples (n=100), that was obviously normally distributed ($P > 0.05$).

Statistical analyses were performed using libraries included in the R environment (R Core Team, 2017). Semivariograms, pseudo cross variograms, ordinary kriging and cokriging were computed using Gstat (Pebesma, 2004), geoR (Ribeiro and Diggle, 2016) and sp (Roger et al., 2013) packages. Lin's concordance correlation coefficient was performed using the epiR package (Stevenson et al., 2017). Maps were plotted with lattice (Sarkar, 2008), and the Taylor Diagram was computed using the plotrix package (Lemon, 2006).

2.3 Results and Discussion

Descriptive statistics of each scenario are presented in Table 2.1. Clay content at 0-20 cm revealed values between 14 and 32 % with a mean of 20 % (s.d. = 4.6 %). Surface soil texture in the field was classified as silt loam, but at some locations measured particle size composition represented a silty clay loam because of higher clay content. While higher

clay contents are expected in deeper soil horizons, in some areas in the field surface material was eroded causing a high clay content even at the soil surface. Apparent electrical conductivity values were 4.6 mS m^{-1} (s.d. = 1.3 mS m^{-1}) for EC_{as} and 14.6 mS m^{-1} (s.d. = 3.9 mS m^{-1}) for EC_{ad}. The Pearson correlation of clay content was significant ($P < 0.01$) with both EC_{as} (0.76) and EC_{ad} (0.67), and with the log-transformed data, it was 0.70 for EC_{as} and 0.57 for EC_{ad}. The magnitude of these correlation coefficients are comparable to those found in other studies by Mueller et al. (2003) in soils of Kentucky and Sudduth et al. (2003) and Bronson et al. (2005) in different fields and regions of the United States, using a Veris 3100 to measure EC_a. In those studies, EC_{as} was the most correlated with surface clay content, since EC_{ad} measurements integrate electrical conductivity between 0 and approx. 90 cm depth. To verify the spatial relationship, the classical cross semivariogram for log-transformed clay content and EC_a data manifests an evident spatial structure that follows a Gaussian model (Figure 2.3).

Table 2.1. Descriptive statistics of clay samples used in each scenario and the validation set (Clay val.) and the electrical conductivity at a shallow (EC_{as}) and deep (EC_{ad}) depth.

Parameter	Clay sc.1	Clay sc.2	Clay sc.3	Clay sc.4	Clay sc.5	Clay val.	EC_{as}	EC_{ad}
			%				mS m^{-1}	
N	96	48	48	24	12	21	7350	7350
Mean	20.0	20.1	19.3	20.1	21.1	20.2	4.6	14.6
Standard Deviation	4.7	4.5	4.0	4.7	5.6	5.7	1.3	3.9
Kurtosis	0.53	-0.16	2.25	-0.04	-0.23	0.35	0.71	2.93
Skewness	1.1	0.8	1.4	0.9	1.0	1.2	0.8	0.8
Minimum	14.0	14.6	14.6	14.6	15.4	14.0	1.4	1.5
Maximum	33.4	31.1	32.5	31.1	31.4	33.4	12.2	50.6

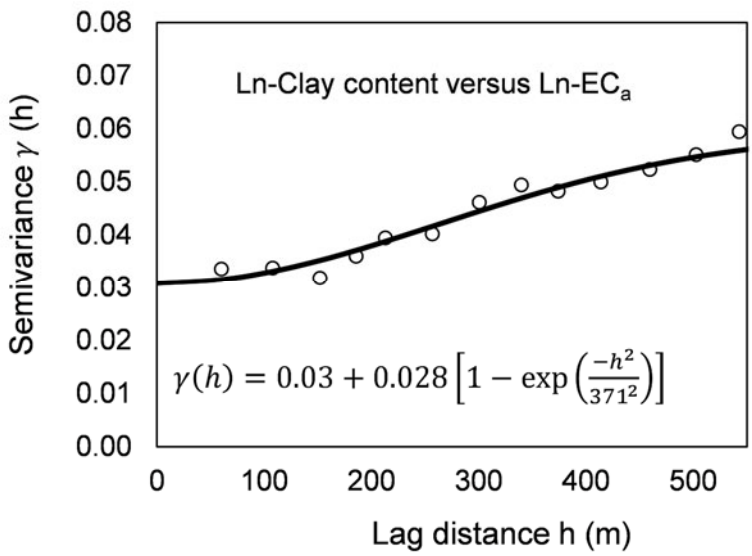

Figure 2.3. Classic cross variogram of Log Clay and Log EC_a.

2.3.1 Semivariograms based on all data

The semivariogram and pseudo cross variogram models applied for kriging and cokriging in scenario 1 including all clay content data are presented in Figure 2.4. The Gaussian model was the best one to describe the spatial structure of clay content, with the semivariance having a parabolic behavior at the start before it reaches an inflection point at about 300 m lag distance (Figure 2.4A). EC_{as} yields a semivariogram with a pattern closer to a spherical model in the range of 0-200 m and then variance increases again at larger lag distances (Figure 2.4C). To fit a common model of coregionalization a nested model was chosen based on nugget, Gaussian and Spherical components. The cross semivariograms between EC_a and clay content, found in other studies (Carrol and Oliver 2005; Heil and Schmidhalter, 2012), revealed a positive structure. Since all data from the secondary variable were used here, the pseudo crossvariogram structure (Figure 2.4D) exhibited a pattern similar to EC_{as} (Figure 2.4C) over the first lag distances. Despite concerns regarding the use of a pseudo crossvariogram for large secondary observation

numbers, the spatial structure remains similar to the classic cross semivariogram presented in Figure 2.3 except for short lag distances.

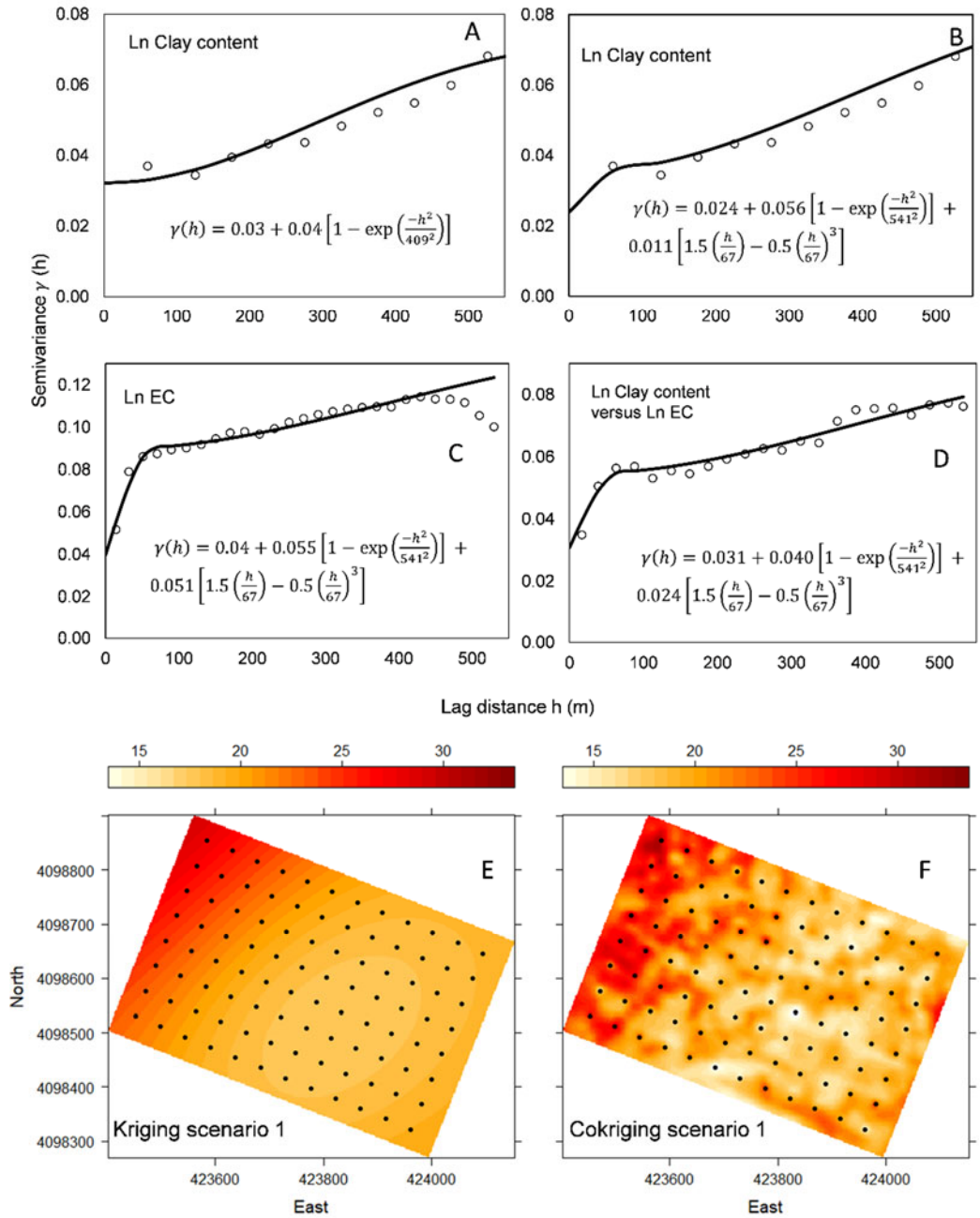

Figure 2.4. Scenario 1 with all data: semivariogram and model for ln-transformed clay content at 0-20 cm used for ordinary kriging (A); semivariograms and linear models of coregionalization for ln-transformed clay content at 0-20 cm (B), ln-transformed electrical conductivity at shallow depth (C) and pseudo cross variogram of ln-transformed clay content and electrical conductivity (D). Maps of clay content for scenario 1 (all measurements) using kriging (E) and cokriging with apparent electrical conductivity at shallow depth (F).

2.3.2 Kriging and Cokriging predictions using all data

Kriged and cokriged clay content maps are presented in Figure 2.4E and Figure 2.4F. In both cases high clay contents were found in the northeastern part of the field, and low clay contents in the center area. On the other hand, spatial differences in the representation of clay content were detected between both estimation methods. The maximum-minimum span of clay content values predicted with kriging was smaller than that obtained from cokriging. Also, cokriged clay content varied over shorter distances than kriged clay content due to the influence of EC_{as} data and their fine resolution. Moral et al. (2010) observed similar patterns in an EC_a map and a clay map using regression kriging with EC_a. Given the relatively coarse resolution of clay content data, kriging remains a smoothing process. On the other hand, the cokriged map better represents the actual clay content variation because variability features are manifested by the secondary variable sampled at finer resolution.

The Gaussian model with its wide effective range produced the relatively smooth spatial distribution of clay content presented in the kriged map in Figure 2.4E. To demonstrate the impact of semivariogram shape especially at short lag distances on the map contours, a spherical model was used for kriging the map displayed in Figure 2.5. Obviously, the semivariogram model fit is less precise than the one displayed in Figure 2.4A. The resulting map in Figure 2.5B reveals a similar overall trend as in Figure 2.4E but with more pronounced small-scale fluctuations introduced by the larger weight for close neighbors in the kriging matrix that was caused by the erroneously small semivariance at short lag distances (Figure 2.5A).

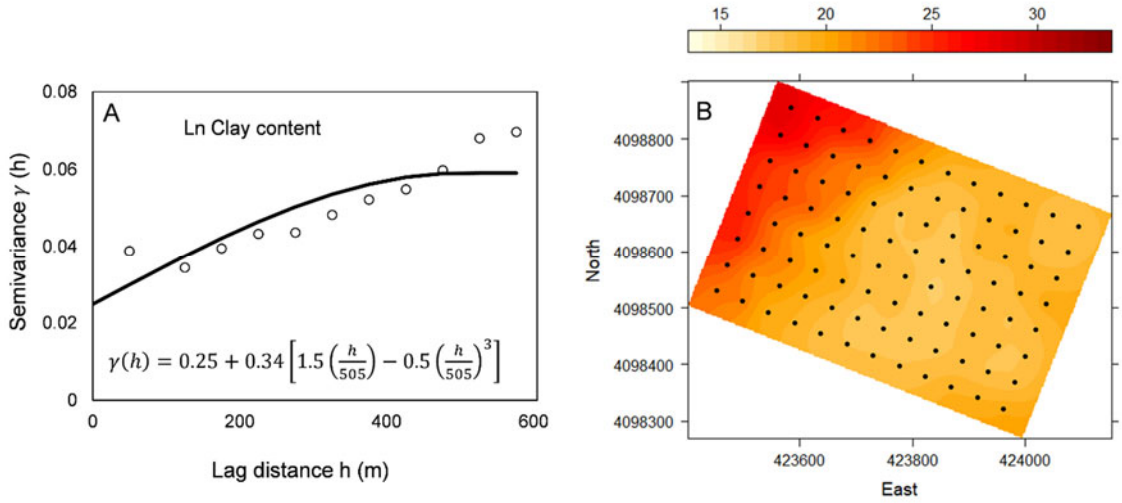

Figure 2.5. Semivariogram and semivariogram model for scenario 1 (A) and kriged map of clay content (B) based on the spherical model.

To validate predictions a leave-one-out cross validation was performed (Figure 2.6). Cokriging decreased the prediction error significantly ($P < 0.05$) (RMSE: 3.16 %) compared to kriging (RMSE: 4.08 %). It is obvious from comparing the results presented in Figure 2.6, that kriging mainly smoothed the spatial process of clay content and the confidence interval of kriged values has a wider range compared with cokriging, the latter revealing a more specific and precise representation of clay content variation between locations. Heil and Schmidhalter (2012) found similar RMSE values (4 %) when predicting clay content using cokriging, a better result than that obtained from regression kriging in their study.

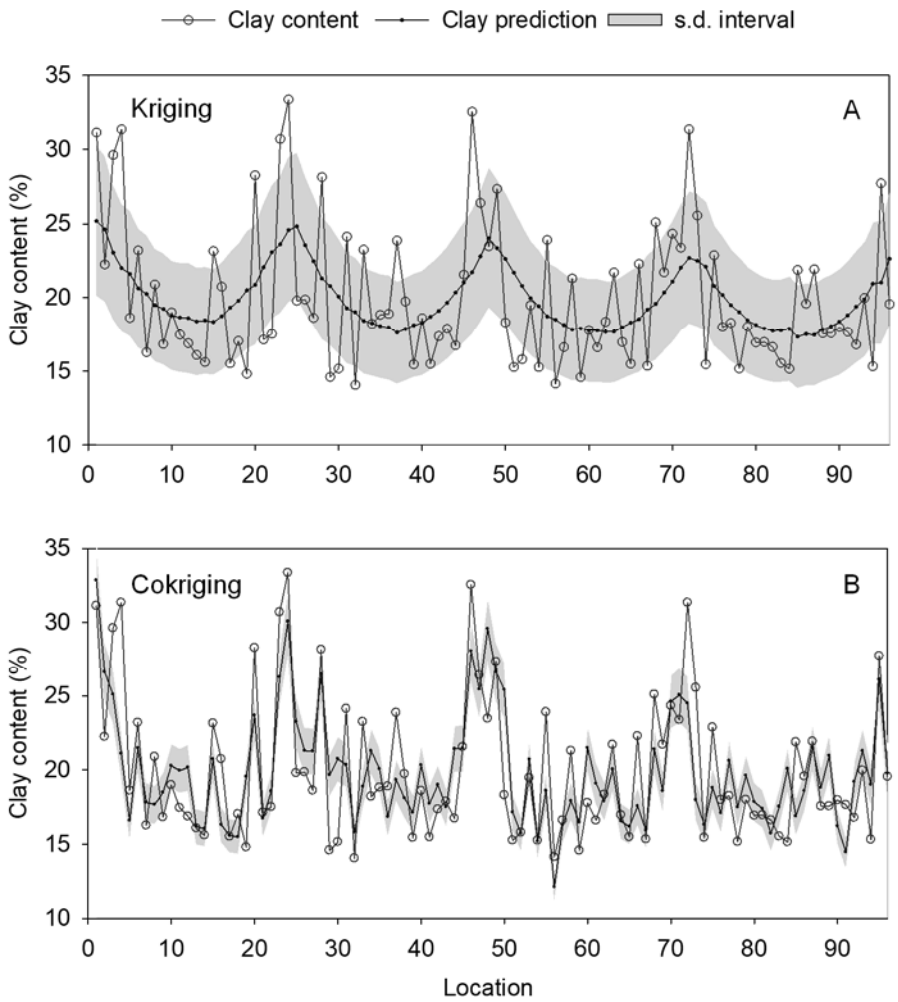

Figure 2.6. Cross validation of predicted clay content at 0-20 cm using kriging (A) and cokriging (B) with all measurements (scenario 1).

2.3.3 Kriging and Cokriging scenarios

Semivariogram models were computed for each scenario (Figs. 2.7 and 2.8). In scenarios 2 and 3, the same numbers of samples was used but in different spatial arrangements that reflect different spatial variability structures of clay content, as obvious from the resulting semivariograms (Figure 2.7). In scenario 4 the semivariogram of clay content appears less structured than in scenarios 2 and 3. In scenario 5 the fitting of the semivariogram model for clay content is less accurate because positive definiteness has to be met. Although we

reduced the number of samples for clay content, the pseudo crossvariogram kept a similar spatial structure over the first lags while differences at large lag distances could be observed. Our results indicate changes in the spatial structure not only by reducing samples but also in the spatial arrangement of sampling points relative to each other as we observe with scenarios 2 and 3, where the scenario 3 is less structured.

Maps obtained with kriging and cokriging are presented in Figure 2.9. Kriged maps exhibit spatial clay content patterns changing for each scenario. Interestingly, the kriged spatial clay pattern differed slightly between scenarios 2 and 3 – a result that can be addressed solely to the arrangement of observations because the number of observations was identical. Kriging predictions depend on observations and semivariograms models. Consequently, with less observations the predictions depend more on models, which increases the uncertainty. On the other hand, for cokriging maps each of the scenarios reveals similar clay content patterns. This result is manifested in the comparison between scenarios 4 and 5, which are both based on a coarse grid sampling distance similar to the one applied by Mueller et al. (2001). The similarity in shape of the cokriging maps is a consequence of the high EC_a sampling density. As was mentioned, with cokriging we can use data from each EC_a location, and predict clay content based on their spatial relationship. Moreover, some loss in resolution is observed in scenarios 4 and 5, and areas with extreme values are more clustered compared to scenarios 2 and 3. This behavior was probably caused by the reduction of clay samples and the semivariogram model fitting.

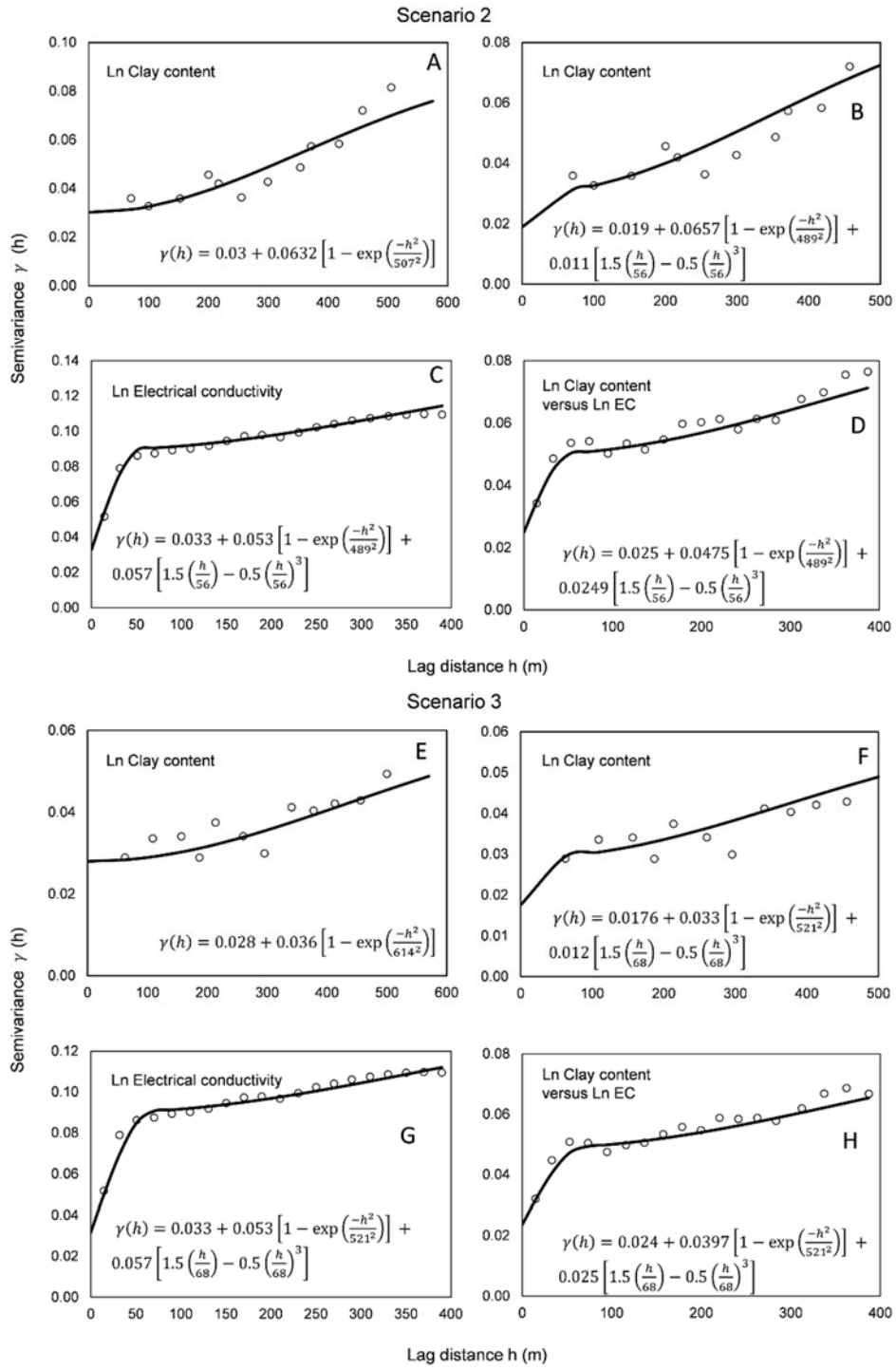

Figure 2.7. Scenarios 2: semivariogram and model for clay content at 0-20 cm used for ordinary kriging (A); semivariograms and linear models of coregionalization for clay content at 0-20 cm (B), electrical conductivity at shallow depth (C) and pseudo cross variogram of clay content and electrical conductivity (D). Scenario 3: semivariogram and model for clay content at 0-20 cm used for ordinary kriging (E); semivariograms and linear models of coregionalization for clay content at 0-20 cm (F), electrical conductivity at shallow depth (G) and pseudo cross variogram of clay content and electrical conductivity (H).

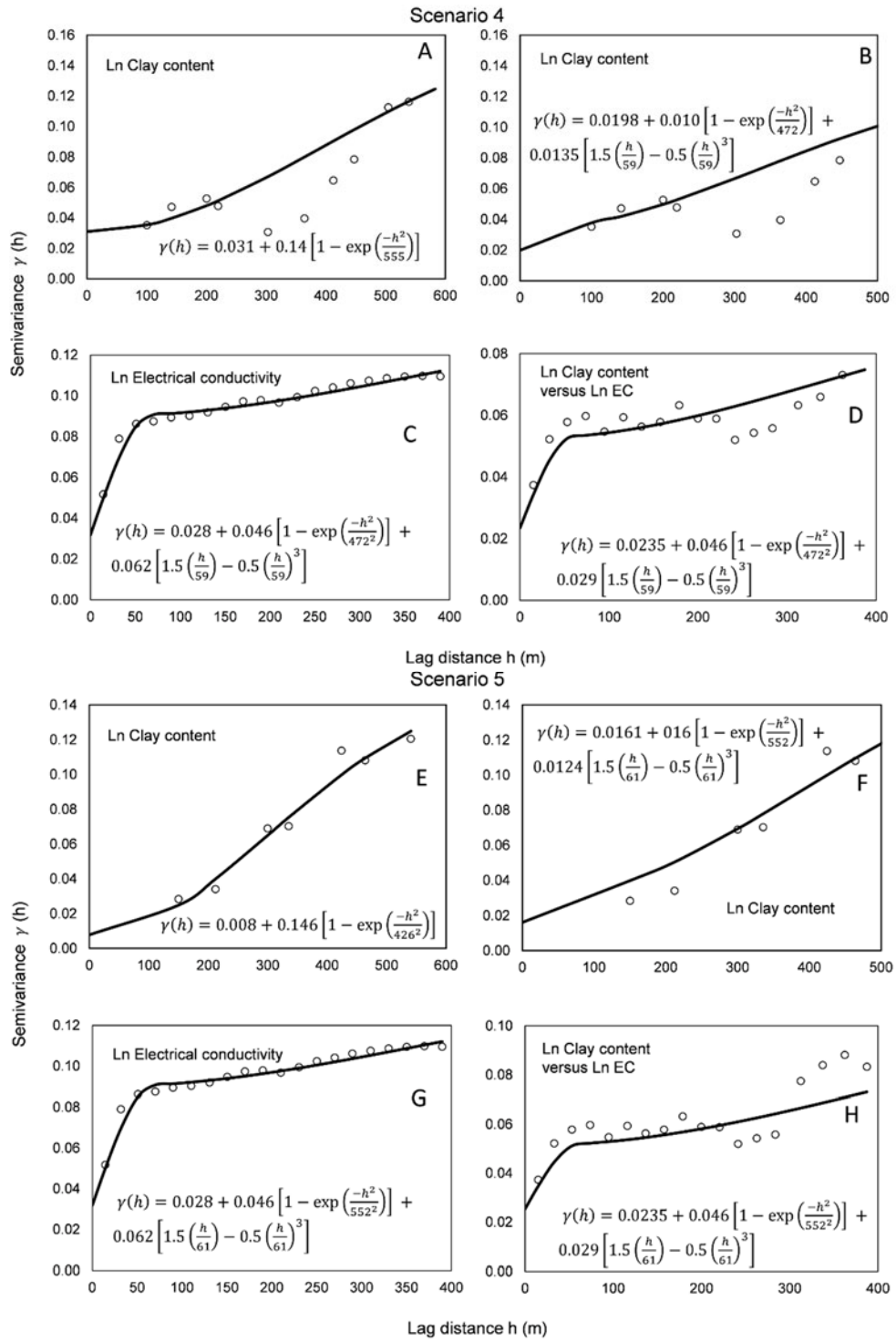

Figure 2.8. Scenario 4: semivariogram and model for clay content at 0-20 cm used for ordinary kriging (A); semivariograms and linear models of coregionalization for clay content at 0-20 cm (B), electrical conductivity at shallow depth (C) and pseudo cross variogram of clay content and electrical conductivity (D). Scenario 5: semivariogram and model for clay content at 0-20 cm used for ordinary kriging (E); semivariograms and linear models of coregionalization for clay content at 0-20 cm (F), electrical conductivity at shallow depth (G) and pseudo cross variogram of clay content and electrical conductivity (H).

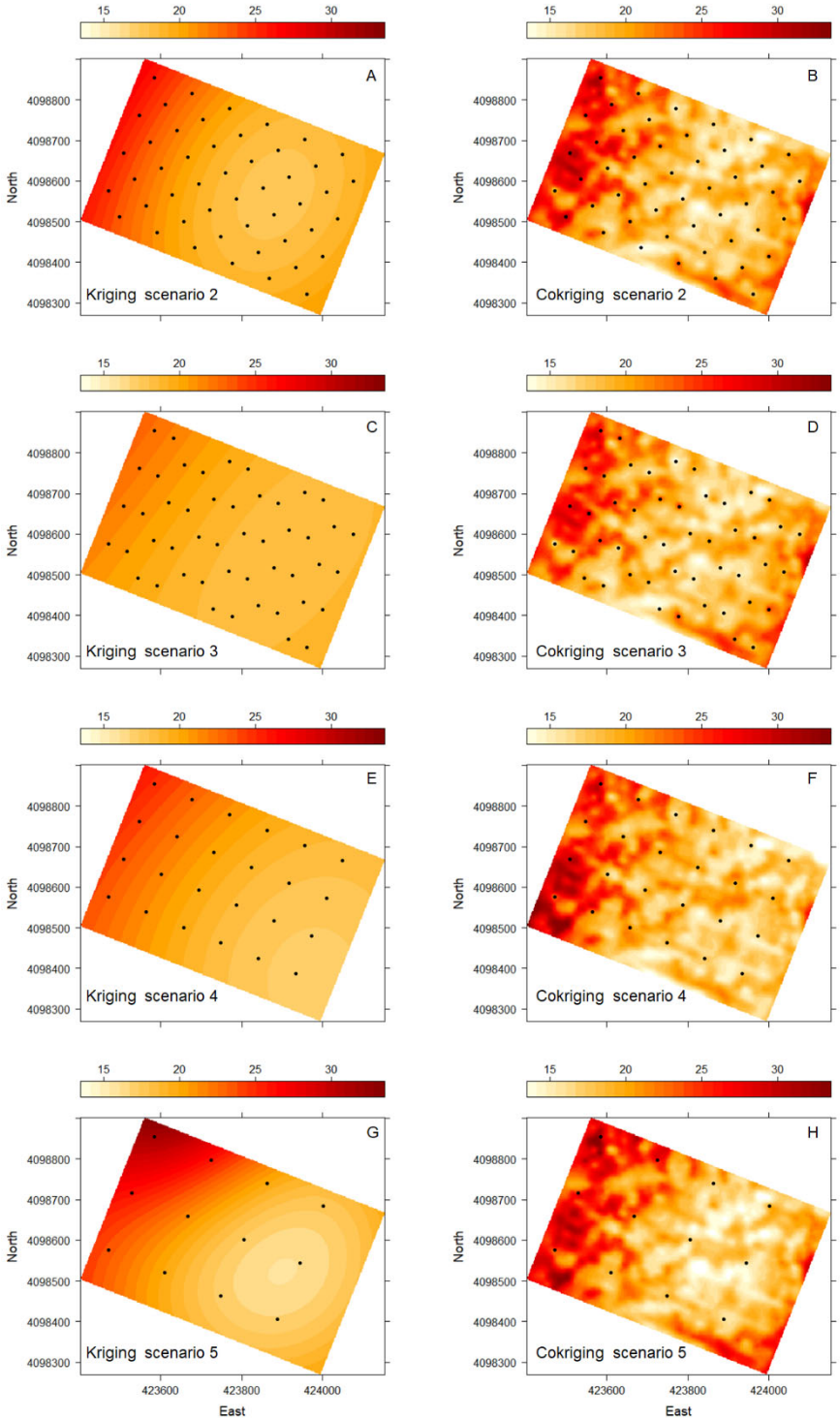

Figure 2.9. Maps of clay content using kriging (A, C, E and G) and cokriging with apparent electrical conductivity at shallow depth (B, D, F and H) in scenarios 2, 3 (48 points each one), 4 (24 points) and 5 (12 points).

Results of leave-one-out cross validations of clay samples in each kriging and cokriging scenario are presented in Table 2.2. This validation only compares the prediction on used measurements. Therefore, the number of samples differs in each scenario. The RMSE was lower with cokriging than kriging, showing significant differences (P<0.05) except for scenarios 3 and 5. The mean error for both kriging and cokriging presented a negative value in all scenarios, with the exception of the scenario when all measurements were used. This result indicates a trend to underestimate measured values, but the bias is low in all cases. On the other hand, a key outcome of this study is that even if the number of sampling points for clay content was decreased, the RMSE did not significantly increase.

Table 2.2. Bias and prediction error of clay content (%) in each scenario using Leave-one-out cross validation. ME: mean error, RMSE: Root mean squared error (RMSE), RSR: RMSE-observation standard deviation ratio. EC_{as} was used as secondary variable for cokriging. Notice, the number of predicted points differs between scenarios.

	Kriging sc. 1	Kriging sc.2	Kriging sc. 3	Kriging sc. 4	Kriging sc. 5
Predicted points	96	48	48	24	12
ME (%)	0.04	-0.06	-0.06	-0.12	-0.23
RMSE (%)	4.08*	3.85*	3.83	4.45*	4.25
RSR	0.86	0.85	0.95	0.94	0.76
	Cokriging sc. 1	Cokriging sc. 2	Cokriging sc.3	Cokriging sc. 4	Cokriging sc. 5
Predicted points	96	48	48	24	12
ME (%)	0.12	-0.11	-0.10	-0.19	-0.17
RMSE (%)	3.16*	3.14*	3.07	3.26*	4.19
RSR	0.67	0.69	0.76	0.69	0.76

* Significant differences (P<0.05) between kriging and cokriging for each scenario.

2.3.4 Sample validations

The error in the prediction of discarded sampling points for each scenario is presented in Table 2.3. As observed in the prediction for measured and used samples (Table 2.2), the RMSE was decreased with significant differences ($P < 0.05$) by using cokriging, while maintaining comparable RSR values in each scenario. In Figure 10, the predictions and Lin's correlation concordance correlation coefficient using both methods are shown. In general, all models have difficulties to predict high clay content values but the smoothing effect is more notorious with kriging (overestimating lower values and underestimating higher values) while cokriging represents the spatial variation at different locations with better accuracy and a higher correlation concordance coefficient. Luca et al. (2007) also observed better prediction quality of organic matter using cokriging with EC_a compared to kriging, and similar quality to simple kriging with varying local means, when they reduced the sample set of organic matter observations.

Table 2.3. Bias and prediction error of clay content (%) for unused samples in each scenario. ME: mean error, RMSE: Root mean squared error (RMSE), RSR: RMSE-observation standard deviation ratio. EC_{as} was used as secondary variable for cokriging.

	Kriging sc. 2	Kriging sc. 3	Kriging sc. 4	Kriging sc. 5
Predicted points	48	48	72	84
ME (%)	-0.16	1.49	0.31	0.10
RMSE (%)	4.35*	4.66*	4.05*	4.12*
RSR	0.87	0.88	0.85	0.89
	Cokriging sc. 2	Cokriging sc. 3	Cokriging sc. 4	Cokriging sc. 5
Predicted points	48	48	72	84
ME (%)	-0.22	0.65	0.02	-0.09
RMSE (%)	3.33*	3.55*	3.37*	3.16*
RSR	0.67	0.67	0.71	0.69

*Significant differences (P<0.05) between kriging and cokriging for each scenario.

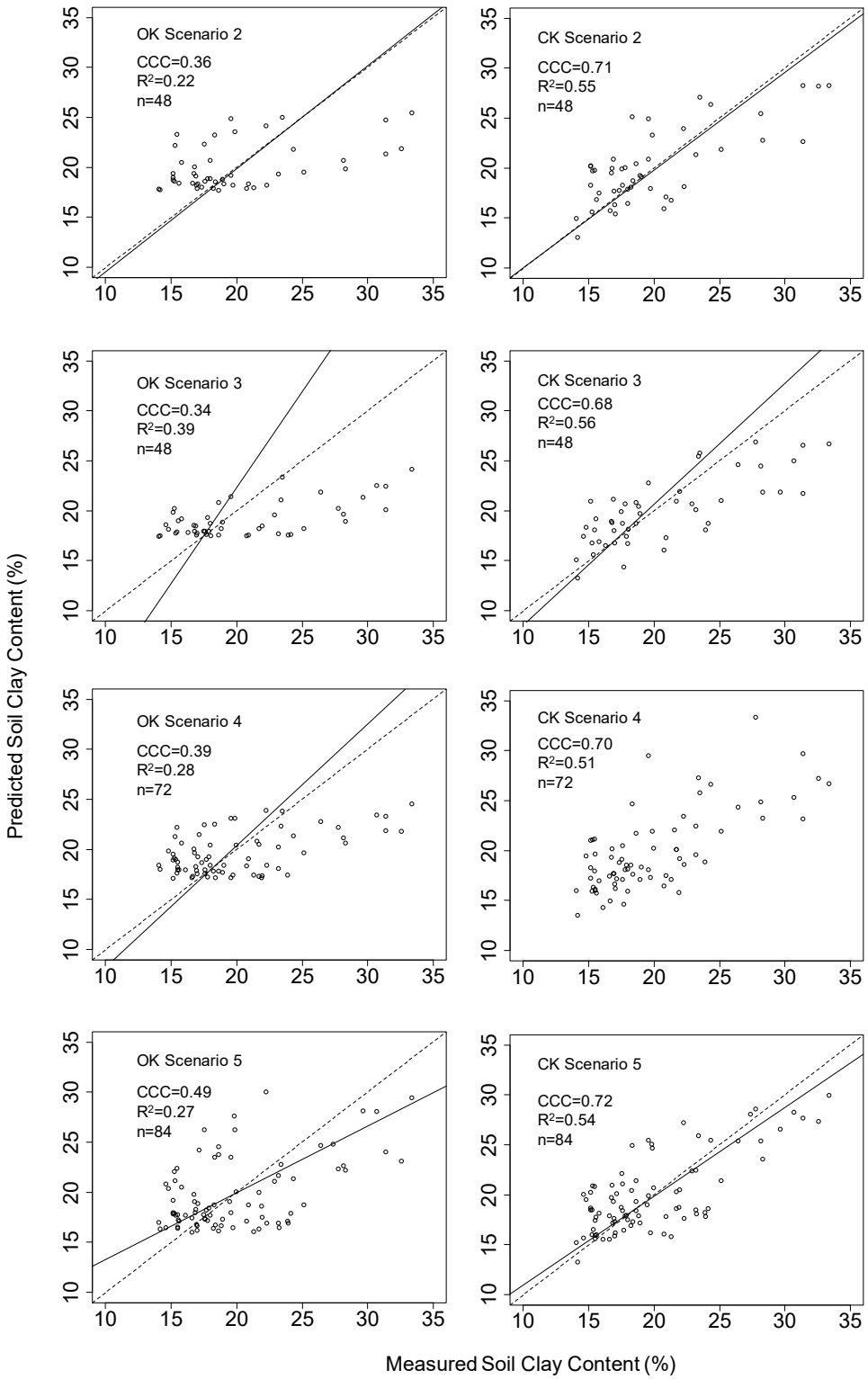

Figure 2.10. 1:1 plots of predicted and measured values. CCC: Lin's concordance correlation coefficient. Dashed line shows the concordance line and solid line shows the linear model.

A validation using an independent data set (Figure 2.1) is presented in Table 2.4. In all cases the RMSE was significantly lower ($P < 0.05$) for cokriging as compared to kriging. In Table 2.5 and Figure 2.11, we observe the results of combining predictions from LOOCV and unused samples to compare the 96 predictions in all scenarios. All cokriging scenarios revealed values for RMSE significantly lower ($P < 0.05$) than kriging scenarios while non-significantly differing among them. The Taylor diagram (Figure 2.11) is a representation of different parameters (RMSE, standard deviation of the reference and predicted values, and correlation between the predicted and reference values) that are being considered simultaneously to compare models against a reference value. In this case, the measured data are the reference. The better the prediction the closer are the parameters to the reference value. This figure shows that the cokriging scenarios are closer to the measured data than kriging scenarios indicated by a smaller RMSE. All models result in lower values of standard deviation compared to measured data, the latter being represented by the quarter of a circle at STD = 4.74. However, these differences are more notorious when using ordinary kriging whereas STD of cokriged values came closer to STD of measured values. Although we could expect that the model with best performance was the one with a large number of measured values included (cokriging scenario 1), the other cokriging models are closer to its predictions. On the other hand, considering our different validations, when using 48 samples the arrangement in scenario 2 seems to be better than the one used in scenario 3 based on a larger STD of the former one while both result in similar magnitudes of correlation and RMSE. The difference is that in scenario 2 the shortest lag distance is larger (70 m) but more data pairs are available in the next closest lags. Our results furthermore suggest the potential to develop clay maps with reduced soil

sampling effort as long as it is accompanied by apparent electrical conductivity measurements. Based on the Taylor diagram, even the ordinary kriging scenario with the highest sampling density was not as good as the lowest sampling density cokriging scenario. This example could be applied and the results verified in fields with similar and differing soils and geographical conditions.

Table 2.4. Bias and prediction error of clay content (%) using an independent validation data set for which locations are shown in Figure 1. ME: mean error, RMSE: Root mean squared error (RMSE), RSR: RMSE-observation standard deviation ratio. EC_{as} was used as secondary variable for cokriging.

	Kriging sc. 2	Kriging sc. 3	Kriging sc. 4	Kriging sc. 5
Predicted points	21	21	21	21
ME (%)	-0.38	-1.01	-0.46	-0.39
RMSE (%)	4.35*	4.88*	4.83*	4.66*
RSR	0.77	0.86	0.85	0.82
	Cokriging sc. 2	Cokriging sc. 3	Cokriging sc. 4	Cokriging sc. 5
Predicted points	21	21	21	21
ME (%)	0.02	-0.33	-0.20	-0.73
RMSE (%)	3.23*	3.55*	3.55*	4.10*
RSR	0.57	0.63	0.63	0.72

*Significant differences (P<0.05) between kriging and cokriging for each scenario.

Table 2.5. Bias and prediction error of clay content (%) of samples combining validation from LOOCV and unused samples in each scenario. ME: mean error, RMSE: Root mean squared error (RMSE), RSR: RMSE-observation standard deviation ratio. EC_{as} was used as secondary variable for cokriging.

	Kriging sc. 1	Kriging sc. 2	Kriging sc. 3	Kriging sc. 4	Kriging sc. 5
Predicted points	96	96	96	96	96
ME (%)	0.04	0.05	-0.78	-0.26	-0.07
RMSE (%)	4.08b	4..10b	4.26b	4.16b	4.14b
RSR	0.86	0.87	0.90	0.88	0.87
	Cokriging sc. 1	Cokriging sc. 2	Cokriging sc. 3	Cokriging sc. 4	Cokriging sc. 5
Predicted points	96	96	96	96	96
ME (%)	0.12	0.06	-0.37	-0.06	0.11
RMSE (%)	3.16a	3.24a	3.32a	3.34a	3.34a
RSR	0.67	0.68	0.70	0.70	0.70

*different letters indicate significant differences (P<0.05) between scenarios.

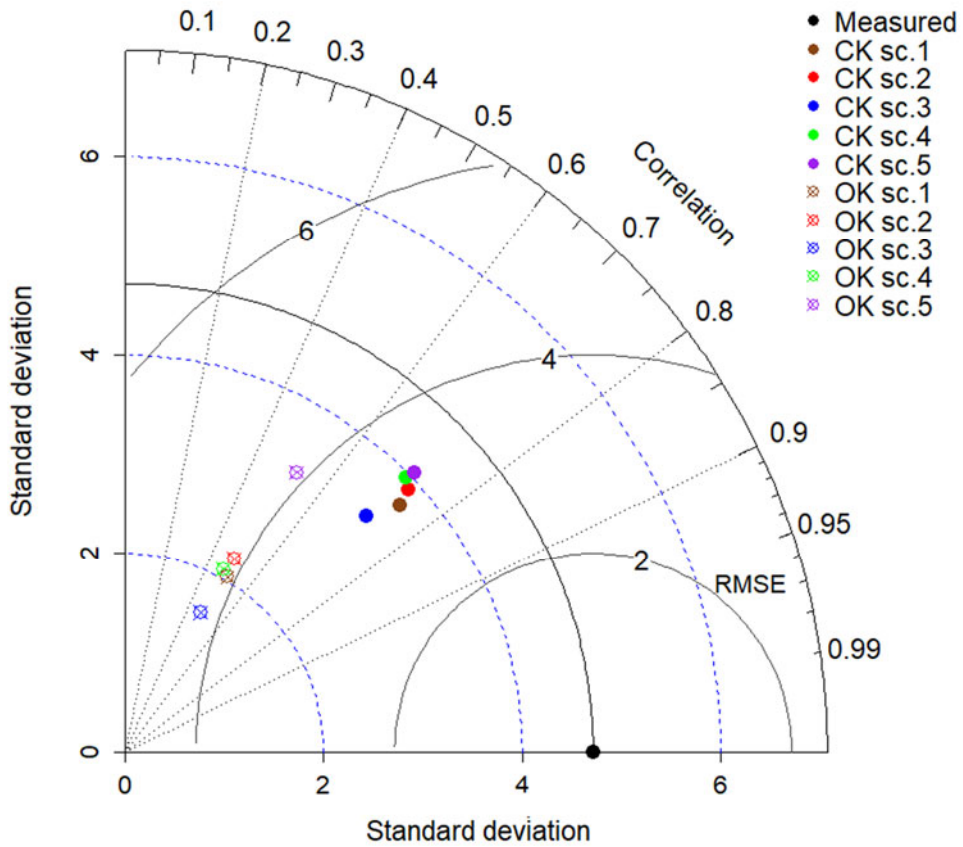

Figure 2.11. Taylor diagram comparing predictions of scenarios 1-5 by using predictions from LOOCV and unused samples at each scenario. The black arc is representing the measured standard deviation

2.3.5 Utilization of EC_a and cokriging

Several studies have shown advantages of using cokriging or other methods that incorporate a secondary variable over ordinary kriging, but without changing the sampling distances of the primary variable. Mueller and Pierce (2003) presented examples of changing grid distance (30 m, 60 m and 100 m) to predict organic carbon by ordinary kriging, cokriging and kriging with external drift. They found small differences in the precision between methods with a 30 m grid, but the methods that include a secondary variable improved the estimation at larger sampling distances. By developing scenarios with a reduced number of samples of the primary variable, we can observe changes in the

estimation, and determine whether we can reduce the number of samples and still obtain a representative map where our estimations shows good accuracy. Although it is always preferred to have the largest number of samples possible, our study has demonstrated that the lower clay sampling density (equivalent to 0.5 samples ha^{-1}) when combined with EC_a has produced satisfactory results. This sampling density is certainly realistic to be used on farms at the field scale.

In general, when we reduce the number of samples it becomes difficult to fit a suitable model for both the semivariogram of the first variable and the cross semivariogram, but with the use of a pseudo cross variograms one can rely more on secondary data. Lark (2002) mentioned that pseudo cross variograms may be used when there is not enough data to calculate the classic cross semivariogram. Otherwise, the cross semivariogram should be preferred. In general, the pseudo crossvariogram is a valid method when none or only few data is available for both variables at the same location or depth (Zhang et al., 1997).

This systematic study proves the usefulness of EC_a to estimate surface layer soil clay content. However, we have to bear in mind that the relationship between soil clay content and EC varies with different soil conditions. The EC_a map by itself represents spatial differences of many different processes occurring in the field (Corwin and Scudiero, 2016). McCutcheon et al. (2006) observed a change from significant to non-significant correlation between clay content and EC_a at different dates in a dryland. Moreover, lack of correlation between field measurements can always occur if one or both sets of data do not strongly vary.

Regarding the time when to measure EC_a, we agree to Corwin's and Scudiero's (2016) recommendation to choose a time for EC_a mapping when the soil is still moist enough to have good contact with the coulters, but not too wet to cause structural damage, compaction and smearing at the soil surface. Whether or not, such an EC data set can efficiently be used in a coregionalization procedure with clay content depends on the resulting spatial variability pattern, and the spatial variability structure. If no common spatial variability structure for clay and EC can be identified, and if there is no well-defined cross semivariogram, then this procedure becomes obsolete. Another consideration is the number of transects that we use to measure EC_a. More transects will generate more data but it involves an increase in time and cost. Triantafilis et al. (2001) have studied the effect of changing transects distance using an EMI sensor to predict clay content. As we expected, the shortest transect distance (24 m) presented the best performance, but when increasing the transect distance it still produced satisfactory results with a quality, that is preferable to results based on univariate kriging of clay content. In addition, obtaining an EC data set can be considered a one-time measurement if conducted under appropriate soil conditions.

2.4 Conclusions

Spatial variation in clay content was identified at the field scale. Estimation of surface clay content through cokriging with EC_{as} as secondary variable has superior quality over ordinary kriging, providing a high resolution map of clay content variation in the field. The use of a pseudo cross variograms for cokriging proves to be useful for small numbers of clay content observation points.

Clay maps derived from cokriging maintained a satisfactory precision even when the number of textural sampling points was reduced because the EC_a data density was effective. The results suggest the potential of combining a reduced number of clay content samples (0.5 point ha^{-1}), that is feasible and realistic for on-farm conditions. Considering the temporal variability of EC_a, this variable should be utilized when soil conditions are appropriate and the spatial relationship with the primary variable is evident.

Copyright © Javier Reyes 2018

Chapter 3 Delineating site-specific management zones and evaluating soil water temporal dynamics in a farmer's field in Kentucky

3.1 Introduction

Understanding and managing soil and crop yield variability remains a long-standing challenge. In agroecosystems and natural systems, soil properties such as clay content, pH, soil organic matter content, nutrient levels and profile depth can vary drastically even within the same field (Downes and Beckwith, 1951; Beckett and Webster, 1971; Koestel et al., 2013). Precision agriculture is an approach in agroecosystem management to distribute resources site-specifically according to this variability and associated varying input demands. The foundation of this concept is the spatial and temporal characterization of soil and crop processes through field measurements taken directly or remotely for maximizing local yield while minimizing environmental risk. Most of the research on management zone delineation has been focused on fertilization, particularly on nitrogen application (Kitchen et al., 2003; Ruffo et al., 2006; Peralta et al., 2015). In other studies, weeds (Peña et al., 2013) and irrigation (Landrum et al., 2014, Haghverdi et al., 2016) were managed site-specifically.

The application of precision agriculture has increased with advances in remote (largely distanced from the object by using platforms such as towers, vehicles, aircrafts, or satellites) and proximal (in direct contact with the object or close to it) sensing tools (Vereecken et al., 2016). Nowadays, georeferenced data describing spatial and temporal variability of soil and crop state variables and related processes can be obtained for farmers'

fields at high resolution. Yield maps, digital elevation models (DEM), maps of normalized difference vegetation index (NDVI) or other canopy reflectance indices and apparent electrical conductivity (EC_a) are among the most frequently used sources for site-specific management decisions. Yield maps are obtained from yield-monitoring systems installed on combines (Schepers et al., 2004). DEMs can be derived from different sources, including existing soil maps, and at a finer resolution Light Detection And Ranging (LiDAR) (James et al., 2006). Many examples exist for utilizing EC_a or electrical resistivity to define management zones based on their relationship with other important state variables, such as soil clay content (Corwin and Lesch, 2003; Sudduth et al., 2003; Schepers et al., 2004; Moral et al., 2010). NDVI can be obtained from different sources, such as proximal sensing (e.g. Greenseeker; Walsh et al., 2012), or remote sensing (e.g. LANDSAT, MODIS; Brown et al., 2006). NDVI is a canopy reflectance index that is strongly related to crop status and fitness. Because it reflects nitrogen demand over substantial parts of the growing period of many agricultural crops, NDVI has been frequently studied as a tool in site-specific nitrogen application decisions (Raun et al., 2002). Informative data can be obtained through remote and proximal sensing approaches in a much cheaper way and higher spatial and in some cases temporal resolution than with collecting soil and plant samples in cumbersome field campaigns at several times during the growing season. It remains unclear, however, what soil and crop information obtained through remote or proximal sensing, including previous years' yield maps, are helpful to understand present year spatial variability of soil and crop stand and to manage the field site-specifically in accordance with previous year information.

The challenge persists to manage field soils site-specifically to maximize biomass production efficiency and environmental benefits. Dividing a field into management zones is a promising strategy to overcome this challenge. Management zones are delineated by separating the field in different areas. Some of the areas have different while other areas have the same response behavior (Kitchen et al., 2005). Whether areas themselves can be considered to have homogeneous characteristics depends on the situation and is not well known yet. Whether or not an area is considered homogeneous depends on the variable selected. For example, the delineation of management zones can be based on crop yield maps. The spatial variability of crop yield has been reported to be related with variables such as soil organic matter content (Mann et al., 2002), clay content (Tremblay et al., 2012), and NDVI (Teal et al., 2006). However, spatial yield patterns vary among different years because different processes during the growing season influence them (Schepers et al., 2004). Especially different weather conditions in different years can cause different spatial yield variability patterns even for the same crop growing in the same field. The key processes and their spatial effect may vary by season making the spatial biomass production and yield difficult to predict between different seasons. Electrical conductivity also varies in space and time, being strongly affected by soil moisture and salinity for instance of sodic soils, although EC can be used to predict other variables when a strong relationship exists (Corwin and Scudiero, 2016). Moreover, EC data behave spatially structured and can be combined in co-regionalization with other variables that remain stable in time such as topography, soil depth and clay content.

The delineation of management zones based on cluster analysis has been proven to be effective to combine impacts of different variables on the outcome (Johnson et al., 2003; Li et al., 2007; Vitharana et al., 2008; Cohen et al., 2012; Peralta et al., 2013). The analysis is centered on finding dissimilarities between observations by using a clustering algorithm through partitioning or hierarchical methods (Kaufman and Rousseeuw, 1990). These dissimilarities can be caused by different response behavior between a target variable and various underlying processes. In a partitioning method, k clusters (data organized in groups) are constructed and data are classified into k groups. Based on a selected index, the optimal number of clusters within a particular domain can be identified. For example, to work on site specific irrigation management (e.g., Sadler et al., 2005) the right amount of water should be applied at the right time but also considering locations and their specific behavior in the field. Spatial differences in topography and soil physical and chemical properties can be found within the same field. Thus, water infiltration and soil water movement also vary spatially when irrigation is applied. Over decades, examples found in the literature (Nielsen et al., 1973; Wendroth et al., 1999) illustrate the spatial and temporal variability of soil water at the field scale. Considering the spatial and temporal variability of soil water at field scale, it may be environmentally and agronomically advantageous to supply irrigation water at variable rates according to field soil water characteristics and the resulting temporal soil water dynamics. Therefore, variables that influence or correlate with soil hydraulic properties and soil water status and dynamics have to be considered in the delineation of areas. Dissimilar soil water temporal variation scales can be expected for different soil properties in different areas of the field. To analyze time-variable behavior at different zones, a wavelet analysis (Grinsted et al., 2004) is a worthy strategy, because it

decomposes a time series data in frequency and time simultaneously allowing to observe periodic variations at different scales and times. In addition, wavelet coherence analyzes and identifies the correlation of pairs of time series data at different time scales. Studies of spatial and temporal changes in soil water using a wavelet analysis are presented by Biswas and Si (2011), Biswas (2014), and Yang et al. (2016).

The challenge of using numerical solutions to delineate management zones is to provide results that are appropriate to be used under farm conditions. Regarding the variable selection, it is essential to consider whether a specific variable represents the field variation of essential processes that underlies site-specific management or what other, indirect variable could provide similar information for site-specific management, while its collection is more affordable than another more directly related variable that may be cumbersome to measure. The objective of this study was to apply easily obtainable data using proximal and remote sensing tools to define management zones in a farmer's field located in Western Kentucky, a typical crop production region in the southeastern United States. Variables should be identified based on different approaches and zones should be delineated by using fuzzy and hard clustering algorithms. Different approaches should be examined to evaluate whether or not they would result in different delineations. A second objective was to evaluate differences or similarities in process behavior among delineated management zones by comparing spatial differences in corn yield and in temporal dynamics of soil moisture.

3.2 Material and methods

3.2.1 Site description and data sampling

The study was conducted at Hillview Farms in Princeton KY, Caldwell County (37° 1'58.02"N, 87°51'33.06"W, 142 m asl). According to the Köppen system, the climate is classified as humid subtropical. The annual precipitation is around 1312 mm (US climate data, 2017), and annual mean temperature is 15 °C. The maximum and minimum mean temperatures occur in June and January, respectively.

The soil in this field belongs mainly to the Crider series (Typic Paleudalfs), while some areas are classified as Nolin series (Dystric Fluventic Eutrudepts) (Soil Survey Staff, 1999). In both cases, the soil texture is classified as silt loam in the surface layer. The experiment covers an area of approximately 27 ha. The field was cultivated with corn (*Zea mays* L.) during the 2014, 2015 and 2017 seasons.

Soil texture at 0-20 cm and 20-40 cm depth and chemical properties at 0-15 cm depth were sampled across a grid of 96 points with a regular distance of 50 m (Figure 3.1). Sand (0.05-2 mm) was separated by sieving, while medium (0.005-0.020 mm) and fine silt (0.002-0.005 mm) and clay (< 0.002 mm) were measured with the pipette method (Gee and Or, 2002) and coarse silt (0.020-0.050 mm) was calculated as residual. Soil organic matter and total nitrogen were determined by LECO combustion, extractable P, K, Ca, Mg, and Zn were measured by Mehlich III extraction. For pH determination, a glass electrode was used in 1:1 soil:water and Sikora buffer for Buffer pH (Jones, 2000). Apparent electrical conductivity (EC_a) was measured in the spring of April 2015 using a Veris 3150 (Veris

Technologies, 2017). The electrodes are configured with a Wenner array and measurements that integrate EC over a shallow depth (about 0-30 cm) and a deep depth (about 0-90 cm) were obtained, defined as EC_{as} and EC_{ad} respectively.

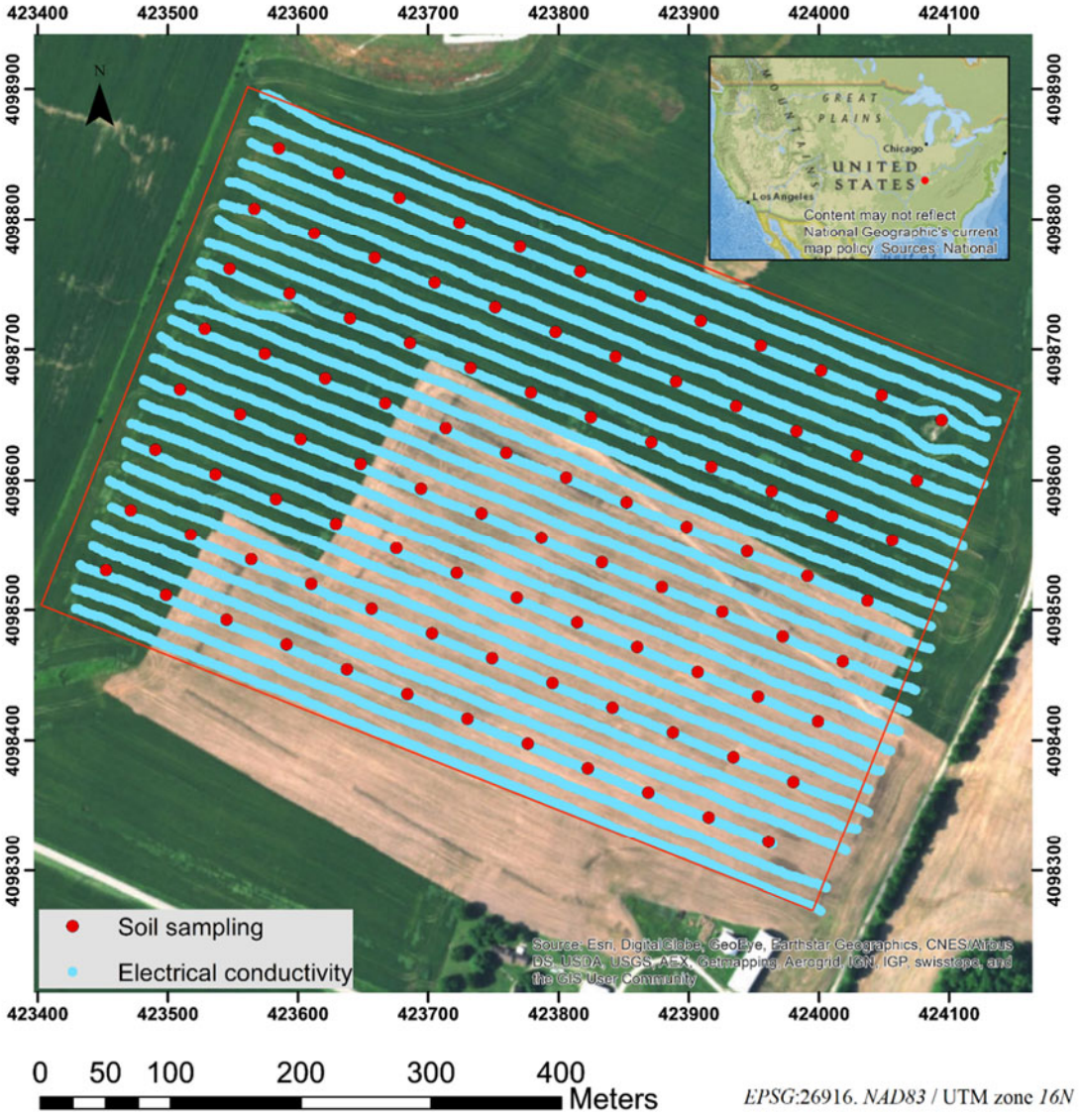

Figure 3.1. Study area and sampling locations for soil texture and chemical properties as well as for electrical conductivity.

A digital elevation model (DEM) was obtained at 1.5 m resolution from LiDAR, provided by the Kentucky Division of Geographic Information. From the DEM, slope and two

widely used topographic indices, i.e., the topographic wetness index (TWI) and the stream power index (SPI) (Moore et al., 1993) were derived. These two indices were computed by using SAGA GIS (Conrad et al., 2015). TWI and SPI were obtained with the following equations:

$$TWI = \ln \frac{A_s}{\tan \beta} \qquad (eq. 3.1)$$

$$SPI = A_s \times \tan \beta \qquad (eq. 3.2)$$

Where A_s is the contributing catchment area (m^2 m^{-1}) and β represents the steepest slope angle (degrees). The spatial pattern of TWI depicts areas that show local water accumulation and therefore high soil water saturation, while SPI indicates the potential erosional power as a result from the combined effect of slope and upstream flow.

Normalized Difference Vegetation Index (NDVI) was obtained from Landsat 8 Operational Land Imager (Level 2 product (SR), U.S. Geological Survey 2017) and was collected during the growing seasons of corn in 2014, 2015 and 2017. NDVI was derived from:

$$NDVI = \frac{NIR - RED}{NIR + RED} \qquad (eq. 3.3)$$

where NIR is the near infrared band (0.85 - 0.88 mm) and RED represents the red band (0.64 - 0.67 mm). High NDVI values are associated with high greenness of vegetation.

Therefore, NDVI indicates crop vigor and crop nitrogen status (Brown et al., 2006). Landsat 8 images are available at a spatial resolution of 30 x 30 m. Based on the image quality and representativeness of different growth stages, images from May 2014, August 2014 and June 2015 were selected.

3.2.2 Data analysis

The statistical analysis was conducted in the R environment (R core team, 2017) and the maps for each variable were produced using RASTER (Hijmans, 2016) and LATTICE packages (Sarkar, 2008). The analysis included measures of central tendency and dispersion, and Pearson correlation using the CORRPLOT package (Wei and Simko, 2016). Kriging and cokriging analysis as methods of interpolation were implemented to create maps by using GSTAT (Pebesma, 2004) and GEOR (Ribeiro and Diggle, 2016) packages. Variables were log-transformed if necessary or underwent Box-Cox transformation. Semivariogram and cross semivariogram models were fitted and applied for the interpolation. For obtaining maps at a fine resolution in a reasonable computing time, all variables were interpolated in a 4-m-grid. For soil texture, a cokriging analysis was previously performed by combining soil clay content with EC_{as} (Reyes et al., 2018). Detailed steps of kriging and cokriging procedures are explained in Nielsen and Wendroth (2003).

Principal component Analysis (PCA) using the FACTOMINER package (Le et al., 2008), was implemented to group the variables into statistical factors and to select key variables that explained variance in different dimensions. The sample size corresponds to the 96 soil

sampling points and the intersected NDVI and topographic attributes for the corresponding locations. PCA is recommended to reduce the dimensionality of multivariate data and to work with highly correlated data (Husson et al., 2010). The Bartlett test of Sphericity and the Kaiser-Meyer-Olkin test were performed to verify the adequacy of the data to be used in PCA. The obtained value was $P < 0.01$ for the Bartlett test of Sphericity and 0.75 for the Kaiser-Meyer-Olkin test suggesting that these data were applicable in PCA.

To delineate management zones, two cluster analysis methods using the CLUSTER package (Maechler et al., 2017) were selected, i.e., a Fuzzy Analysis Clustering (FANNY) and a Clustering for Large Applications (CLARA). FANNY is an unsupervised soft clustering method focused on reducing the objective function defined as:

$$\sum_{v=1}^{k} \frac{\sum_{i,j}^{n} u_{(i,v)}^{r} u_{(j,v)}^{r} d(i,j)}{2 \sum_{j}^{n} u_{(j,v)}^{r}} \quad (eq\ 3.4)$$

where n is the number of observations, k is the number of clusters, r is the membership exponent and $d(i,j)$ is the dissimilarity between observations i and j.

Each data point has a membership coefficient between 0 and 1 for each cluster and it is assigned to the cluster with higher membership coefficients. A membership exponent of 2 could induce a complete fuzziness while values close to 1 reduce the fuzziness. For this study a conventional value of 1.35 (Odeh et al., 1992) was used and Euclidean distance.

CLARA is a hard clustering method. It is based on the same algorithm as the partitioning around medoid method (PAM) described in Kaufman and Rousseeuw (1990). However, in CLARA the data are divided in subsamples of fixed size. Then each subsample is partitioned in k clusters. The difference between the hard cluster and the fuzzy cluster is that the data are entirely assigned to one cluster in the hard cluster analysis; consequently, it is not possible to observe degrees of membership.

To apply the cluster analysis, the attributes to be included have to be selected. For this purpose, all variables were standardized and three approaches were selected to be applied in the interpolated maps:

a) Using maps of retained principal component factor scores. These factors are obtained by using the component score coefficient matrix and standardized variables (Yao et al., 2014). The retained components were selected according to the percentage of variance explained.
b) Selecting a key variable of each of the retained principal components. The selection was based on the factor loading scores obtained for each variable.
c) Combining variables from field measurements with easily obtainable remote sensing data. The selection of these variables was based on factor loadings with high contribution in the first component.

The Silhouette width (Kaufman and Rousseeuw, 1990) was used to evaluate the most appropriate number of clusters. This method was chosen because it can be applied to both hard and soft clustering and is defined as:

$$s(i) = \frac{b(i) - a(i)}{max\{a(i), b(i)\}} \quad (eq. 3.5)$$

where *a(i)* is the average dissimilarity between *i* and all other points of the cluster to which *i* belongs. For all other clusters *C, d(i,C)* is the average dissimilarity of *i* to all observations of C, then *b(i)* is the minimum of *d(i,C)*, which can be seen as the dissimilarity between *i* and its "neighbor" cluster. The individual Silhouette and the average value for each cluster is obtained. The values are in the range between -1 and 1. Negative values indicate that the data was assonated to the wrong cluster while values closer to 1 indicate a very well clustered data. Consequently, the best number of divisions will be the number of clusters with the largest average silhouette width.

To study the representativity of the management zones obtained, dissimilarities between clusters were quantified by observing two variables: crop yield and temporal dynamics of soil water tension. To evaluate yield differences among delineated areas, corn grain yield from the years 2014, 2015 and 2017 were used. ANOVA was performed to observe significant differences ($p < 0.05$) in corn yield. HDS Tukey test was used as *post-hoc multiple comparison.*

Temporal dynamics of soil water tension at different locations were observed as well. These measurements were made during the spring season of 2016 using watermarks (Fisher

and Gould, 2012) connected to antennas at 4 locations for each delineated area. Data were collected each hour, and sensors were located at three depths: 20 cm, 40 cm, and 60 cm. The method of analysis was the wavelet transform (e.g., Wendroth et al., 2010) by using the BIWAVELET package (Gouhier et al., 2016). The wavelet transform is a technique that can be used to analyze time series to identify cyclic variations at different frequencies or scales. This analysis includes a continuous wavelet transform for individual variables and a bivariate analysis by performing a wavelet coherence analysis (Grinsted et al., 2004; Yang et al., 2016). The data had to be transformed with a wavelet function. In this study a Morlet wavelet was chosen as mother wavelet, which is defined as:

$$\psi_0(\eta) = \pi^{1/4} e^{i\omega_0 \eta}\, e^{-\frac{1}{2}\eta^2} \qquad (eq. 3.6)$$

where ω_0 is the dimensionless frequency and η is the dimensionless time. The Morlet wavelet was selected because it provides a good resolution for scale and frequency. When ω_0=6, the Fourier period is almost identical to the scale. The continuous wavelet transform with uniform time steps (δt) at different scales (s) of a data series xn is defined as:

$$W_n^X(s) = \sqrt{\frac{\delta t}{s}} \sum_{n'=1}^{N} xn' \psi_0 \left[(n' - n)\, \frac{\delta t}{s}\right] \qquad (eq. 3.7)$$

The wavelet coherence can be considered as a correlation coefficient for common frequencies and locations. It is defined as:

$$R_n^2(s) = \frac{|S(s^{-1}) W_n^{XY}(s))|^2}{S(s^{-1})|W_n^X(s)|^2) \times S(s^{-1})|W_n^Y(s)|^2)} \qquad (eq. 3.8)$$

where S is a smoothing operator and W_n^{XY} represents the cross-wavelet of the individual wavelet transforms $W_n^X(s)$ and $W_n^Y(s)$ calculated as $W^{XY}=W^X*W^Y$, where the asterisk denotes complex conjugation.

A significance test ($p < 0.05$) was performed, contrasting the null hypothesis that the signal is generated by a stationary process with a given background power spectrum (Grinsted et al., 2004). In the BIWAVELET package, this test is available only for the Morlet function.

3.3 Results and Discussion

The descriptive statistics of all measured variables are summarized in Table 3.1. In general, the average values for soil properties are similar to what is expected for fields located in Kentucky (Karathanasis, 1987; Landrum et al., 2014). The silt fraction is predominant at both soil depths, but an increase in clay content is observed in the second layer. Some variables present a high coefficient of variation such as EC_{as} and other chemical properties (P, K, Mg). On the other hand, the variables derived from topography (slope, TWI, SPI) also show a high coefficient of variation. The Pearson correlation (Figure 3.2) displays some significant relationships ($p < 0.01$): OM and N show the highest correlation. Clay content at both depths is strongly correlated with EC_{as}, EC_{ad}, slope and Mg. NDVI obtained in June has significant correlations with soil properties, especially silt content in the surface layer.

Table 3.1. Descriptive statistics of all measured variables. Chemical properties correspond to the surface layer (0-15 cm). Sample size corresponds to the 96 soil samples and the intersected NDVI and topographic attributes for the corresponding locations.

Parameter	OM (%)	N (%)	pH	P (kg ha^{-1})	K (kg ha^{-1})	Ca (kg ha^{-1})	Mg (kg ha^{-1})	Zn (kg ha^{-1})	Clay 0-20 cm (%)	Silt 0-20 cm (%)
Mean	1.6	0.092	5.4	104	334	3568	164	4.1	19.8	77.9
SD	0.3	0.002	0.6	75	103	1049	70	1.4	4.6	5.7
Skewness	0.1	0.019	0.1	0.7	0.8	0.9	1.7	0.3	1.1	-1.9
Kurtosis	-0.3	-0.597	-0.5	-0.5	0.0	0.7	3.0	-0.3	0.7	4.6
CV(%)	19.2	17.6	11.1	72.4	30.7	29.4	42.8	34.6	23.0	7.3

Parameter	Clay 20-40 cm (%)	Silt 20-40 cm (%)	EC_{as} (mS m^{-1})	EC_{ad} (mS m^{-1})	Slope (%)	TWI	SPI	NDVI Aug-14	NDVI Jun-15	NDVI May-14
Mean	25.6	71.3	0.9	14.8	4.6	5.8	-1.8	0.55	0.83	0.27
Stdev	5.7	6.6	0.6	3.9	1.3	1.6	0.9	0.02	0.03	0.01
Skewness	-0.3	-0.5	0.9	0.9	0.7	0.9	0.4	-1.97	-1.33	0.36
Kurtosis	-0.8	0.2	0.1	2.4	0.2	0.3	-0.9	6.02	3.68	-0.36
CV(%)	22.3	9.3	64.1	26.3	27.5	28.1	-50.5	3.15	4.19	2.76

OM: organic matter, TWI: topographic wetness index, SPI: stream power index, SD: standard deviation, CV: coefficient of variation.

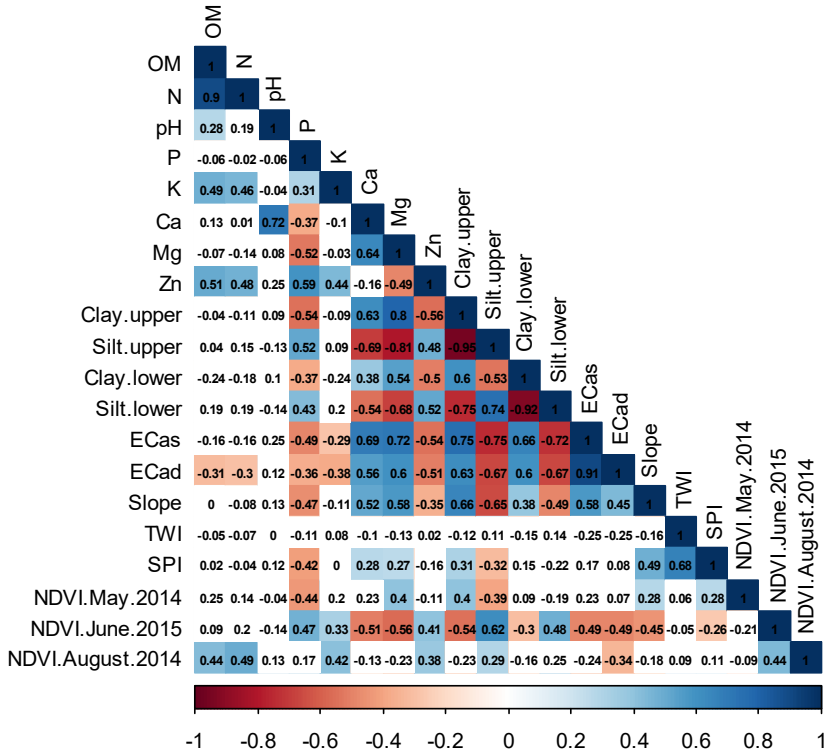

Figure 3.2. Pearson correlation between measured variables. Colored cells represent significant correlation ($p < 0.01$).

3.3.1 Geostatistical interpolation

Maps for each variable were interpolated using ordinary kriging or cokriging in a 4-m-grid. In Figure 3, maps of spatial distributions for selected variables are depicted: clay content 0-20 cm, 20-40 cm, NDVI June 2015, soil organic matter, total soil nitrogen, extractable P, slope, TWI, and EC_{as}. Each of these variables reveals high spatial variability across the field. Highest clay content values are observed in the northwest part of the field. Interestingly, this area also shows low NDVI values and a high slope percentage, similar to results reported by Odeh and McBratney (2000). On the other hand, the patterns observed between organic matter (OM) and total N content are analogous but differ from those of other variables (Figure 3.3). Both OM and N present the lowest values in the southeast and some parts of the northwest. A possible explanation for these differences could be the fact that in previous years the farmer had planted Burley tobacco (*Nicotiana tabacum*) in the southeast (this area can be observed in Figure 1), which corresponds to the area with the highest extractable P content. Tobacco has high nitrogen demand and requires more intensive management than other field crops (MacKown et al., 2000). On the other hand, TWI also reveals a high spatial variability, however, with a pattern different from those of other variables. In general, only small parts of the field show high TWI values implying the potential to have saturation overland flow (Quinn et al., 1991), therefore runoff can occur in case of substantial precipitation or excessive irrigation. On the other hand, areas with low TWI values will potentially dry up first.

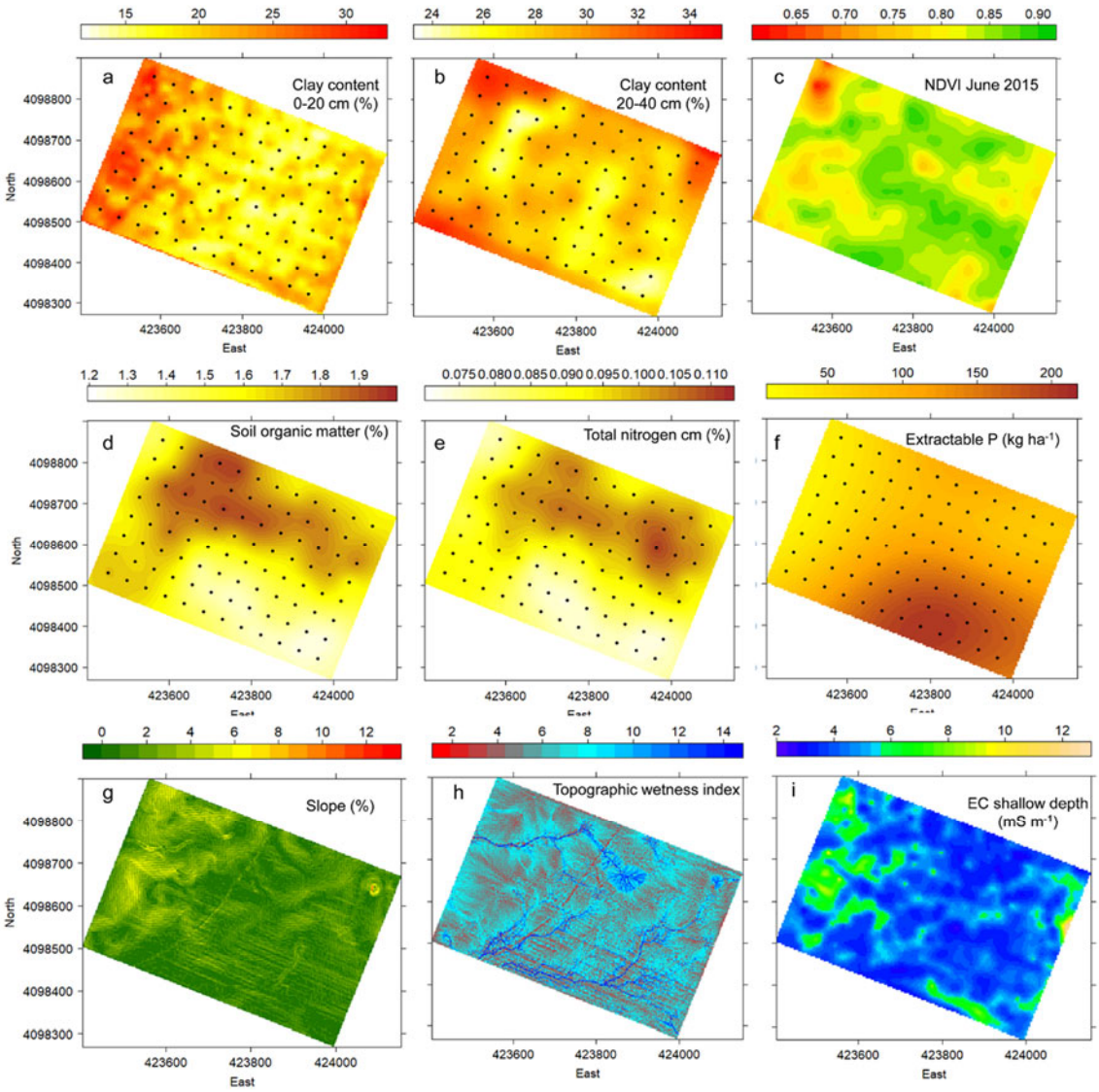

Figure 3.3. Maps of spatial distribution of clay content at 0-20 cm (a), and 20-40 cm (b), NDVI June 2015 (c), organic matter (d), total nitrogen (e), extractable phosphorous (f), slope (g), topographic wetness index (h), and apparent electrical conductivity (i) at a shallow depth (0-30 cm). Black dots represent the soil sampling grid.

3.3.2 Principal components analysis

After performing PCA, three first components were retained that explain 65% of the total variance. The factor loadings for the variables and the three retained components are displayed in Table 3.2. Figure 3.4 presents the factor loadings of the first three components. The factor loadings most associated with the first component, which explains 40 % of the

total variance, were clay and silt at both depths, apparent electrical conductivity (both depths) and slope. OM and total N strongly contributed to the second component which explained 15% of the total variance. In the third component, representing 10 % of the total variance, the highest contributions came from indices related to topography (TWI and SPI). It can also be observed in Figure 4 that clay content is grouped with slope, Mg content, and EC_a. Silt content is grouped with NDVI measured in June 2015 and with P content. These results are consistent with the maps presented in Figure 3.3, where high spatial variability for all variables was evident, however, revealing different patterns. Contributions of the same variable to particular processes and their relationships vary for different fields and soil conditions. For example, the highest factor loadings for the first component were reported for different variables in other studies: pH, slope (Vitharana et al., 2008), and EC_a (Van Meirvenne et al., 2016) in north-west Europe; elevation and soil depth in Argentina (Peralta et al., 2015); organic carbon and available N (Li et al., 2007) in East China. Furthermore, the relationships among variables varied between those studies.

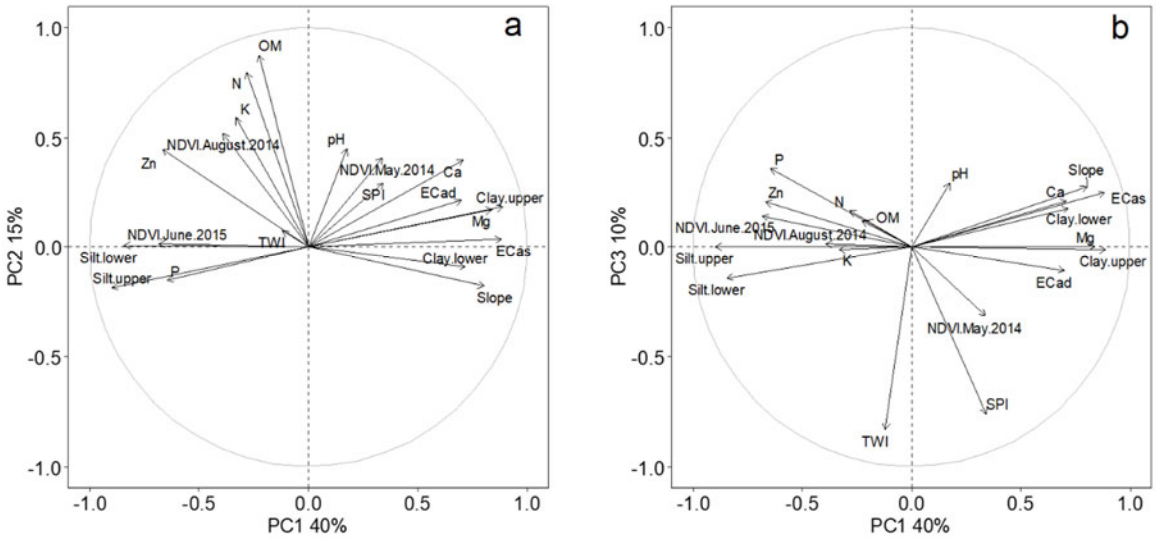

Figure 3.4. Principal component analysis map of variable for: a) PC1vs PC2 and b) PC1 vs PC3.

Table 3.2. Factor loadings of each variable for the first 3 components. In parenthesis is the percentage of explained variance for each component. Chemical properties correspond to the surface layer (0-15 cm).

Variable	PC1 (40 %)	PC2 (15%)	PC3 (10%)
OM	-0.23	0.88	0.12
N	-0.28	0.80	0.17
pH	0.18	0.45	0.29
P	-0.65	-0.15	0.36
K	-0.33	0.59	-0.01
Ca	0.71	0.40	0.21
Mg	0.84	0.17	0.01
Zn	-0.67	0.45	0.21
Clay upper (0-20 cm)	0.89	0.18	-0.01
Silt upper (0-20 cm)	-0.90	-0.19	0.01
Clay lower (20-40 cm)	0.72	-0.09	0.18
Silt lower (20-40 cm)	-0.84	0.01	-0.14
Slope	0.88	0.04	0.25
EC_{as}	0.70	0.21	-0.11
EC_{ad}	0.80	-0.18	0.28
TWI	-0.12	0.07	-0.83
SPI	0.34	0.29	-0.76
NDVI August 2014	-0.39	0.52	0.02
NDVI June 2015	-0.68	0.01	0.14
NDVI May 2014	0.34	0.41	-0.31

OM: soil organic matter content, EC_{as}: apparent electrical conductivity shallow depth, EC_{ad}: apparent electrical conductivity deeper depth, TWI: topographic wetness index, SPI: stream power index.

3.3.3 Potential Management zone delineation

A cluster analysis was established using the criteria described above: a) based on PCA maps of retained components (PC1, PC2 and PC3); b) based on one key variable for each retained component, where Clay at 0-20 cm, OM and TWI were selected; and c) selecting relevant variables for the first component. In c), clay content at two depths in combination with NDVI in June 2015 and slope were chosen. In Figure 3.5, the average silhouette width for a different number of clusters by using FANNY and CLARA is displayed. In both cases, results are similar and the optimal number of divisions is 2 when the analysis is based on criteria a) and b). On the other hand, 3 divisions are optimal for criterion c). According to Kaufman and Rousseeuw (1990), the results found for Maximum Average Silhouette Width can be considered as reasonably structured clusters (in the range of 0.5-0.7).

Therefore, results presented here can be considered appropriate to provide a well-structured division of the field. The resulting cluster zone maps are presented in Figure 3.6. Similarities between the maps based on criteria a) (Figure 3.6a and 3.6b) and b) (Figure 3.6c and 3.6d) by using both cluster methods are obvious. Criterion c) (Figure 3.6e and 3.6f) presents a zone in the northwest part (area 3) that has resemblance with area 2 observed for a) and b). The additional division resulting from criteria in c) can be considered as a transitional zone in the middle part of the field. Nevertheless, all the criteria and methods result alike with respect to the Northwest area having strong dissimilarities with the rest of the field. As the farmer's and our own field observations confirmed, this area is characterized as more eroded and the soils in this area reveal higher clay contents and slopes than the rest of the field. Combining both effects, it is understandable that a soil with high clay content and steep slope, exhibits lower water infiltration and more run-off compared to a soil with only high slope or only high clay content.

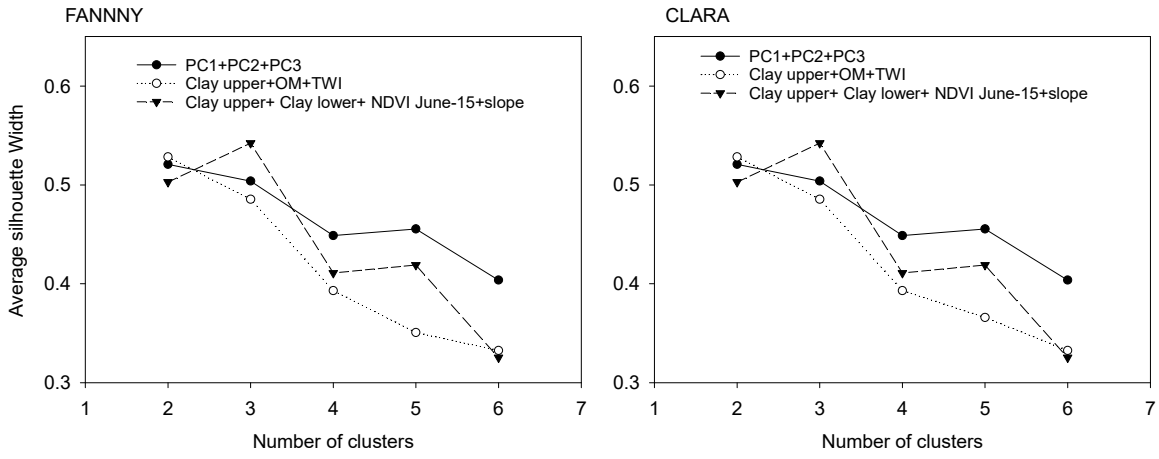

Figure 3.5. Average silhouette width for different number of cluster using FANNY and CLARA.

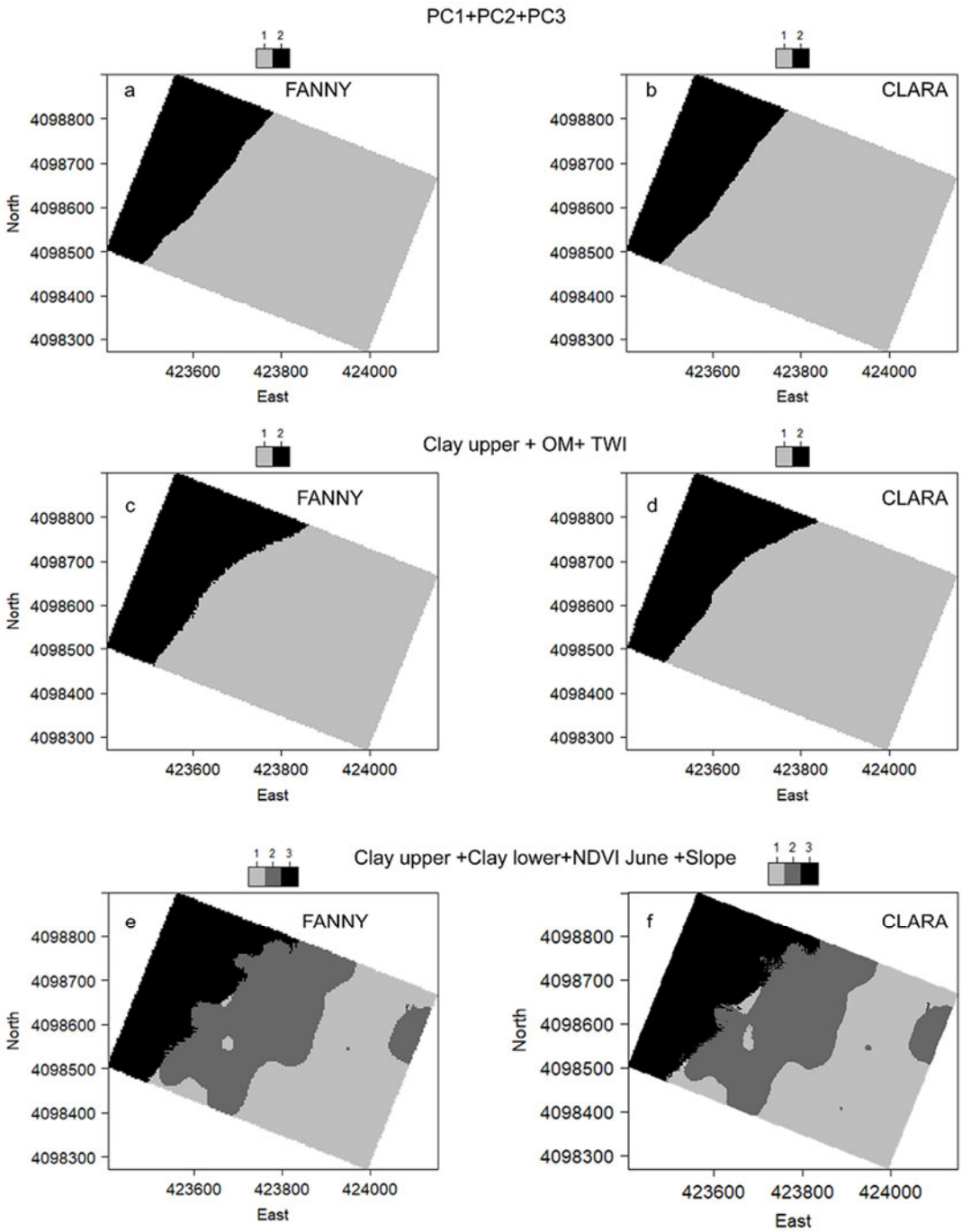

Figure 3.6. Maps of delineated management zones. Based on maps of principal components factor scores by using a) FANNY and b) CLARA; based on Clay content at 0-20 cm, Organic matter content and Topographic wetness index by using c) FANNY and d) CLARA; based on Clay at 0-20 cm and 20-40 cm, NDVI at June 2015, and Slope by using e) FANNY and f) CLARA.

Other studies have demonstrated the capability of using PCA maps for cluster analysis (Li et al., 2007; Yao et al., 2014). Moreover, this implies that either all measured variables involved need to be used or a preselection has to be made using another method (e.g., stepwise regression). On the other hand, the selection of one key variable for each retained component resulted in maps comparable to using all variables, so it could be more appropriate and sufficient to use the concept of choosing key variables as a criterion. Nevertheless, it remains challenging to identify one key variable without any *a priori* evaluation of different variables from a data set. The same criteria can be applied for other fields in case their characteristics are comparable.

In farmers' fields in this part of the south-eastern U.S., differences in local topography, as those observed in the field of this study are typical, and they have a great influence on the spatial variability of soil properties and, consequently, on the spatial variability of crop yield. In Figure 3.7, a cross section of an elevation profile from this experimental field is displayed with a division of the three management zones as based on criterion c). Zones 1 and 2 behave not so different with regard to slope, although zone 2 is higher in clay content (Figure 3.3a-b). On the other hand, zone 3 clearly reveals the steepest convex slope, which tends to cause frequent and more severe runoff and erosion events.

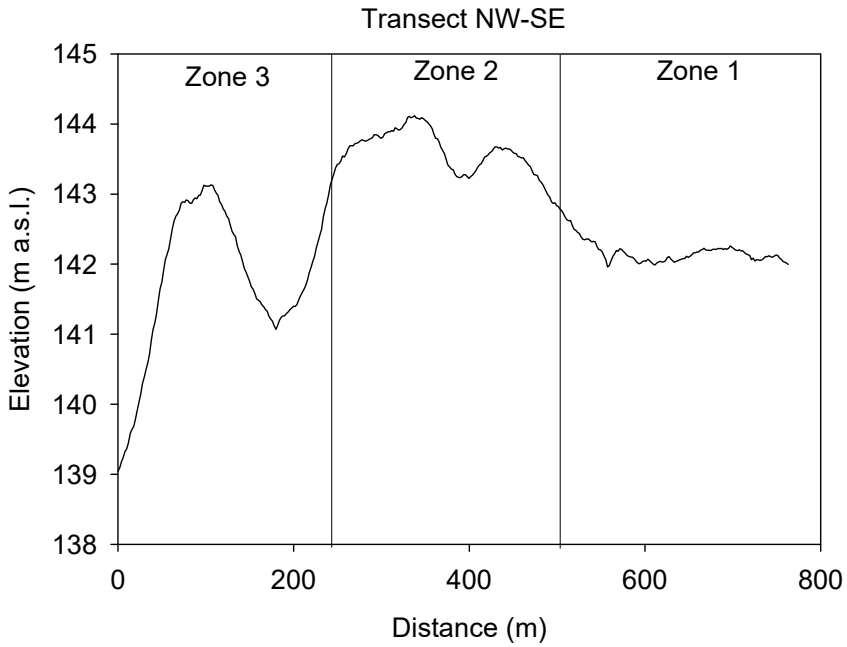

Figure 3.7. Elevation profile along a transect from NW to SE of the field.

In general, many different processes occur in a field at different scales. Some of them are permanently visible, others only temporally. Consequently, even if the desire is to classify the field in different zones, different variables can have some degree of pertinence to another. For this reason, fuzzy cluster analysis is preferred over the hard clustering method for data presented in a continuum. Moreover, the CLARA algorithm is a promising tool to perform a cluster analysis at the field scale with few divisions and using large data sets from high-resolution sources or generated by interpolation. By performing cluster analysis with R, memory limitations can cause a problem with larger datasets, while techniques with reduced memory usage such as CLARA could be more convenient. Nevertheless, free source software to delineate management zones by using clustering analysis is available and has been presented in other studies (Li et al., 2007; Moral et al., 2010).

The delineation of management zones is based on a numerical solution that separates the field according to data dissimilarities. However, the results will not always be suitable for practical use. In Figure 3.8, the result of dividing the field in two areas using the FANNY algorithm only based on EC_{as} as a variable is displayed. EC_a has been proven to be a useful variable for defining management zones (Johnson et al., 2003; Fleming et al., 2004; Moral et al., 2010; Peralta et al., 2013). Based on this map, it may appear difficult to apply a differentiated management in isolated sectors classified as zone 1 or 2 because it would require highly precise variable-rate technology. However, data can be further processed. For example, point data could be spatially aggregated, or combined with data from other relevant variables to perform a clustering. In this study, EC_{as} was not directly applied in the delineation procedure but as ancillary data to produce the clay content maps presented in Figure 3.3i.

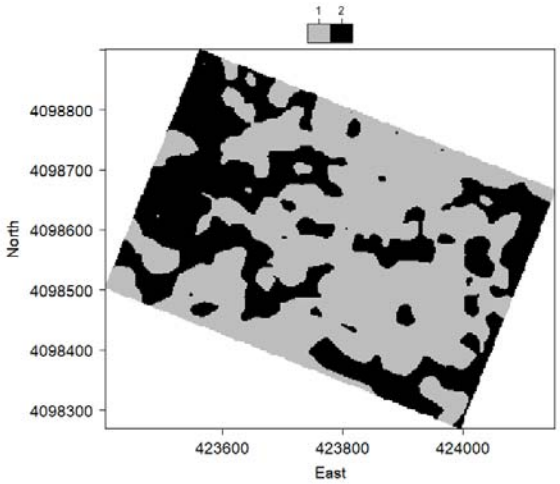

Figure 3.8. Management zones obtained from a FANNY analysis by using apparent electrical conductivity at a shallow depth (0-30 cm).

3.3.4 Evaluating management zones

Table 3.3 provides average corn yields for 2014, 2015 and 2017 at each of the delineated zones presented in Figure 3.6. In all cases, significant differences ($p < 0.05$) were found

when comparing areas. This result indicates that the yield was different for each zone even when the field was divided in 3 zones. As expected, the zone with low yield was the one with highest clay content, largest slopes and lowest NDVI in June. Spatial yield patterns can turn out differently caused by each year's specific weather conditions (Eghball and Varvel, 1997; Schepers et al., 2004). Despite this fact, these results manifest consistent zonal differences across this field that could be evaluated for site-specific management.

Table 3.3. Average corn yield among different management zones by using different variables and cluster algorithms.

Variables selected	Cluster zones	Corn Yield 2014 Mg ha^{-1}		Corn Yield 2015 Mg ha^{-1}		Corn Yield 2017 Mg ha^{-1}	
		FANNY	CLARA	FANNY	CLARA	FANNY	CLARA
PC1 + PC2 + PC3	1	12.5 a	12.5 a	12.5 a	12.5 a	13.3 a	13.3 a
	2	11.5 b	11.4 b	11.6 b	11.5 b	12.8 b	12.6 b
Clay 0-20 cm + OM + TWI	1	12.5 a	12.5 a	12.4 a	12.4 a	13.3 a	13.3 a
	2	11.6 b	11.4 b	11.9 b	11.8 b	12.8 b	12.7 b
Clay 0-20 cm + Clay 20-40 cm +Slope + NDVI June 2015	1	12.6 a	12.6 a	12.6 a	12.5 a	13.4 a	13.4 a
	2	12.2 b	12.2 b	12.1 b	12.1 b	13.2 b	13.2 b
	3	11.4 c	11.5 c	11.6 c	11.6 c	12.7 c	12.5 c

PC: principal component, OM: soil organic matter, TWI: topographic wetness index. *different letters indicate significant differences (P<0.05) between clusters zones.

Another aspect to consider is the temporal stability of processes occurring in the delineated areas. In other words, the delineation presented above stands only for a time span that is represented by the underlying variables of the respective delineation. Would the same variables measured at a different time have resulted in the same delineation zones? Variables such as clay content, slope or TWI maintain rather stable over time but others such as NDVI could vary during a growing season and even between different years. NDVI is an indicator of crop vigor (Teal et al., 2006) and, in case of corn in south-eastern US, spatial differences of NDVI can appear during growth stages with a high demand of water and nutrients (June-July). Due to its nature, this variable is affected by seasonal effects,

weather conditions and soil and crop nutrient status. Anyway, NDVI has been shown to be a useful crop yield predictor (Wendroth et al., 2003). An example of how the delineation zones change when they are based on different NDVI data sets is presented in Figure 3.9, where zones were delineated using criterion c, but replacing NDVI in June 2015 with NDVI in June 2017. Figure 3.9a shows some differences compared with Figure 3.3c, although the northwest zone still exhibits lower values. When using the FANNY algorithm to divide the field in 3 areas, the patterns in Figure 3.9b and Figure 3.6e are similar. In this example, some differences in NDVI were identified during different years, manifested as extreme values in certain areas. Nevertheless, these differing NDVI data in addition to other rather stable variables resulted in similar delineation zones.

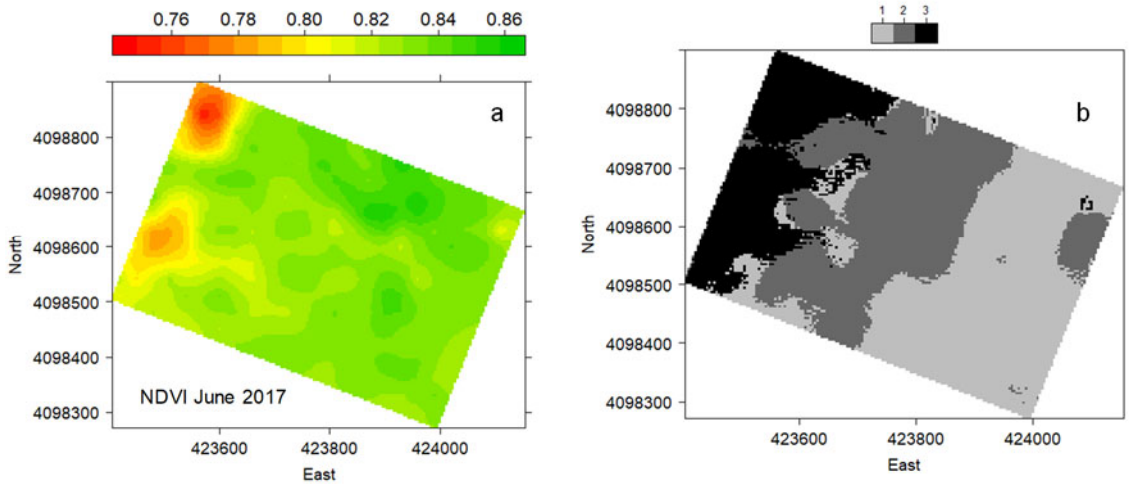

Figure 3.9. a) NDVI map of June 2017. b) Delineated zones using FANNY and based on Clay at 0-20 cm and 20-40 cm, Slope and NDVI at June 2017.

Regarding soil moisture, it was expected in this study, that the soil textural composition in different zones of the field affects the temporal dynamics of soil water tension. For example, in a zone with relatively low clay and high silt content, changes in tension at a

given depth as a consequence of rainfall or evapotranspiration would occur at a slower rate than in a zone with a higher clay and lower silt content due to the different shape of the soil water retention curve and hydraulic conductivity function in the different zones. Therefore, the question addressed here was whether the three different delineated zones would reveal differences in temporal soil water tension dynamics and whether these differences would depend on the similarity or diversity between different zones. For this purpose, soil water tension at three depths during the spring season of 2016 was monitored at different locations, distributed across the different zones at 1-hour intervals. This variable and the experimental set-up used here is widely applied for scheduling irrigation (Liang et al., 2016). Due to similarities in the delineation derived from different approaches, this analysis was centered on the comparison of three areas using FANNY (Figure 3.6e). In Figure 3.10, the soil water tension at different depths for each area and daily precipitation are presented. Between rainfall events soil water tension increases as a consequence of evapotranspiration, however, with different behavior in each zone. Zone 3.3, identified with high clay content and slope shows the steepest tension increase during drying, not only at 20 cm depth near the surface but also at 40 and 60 cm. On the other hand, during days with precipitation tension reaches lower values than the other two areas. Values in zone 1 are less fluctuating but more alike to zone 2. This behavior is interpreted as a consequence of higher silt content and higher water capacity than in the clay soil.

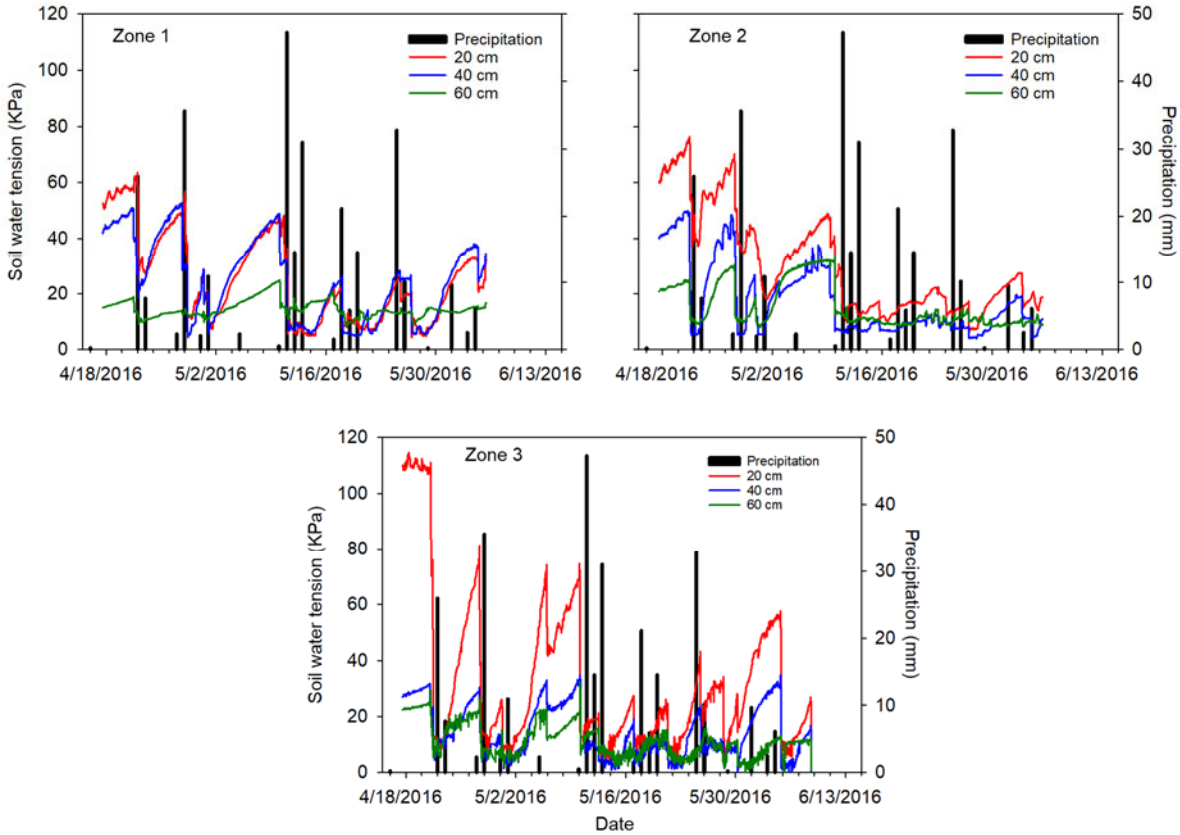

Figure 3.10. Soil water tension and precipitation at different cluster areas over time.

In the following, the temporal dynamics of soil water tension and their variability at different scales should be analyzed in order to detect similarities or differences in their dynamics, and to understand how different temporal behavior over the time period is manifested in wavelet spectra. Results of wavelet analysis for each zone and depth are presented in Figure 3.11. This analysis allows identifying cyclic patterns at different frequencies and at different points or periods in times, here represented in periods of 1 hour with temporal scales that range from hours to several days. Furthermore, time-specific periodic features become apparent. Results show that temporal fluctuation behavior shows some differences among zones and depths. High spectral density values were found for a

frequency equivalent to 5-10 days, which coincides with the occurrence of rainfall events. In addition, a significant cyclic pattern at lower frequencies during rainfall periods was identified.

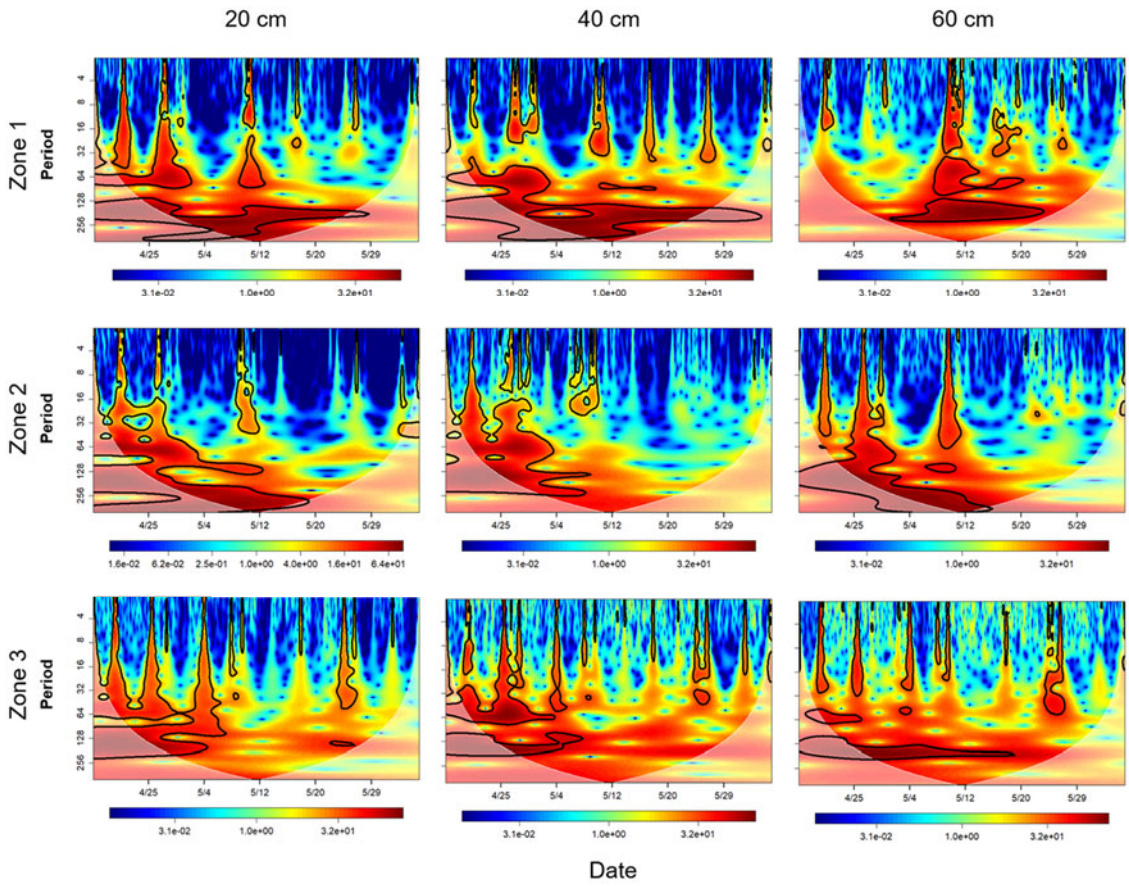

Figure 3.11. Continuous wavelet transform at different depths for each cluster zone. Period resolution is 1 hour. Significant differences ($p < 0.05$) against red noise is shown as a thick contour. The light shade represents the area outside of the cone of influence.

The wavelet coherence between time series observed at the same location but at different depths is presented in Figure 3.12. As expected, the coherence is significant ($p < 0.05$) at frequencies of 5-10 days between layers for the same zone. In zone 3, a strong coherence for frequencies of 1-2 days is found. The phase represented by arrows presents mainly an in-phase behavior, which means that changes in soil water tension occur synchronously or

without a substantial lag at different depths. The coherence is higher when layers of 20 and 40 cm are compared, and decreases when other combinations (20 vs 60 cm or 40 vs 60 cm) are contemplated owing to the fact that redistribution of rain water and removal of water through evapotranspiration occurs faster in shallow layers than at greater depths monitored here. This finding can also be attributed to the fact that results at 60 cm represent the wettest soil conditions with small fluctuations (Figure 3.10).

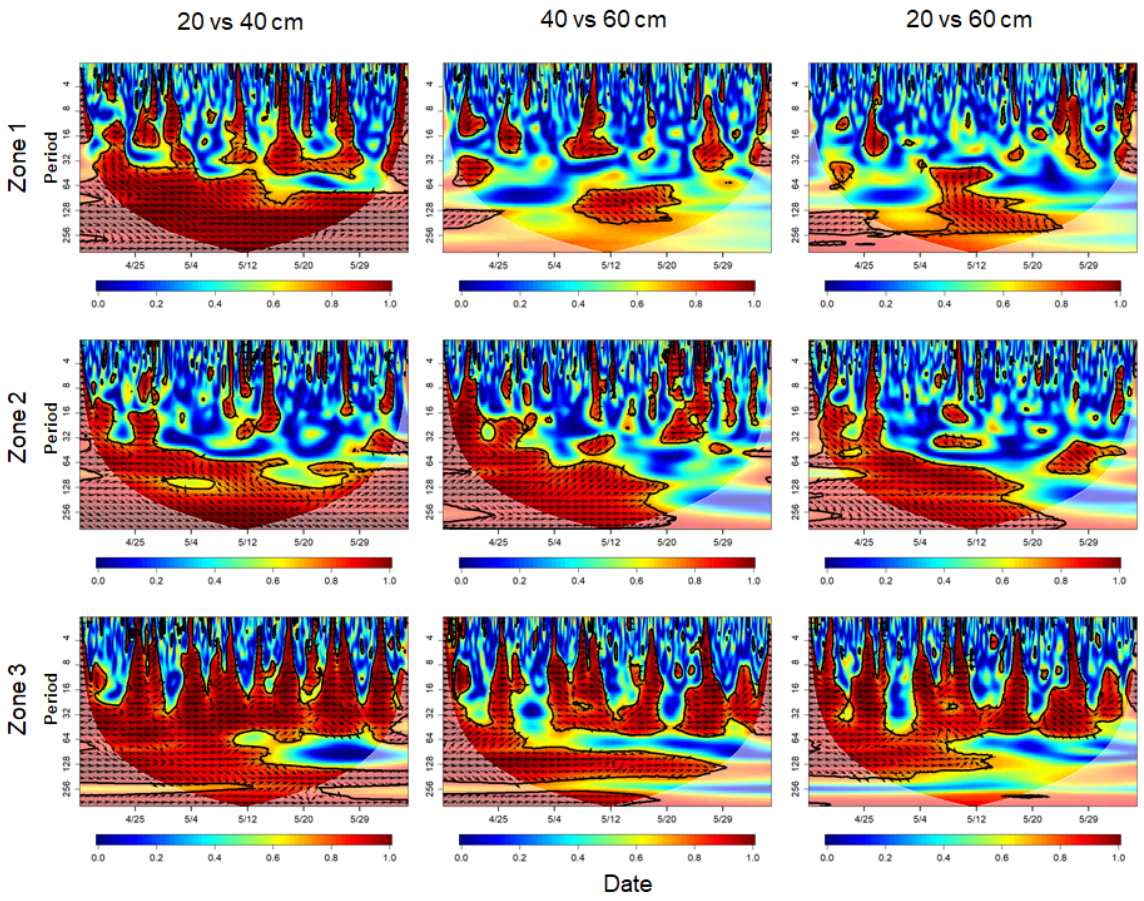

Figure 3.12. Wavelet Coherence between depths for individual cluster zones. Period resolution is 1 hour. Significant differences ($p < 0.05$) against red noise is shown as a thick contour. The light shade represents the area outside of the cone of influence. Arrows indicate the relative phase relationship: Right: in-phase; Left: anti-phase; Down: first series leading second series by 90°; Up: second series leading first series by 90°.

Wavelet coherence for soil water tension between areas is presented in Figure 3.13. Significant values ($p < 0.05$) were observed primarily when comparing zones 1 and 2 at 20

and 40 cm. On the other hand, zone 3 in general does not have high coherence with the other two zones. This result shows that clusters 1 and 2 at 20 and 40 cm depth are zones in which the soil water temporal dynamics are significantly correlated. On the other hand, the temporal variation presents differences in space when we compare the other possible combinations (i.e. 1 vs. 3 and 2 vs. 3 at each depth and 1 vs. 2 at 60 cm). The phase relationship shows that arrows mainly point downward, indicating that at the same depth, there is a lag in the process of soil water tension between zones, i.e., the first series leads the second by a phase shift of 90 degrees. This shows that temporal changes in soil water tension do not occur synchronously although the patterns present high correlation, which is caused by the delay due to different soil hydraulic properties in the different textural zones. Yang et al. (2016) also found high coherence during rainfall events. Moreover, when comparing different zones, dissimilarities in temporal variability were observed: Zone 3 (Northwest part of the field) reveals the most severe changes in time. Between rainfall events, the soil dries out faster in zone 3 than the other zones. On the other hand, when high precipitation amounts are received, soil water tension can reach values closer to saturation within a shorter time. This result manifests what commonly occurs in clayey soils, and it is due to their water retention characteristics. Combined with the fact that this is the area with the highest slope, it is not recommended to manage zone 3 in the same way as zones 1 and 2 for its limited water capacity and infiltrability. In case of irrigation, the optimal time, frequency and rate of water application has to differ among management zones in this field. For example, the clayey zones should be irrigated more frequently with low rates compared with the other zones in order to apply the required amount of water at a rate that would not cause runoff but that can be taken up by the soil.

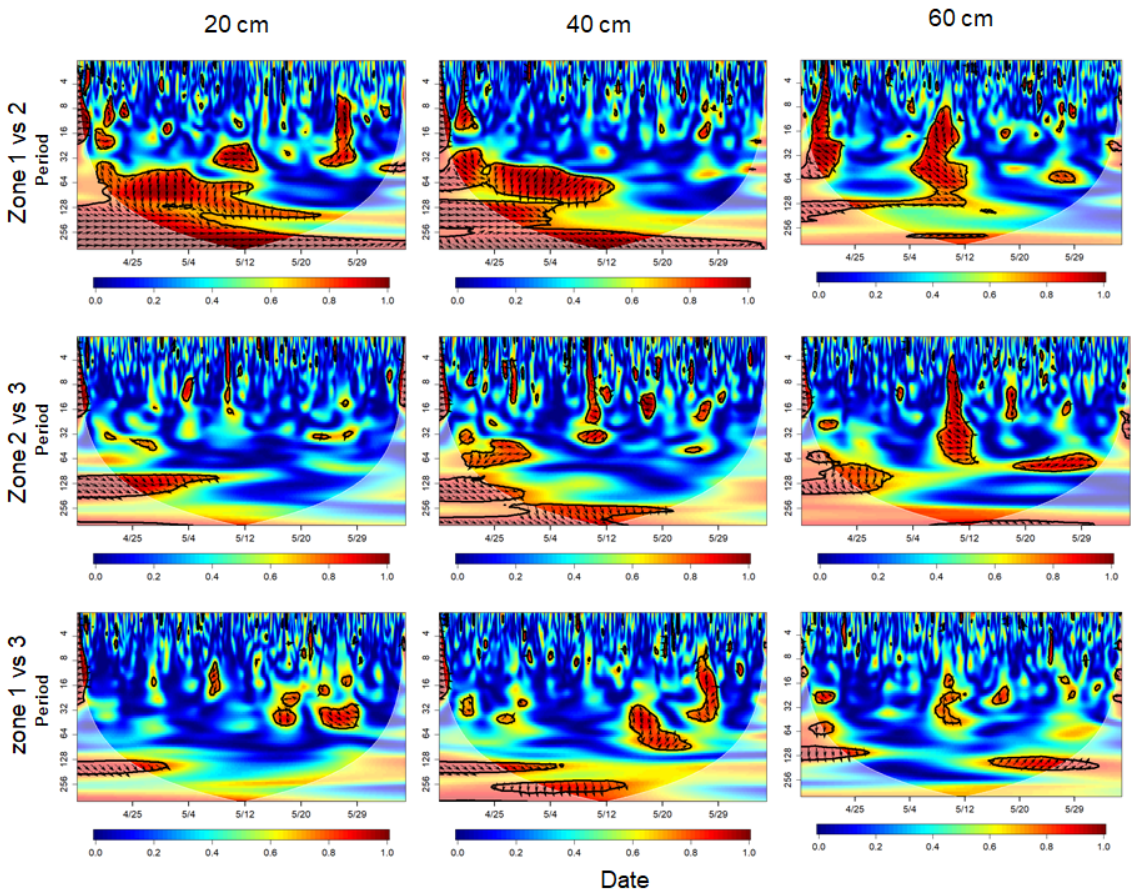

Figure 3.13. Wavelet Coherence between cluster zones at different depths. Period resolution is 1 hour. Significant differences ($p < 0.05$) against red noise is shown as a thick contour. The light shade represents the area outside of the cone of influence. Arrows indicate the relative phase relationship: Right: in-phase; Left: anti-phase; Down: first series leading second series by 90°; Up: second series leading first series by 90°.

3.4 Conclusions

Spatial differences in local topography are a key driver of spatial variability in the studied field. Areas with high slope were eroded, resulting in higher clay content closer to the soil surface. This might explain lower crop productivity as reflected by NDVI and crop yield, and influenced the soil organic matter and total nitrogen content in the soil.

Cluster analysis resulted in a division of 2 or 3 areas depending on the underlying criteria. A method based on PCA maps revealed a similar delineation compared to selected key variables, which in this study were clay content, soil organic matter content and topographic wetness index. For larger data sets, CLARA proves to be as good as the FANNY clustering and for being used appropriately in fields with large data sets and a small number of divisions.

Delineated areas changed when different variables were selected, but showed concordance at identifying the most restrictive zone for agricultural practices. With all the different delineation approaches, crop yields significantly differed between delineated zones. Soil water dynamics were affected by precipitation and their behavior contrasted among zones, possibly due to site-specific soil hydraulic properties. The results from this study emphasize the need for delineating functional subunits in farmers' fields and the methodology manifests a feasible way to delineate site-specific management zones to improve the productivity of this field as shown in the various ways to evaluate the delineation. The method of dividing this field into different functional and management units obtained in this study are suitable for practical use.

Copyright © Javier Reyes 2018

Chapter 4 Evaluating and Predicting Soil Water Status in a Farmer's Field in Western Kentucky

4.1 Introduction

Spatial and temporal variation of soil processes occurs at different scales. At the field scale, the spatio-temporal variation of soil water in the vadose zone is one of the key variables to be considered for soil and crop process dynamics and management. Several works have shown how soil moisture varies at different locations in the field (Nielsen et al., 1973; Bell et al., 1980; Wendroth et al., 1999; Weihermüller et al., 2007). Several factors affect this spatial variation, including landscape topography, agricultural management, variability in soil texture and structure, lateral flow and water distribution in the soil profile (Vereecken et al., 2014). Soil water also varies in time. Regarding its behavior, Vachaud et al. (1985) proposed the concept of temporal stability of spatial variability. This means that the driest locations in the field tend to maintain as the driest spots at different times and so do the wet spots. Several works have corroborated this pattern (Wendroth et al., 1999; Grant et al., 2004; Hu et al., 2010). If a temporal stability is found in a field, it is possible to identify sampling locations that can be used to improve the sampling efficiency while maintaining a good accuracy. On the other hand, the temporal variability could be stationary or non-stationary depending on the time scale and crop and soil attributes; thus, further work is required to have better understanding of soil water dynamics at the field scale.

The development of computer technology and simulation algorithms of ecological processes has brought several numerical and analytical agroecosystem models used to simulate agricultural, soil and crop processes (Vereecken et al., 2016). These models

provide the opportunity of developing management scenarios and predict relevant variables which would make the model useful as a decision-support tool. Different models have been developed to study soil-water dynamics such as RZWQM2 (Ma et al., 2002), SWAP (Jiang et al., 2001), and HYDRUS 1D/2D/3D (Šimůnek et al., 2017). The Root Zone Water Quality Model (RZWQM2) is a one dimensional model that has been widely used. The model reflects the current state of knowledge on the interactions between weather, soil properties, hydrology, agricultural management practices, crop growth, and chemical transport (Ahuja et al., 2000). Studies on water balance (Cameira et al., 2005), crop growth (Anapalli et al., 2005), nitrogen fertilization (Qi et al., 2012) and climate change (Wang et al., 2016) describe some of the model applications.

This study is located in a relatively humid region of the south-eastern United States, however, the water use for practices such as irrigation has increased in recent years (Boyer et al., 2014). The application occurs mainly during short-term periods of drought in the summer. Irrigation is primarily used to optimize and stabilize crop yield at times of water shortage during the growing period. The timing of irrigation depends on the soil water status, although due to the spatial variation of soil moisture at the field scale, there can be zones that indicate sufficient water while other zones reflect the need to initiate irrigation at the same time. To increase water use efficiency, spatial differences should be studied and concepts for site-specific irrigation management be derived (Evans and Sadler, 2008). The objectives of this study were therefore: 1) to study the soil water temporal dynamics in different zones of a field grown with wheat and corn thereafter in a farmer's field located

in Western Kentucky and 2) to evaluate the accuracy of RZWQM2 in predicting soil water tension dynamics in different field zones and soil depths.

4.2 Material and Methods

4.2.1 Site description and data sampling

The study was conducted at Hillview Farms located in Princeton KY, Caldwell County (37° 1'58.02"N, 87°51'33.06"W, 142 m asl). According to the Köppen system, the climate is classified as humid subtropical. The annual precipitation is around 1312 mm (US climate data, 2017), and mean annual temperature is 15 °C. The maximum and minimum mean temperatures occur in June and January, respectively. The soil in this field belongs mainly to the Crider series (Typic Paleudalfs), while some areas are classified as Nolin series (Dystric Fluventic Eutrudepts) (Soil Survey Staff, 1999); both soil series are classified as silt loam in the surface layer. The experiment covers an area of approximately 27 ha. The field was cultivated with double crop soybean (*Glycine max*) - winter wheat (*Triticum aestivum* L) in 2015/2016 and with corn (*Zea mays* L.) in 2017 seasons. Yield maps were obtained for each crop after harvesting.

Disturbed soil samples were obtained at 5 depths (0-20, 20-40, 40-60, 60-80, and 80-100 cm) for particle size analysis. Soil texture was separated in sand (0.05-2 mm), silt (0.002-0.05 mm) and clay (< 0.002 mm) using the pipette method (Gee and Or, 2002); procedures are explained in Reyes et al. (2018). Soil chemical properties were obtained in the upper four layers (0-80 cm depth). Soil organic matter and total nitrogen were determined by LECO combustion. Extractable P, K, Ca, Mg, and Zn were measured by Mehlich III

extraction. For pH determination, a glass electrode was used in 1:1 soil:water and Sikora buffer for Buffer pH (Jones, 2000). Soil samples where obtained at 96 locations in a 50x50 m grid. Soil water tension was measured at 48 locations and at three depths (20, 40, 60 cm) per location (Figure 4.1). Soil water tension measurements were made during the spring season of 2016 under wheat and in summer 2017 under corn by using watermarks (Fisher and Gould, 2012) connected to wireless radio network of antennas. Data were collected each hour.

A digital elevation model (DEM) was obtained at 1.5 m resolution from LiDAR, provided by the Kentucky Division of Geographic Information. From the DEM, topographic parameters such as elevation and slope were obtained. Satellite Images from Landsat 8 Operational Land Imager (Level 2 product (SR), U.S. Geological Survey 2017) were collected during the growing seasons of wheat (2016) and corn (2017). Different variables were obtained from Landsat images, including leaf area index (LAI), normalized vegetation index (NDVI), Evapotranspiration (ET). Their values were computed using the WATER package (Olmedo et al., 2017) under the R environment. Equations are based on the METRIC model (Allen et al., 2007).

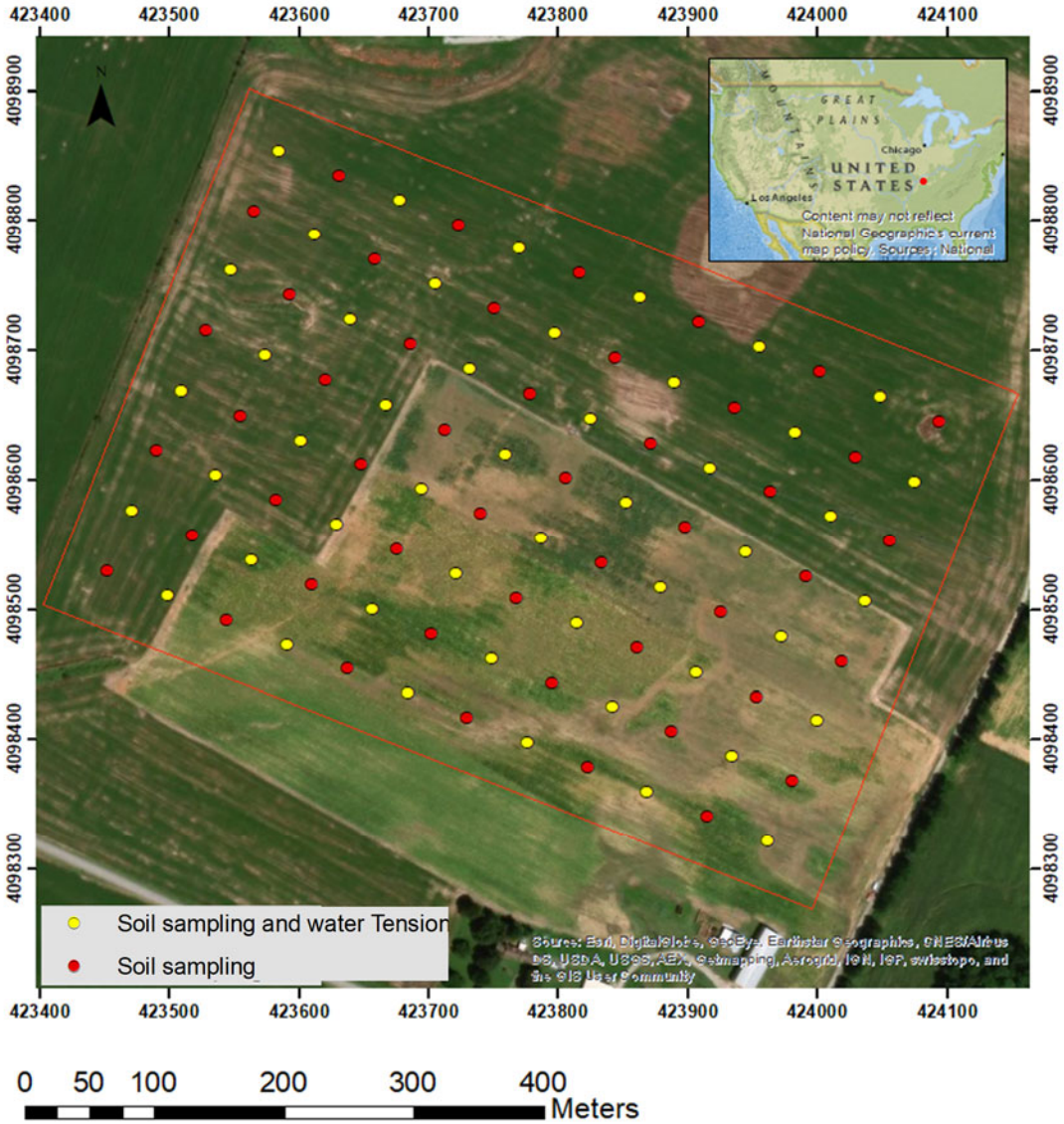

Figure 4.1. Study area and sampling locations. Soil textural and chemical properties measurements were done at both red and yellow bullets.

Combining field, proximal sensing and remote sensing data, the field was divided in three zones that represent spatial variability of soil and crop processes (Figure 4.2). The criteria and parameters used are explained in chapter 3, where zone 1 represents an area with better soil and topographic characteristics for crop production than zone 3 which is an area with restricted growing conditions. Zone 3 is an eroded area with a pronounced slope, while

zone 2 represents a transitional area. Considering this field division, the analysis was centered on evaluating the soil water dynamics at different zones and depths under wheat and corn crops.

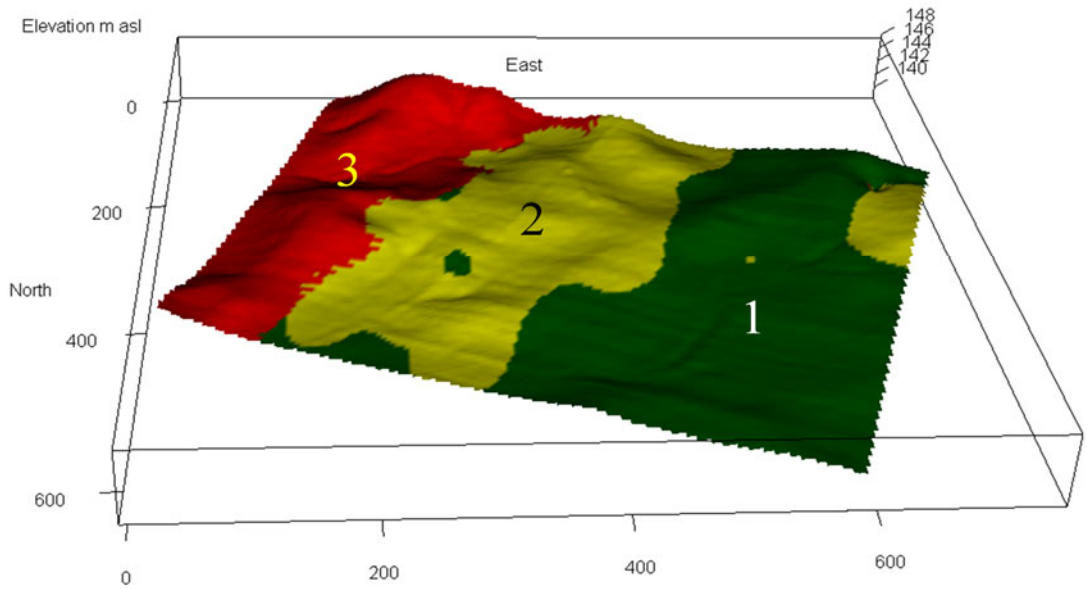

Figure 4.2. Topographic model of the delineated zones in the field. The area corresponds to the red rectangle showed on Figure 4.1.

4.2.2 Model evaluation and calibration

The Root Zone Water Quality model (RZWQM 2.0, Ma et al., 2000) was used in this study to simulate the soil water status. This model uses numerical one-dimensional approaches and modified forms of the Brooks-Corey equations (Brooks and Corey, 1964) to describe the soil hydraulic property functions, i.e., the water retention curve and the hydraulic conductivity function. The Green-Ampt equation is applied for infiltration during rainfall or irrigation and the Richards equation is used for redistribution between rainfall or irrigation events. The crop water uptake can be simulated using DSSAT modules (Ahuja et al., 2000, Ma et al., 2011). Complementary to the soil data, hourly weather data was

obtained from a weather station (located about 2 km distance) during 2015-2017. The lower boundary was set as unit gradient with a depth of 1.5 m. Spatially averaged data of representative locations with data of soil water tension and soil properties at each zone (Figure 3.2) and depth was used as input in the model. Soil water retention curve and hydraulic parameters were estimated based on soil textural class parameters. Measured soil water tension on the first day of simulation were setup as initial conditions. Calibration to predict soil water tension at each zone was done manually, while trying to minimize the difference between simulated and observed soil water tension values. As it was recommended by Ma et al. (2011), changes were focused on the physical parameters, including saturated hydraulic conductivity, total porosity and macroporosity, soil water content at 33 and 1500 kPa suction and lateral hydraulic flow. Input and output parameters were checked to have a physical meaning according to the literature.

Statistical indices were used to evaluate the model predictions. The mean error (ME) is a criterion to evaluate the bias. To identify the accuracy, the root mean square error (RMSE) and Nash-Sutcliffe model efficiency (NSE, Nash and Sutcliffe, 1970) were applied. These indices were calculated according to:

$$ME = \frac{1}{n}\sum_{i=1}^{n}\left(p_{(i)} - o_{(i)}\right) \qquad \text{(eq. 4.1)}$$

$$RMSE = \sqrt{\frac{1}{n}\sum_{i=1}^{n}\left(p_{(i)} - o_{(i)}\right)^2} \qquad \text{(eq. 4.2)}$$

$$NSE = 1 - \sqrt{\frac{\sum_{i=1}^{n} \left(o_{(i)} - p_{(i)}\right)^2}{\sum_{i=1}^{n} \left(o_{(i)} - \bar{o}\right)^2}} \qquad \text{(eq. 4.3)}$$

where p_i and o_i are the predicted and observed values at location i, $\bar{o}$ is average of observed values, and n represents the total number of observations.

4.3 Results and discussion

4.3.1 Soil properties and crop yield

Soil properties at different depths and zones are presented in Table 4.1. In general, these values have similarity with other studies performed in this region, although the pH is slightly more acidic relative to what is commonly observed on the surface layer of a Crider soil series (Karathanasis and Wells, 1990; Mueller et al., 2004). As expected, available nutrients and soil pH decreased with depth. An increase in clay content was found as well. When comparing the management zones presented in Figure 4.2, some differences were detected. As mentioned before, zone 3 presents the most restrictive conditions for crop growth. The restrictive conditions in this zone are reflected in a clay content that is higher than in the other two zones and also higher than expected for a Crider soil series. Soil organic matter, available phosphorous and potassium contents are lower compared with the other two zones, while calcium and magnesium concentrations are higher. Average wheat and corn yields obtained from a combine harvester map for each of the three zones are provided in Table 4.2. A one-way ANOVA test was performed to compare crop yield

among zones. It showed that grain yield presented significant differences ($p > 0.05$) between each zone. Although crop yield variation is strongly affected by seasonality, as a result, yield even for the same crop can vary in different years (Eghball and Varvel, 1997; Schepers et al., 2004). This information has concordance with the spatial variability of several properties in the field.

Table 4.1. Soil Properties at different zones and depths.

Zone	Depth	OM	N	P	K	Ca	Mg	Silt	Clay	pH
	cm	%		kg ha^{-1}				%		
1	0-20	1.9	0.10	87	378	3627	151	79.6	18.7	5.6
	20-40	0.8	0.06	25	278	3552	205	72.1	25.9	5.5
	40-60	0.6	0.05	20	277	3665	340	68.4	28.9	5.3
	60-80	0.4	0.04	36	254	3010	522	68.6	28.4	4.9
	80-100							68.2	28.0	
2	0-20	1.7	0.10	76	306	3656	152	77.4	20.3	5.6
	20-40	0.8	0.06	16	248	3958	222	72.4	24.2	5.4
	40-60	0.5	0.06	7	230	3967	324	69.1	27.5	5.2
	60-80	0.4	0.05	9	216	3812	462	68.5	27.2	4.7
	80-100							67.1	28.3	
3	0-20	1.6	0.09	27	262	4425	244	67.5	27.1	5.4
	20-40	0.6	0.05	8	219	4520	285	63.2	29.9	5.6
	40-60	0.4	0.04	7	210	4234	458	63.4	31.4	5.0
	60-80	0.3	0.03	6	206	3465	623	62.1	31.5	4.6
	80-100							61.1	32.5	

Table 4.2. Wheat and corn yield in each field zone.

Field Zone	Wheat-2016	Corn-2017
	kg ha^{-1}	
1	5087 a	12644 a
2	4861 b	12268 b
3	4657 c	11445 c

Different letters indicate significant differences ($p<0.05$).

Measured soil water tension in different zones and depths is depicted in Figure 4.3. Under both crops (wheat in 2016 and corn 2017), it is observed that the soil water tension varies

between zones. This is consistent with the differences detected with the other soil properties. Soil water tension values and variations are higher in surface layer and less pronounced in deeper layers. When rainfall occurs, the soil water tension decreases. Yang et al. (2016) have mentioned that precipitation is one of the main driving force in temporal changes and its impact decreases at deep layers compared to shallow soil depths. On the other hand, low rainfall amounts are barely recognized with regard to soil water tension fluctuations in some periods. This behavior can be caused by drying of the surface soil. At some level of drying, the water infiltration and transport through the soil profile becomes extremely slow and the amount of rainfall may not have been sufficient to reach the uppermost sensor at 20 cm depth. Results presented in chapter 3 showed that temporal variation of soil water tension among different zones and depths do not present good correlation when a wavelet coherency analysis was performed. Zone 3 behaves particularly different compared with the others zones and presents more restrictions for crop growth. This is caused by higher clay content, higher slope among other variables and expressed in lower crop yield than in the remaining zones in this field.

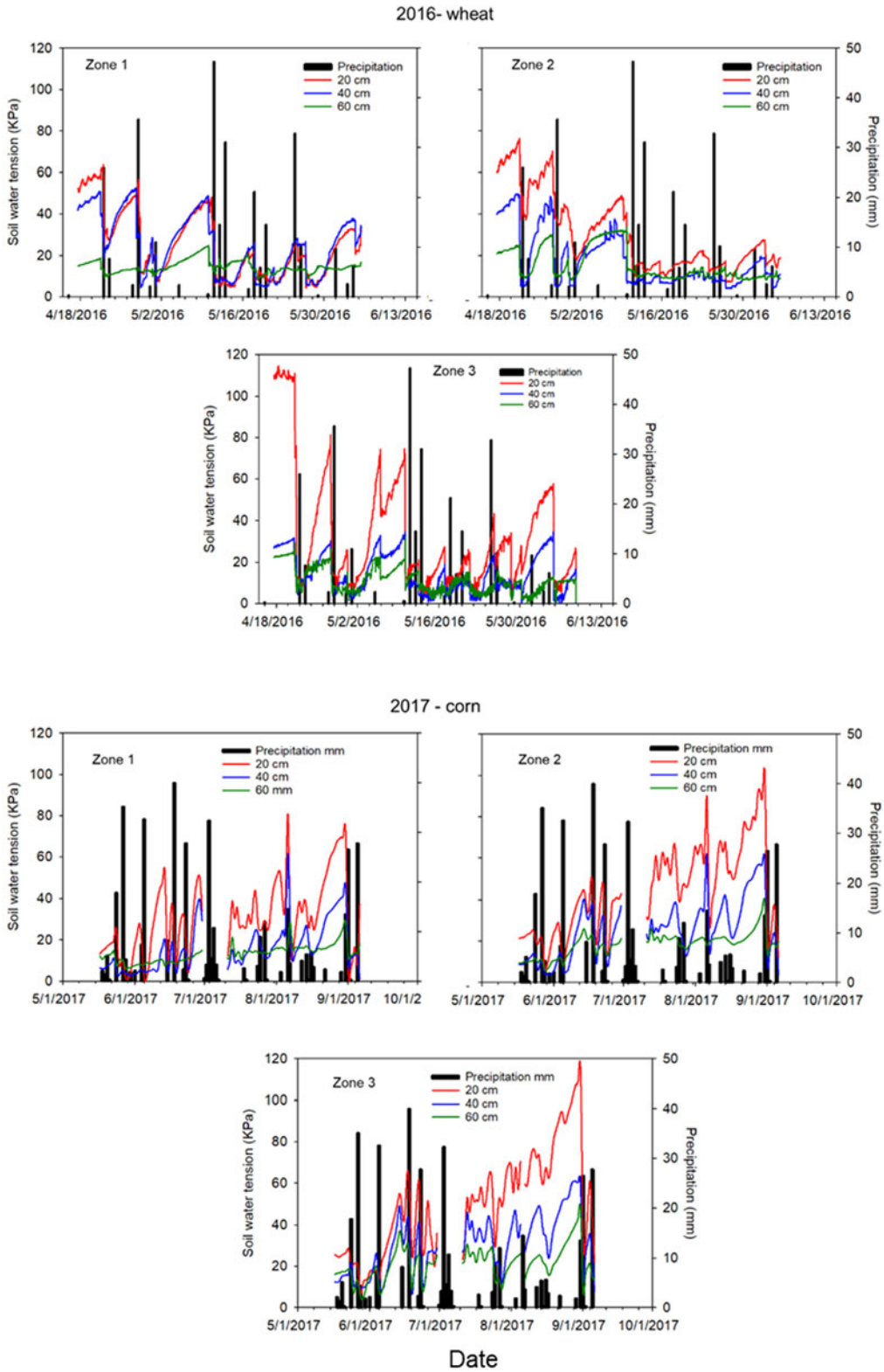

Figure 4.3. Soil water tension at 20, 40 and 60 cm depth and daily precipitation under wheat (2016) and corn (2017) crops.

4.3.2 Predicted soil water status

The measured and RZWQM2-predicted soil water tension is presented in Figure 4.4 for the wheat growing season and in Figure 4.5 during the corn growing season. The error of predictions of soil water tension after performing the calibration are presented in Table 4.3. The model predictions follow the pattern of soil water tension dynamics in time. On the other hand, the bias in the prediction do not presents a trend in different zones and layers under both crops. The NSE values reflect the efficiency of model predictions. A value close to 1 indicates that the prediction is accurate and close to measured data; a value of 0 implies that the accuracy of the prediction is close to using the overall average, and negative values denote that the use of the overall average for the entire time series is better than using model predictions. (Nash and Sutcliffe, 1970). Ma et al. (2011) indicate that with a NSE value of > 0.7 the model prediction could be considered acceptable. Table 4.3 shows that only under wheat at 20 cm depth simulations reach NSE values > 0.7 and under corn come close to this value only at 20 cm depth.

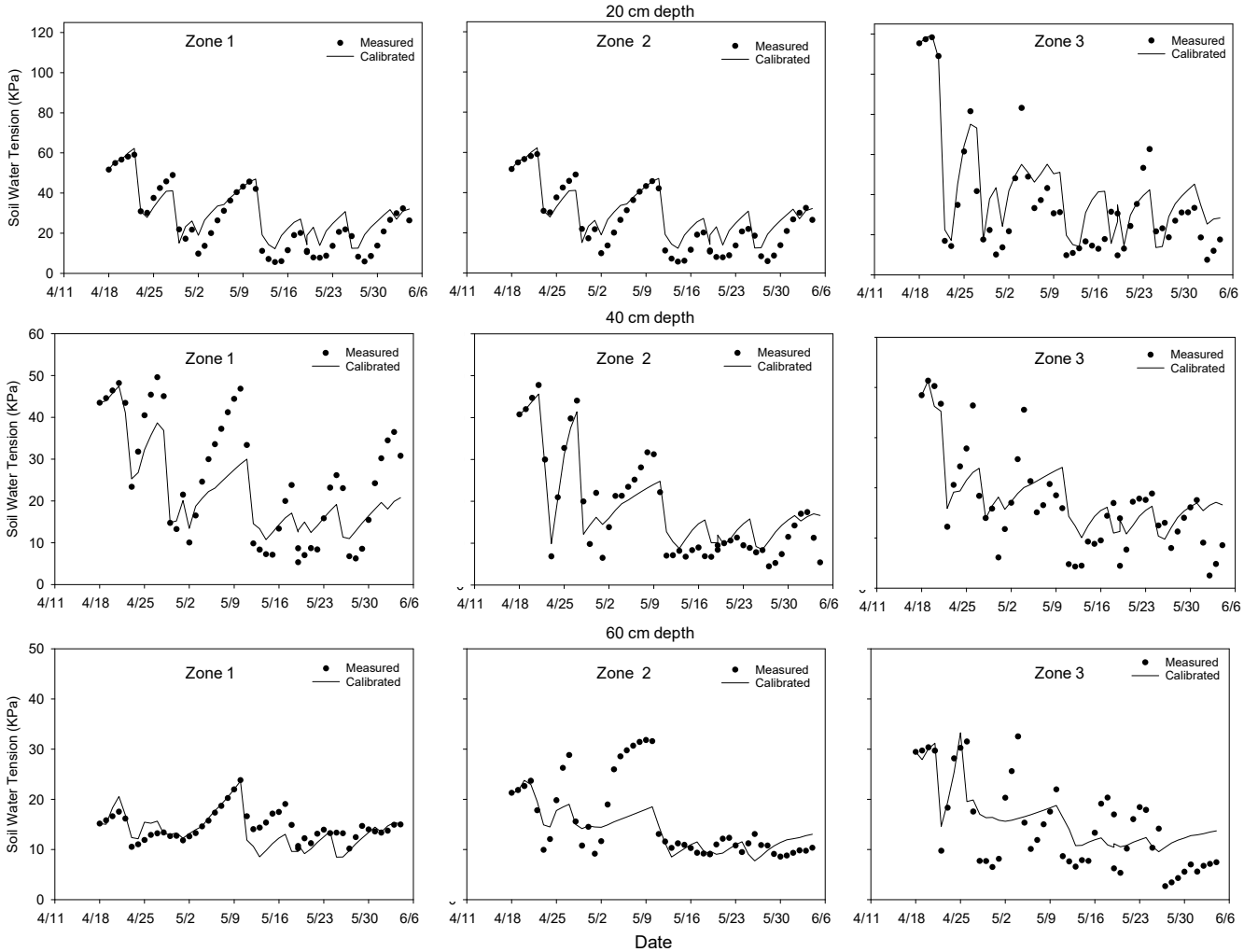

Figure 4.4. Predicted and measured soil water tension under wheat crop (2016) at different zones and depths.

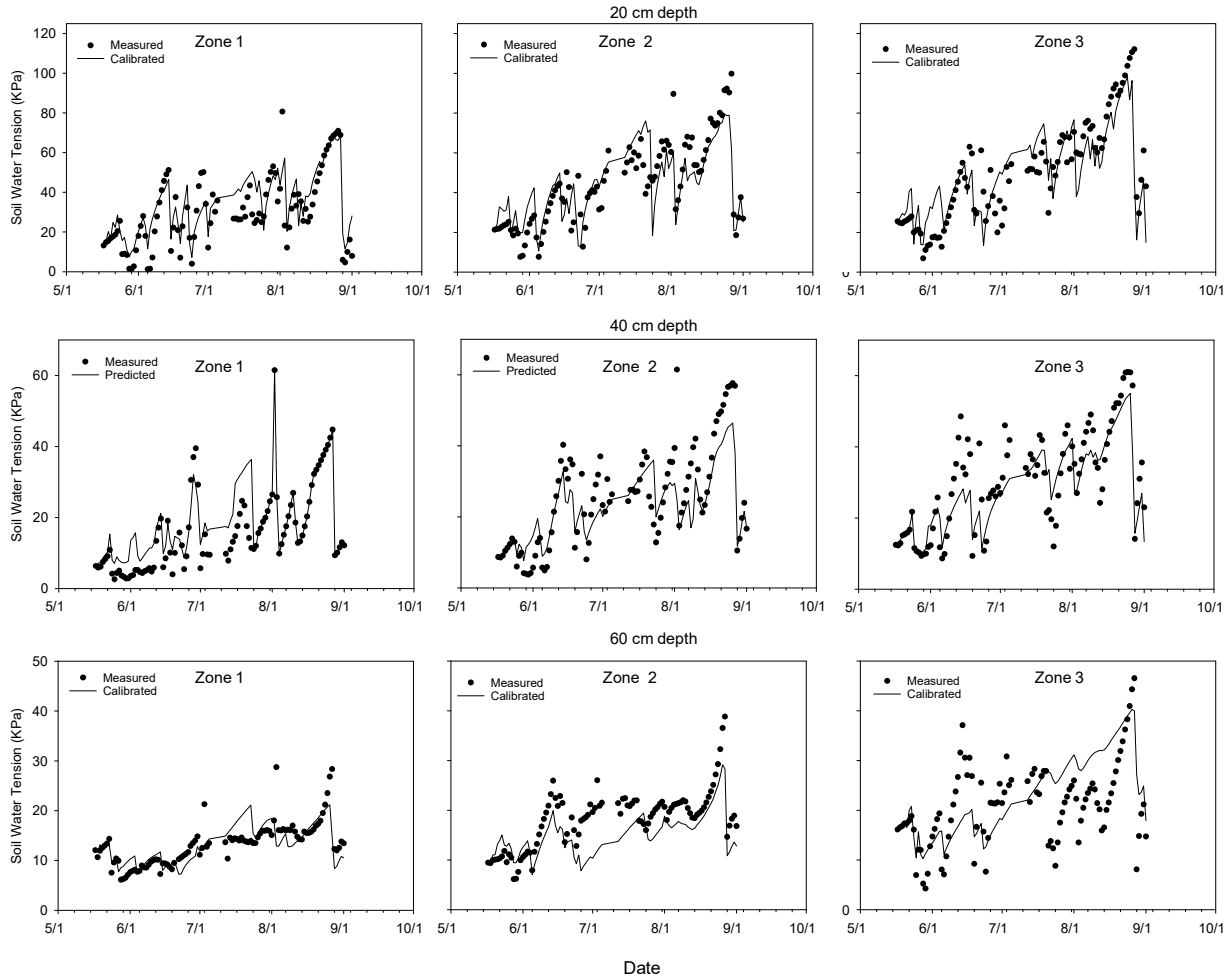

Figure 4.5. Predicted and measured soil water tension under corn crop (2017) at different zones and depths.

Comparing soil water tensions under the two different crops considering ME, RMSE and NSE, reveals that predictions turned out better under wheat than corn. This result could be due to the difference in number of measurements per location rather than to a crop/season issue. Differences in accuracy can also be observed between zones. The predictions were less accurate in zone 3 than in the other zones, especially in 2016. This result could be due to the topography of this area, considering that the slope does not affect surface runoff simulation in RZWQM2 (Ma et al., 2011), and to problems in describing water infiltration and redistribution in the clayey soil of this zone.

The model reveals special sensitivity to changing physical parameters, including the soil water content at 33 and 1500 kPa suction, macroporosity and lateral hydraulic flow (Ma et al., 2007). Our results were adequate to estimate predictions in the surface layer but the accuracy decreased in deeper layers, consequently, further calibration is needed to better predict soil water tension at 40 and 60 cm depth. The prediction of soil water tension at lower layers depend on the accuracy in the estimation of water movement from upper layers. Wu et al. (1999) observed that soil water predictions were more dynamic than observations in lower layers and the predictions were less dynamic than measurements in upper layers. We need to consider that temporal dynamics decrease with increasing depth. Consequently, it is more difficult to predict minor fluctuations. The range of fluctuations is lower at 60 cm depth which results in lower RMSE despite a lower NSE when compared with the upper layers.

Table 4.3. Bias and prediction error of calibrated soil water tension predictions using RZWQM2 under wheat and corn at each zone.

		Wheat 2016		
Zone	Parameter	20 cm depth	40 cm depth	60 cm depth
Zone 1	ME (KPa)	4.43	-3.17	-0.85
	RMSE (Kpa)	7.43	7.90	2.65
	NSE	0.78	0.69	0.15
Zone 2	ME (KPa)	-1.61	1.14	-1.83
	RMSE (Kpa)	6.98	4.58	5.68
	NSE	0.85	0.86	0.45
Zone 3	ME (KPa)	7.28	1.51	1.37
	RMSE (Kpa)	14.63	6.17	6.25
	NSE	0.75	0.60	0.49
		Corn 2017		
Zone	Parameter	20 cm depth	40 cm depth	60 cm depth
Zone 1	ME (KPa)	4.19	2.97	-0.04
	RMSE (Kpa)	10.19	5.95	3.34
	NSE	0.68	0.66	0.40
Zone 2	ME (KPa)	-0.09	2.19	3.27
	RMSE (Kpa)	12.27	7.81	4.95
	NSE	0.67	0.64	0.27
Zone 3	ME (KPa)	-0.03	1.89	-2.08
	RMSE (Kpa)	14.26	7.28	7.63
	NSE	0.67	0.63	0.14

4.3.3 Potential use of model predictions

The use of agro-system models as a decision-making tool is one of the potential applications. Several experiments have shown the potential of applying RZWQM2 to support decisions (Ma et al., 2009; Saseendran et al., 2014; Kisekka et al., 2017). In our study, the calibration shows the impact of accurate soil and hydraulic properties in predicting the soil water status. As expected, reliable field measurements are required to provide accurate process descriptions and to reflect field spatial variability. While accurate field data could require high sampling density, it could be reduced when combined with ancillary variables (i.e., proximal and remote sensing information). On the other hand, soil water content can be estimated from remote and proximal sensing data (Lambot et al., 2006; Hong and Shin, 2011, Adams et al., 2013), but due to the resolution, depth level and

spatio-temporal variation, these are mainly punctual observations at specific dates so it should be only used as reference of spatial field variability. If we obtain a good prediction of soil water status, it can be used for practices such as irrigation or fertilization. For example, Liang et al. (2014) shows the use of soil water tension to estimate volumetric water content using the van Genuchten (1980) model to schedule irrigation. In summary, potential application of models such as RMZWQ2 for site specific management, relies on obtaining appropriate data and field characterization combined with appropriate model calibration.

4.4 Conclusions

Soil water status varies between delineated zones. When RZWQM2 model was applied, the predictions presented better accuracy under wheat compared to corn. Better accuracy to predict soil water tension was observed at the surface depth (20 cm depth) compared with the 40 and 60 cm depths. Similarly, the accuracy of predictions decreased in the most restricted area (zone 3) compared to the other zones. The differences observed in both soil water status measured and predicted can be attributed to spatial differences in topography and soil characteristics. The prediction improved after calibrating the model by adjusting soil physical parameters, having NSE > 0.7 in surface layers, but further calibration is needed to improve the simulation result in deeper layers. RZWQM2 shows the potential to estimate soil water status and predict spatial differences at the field scale. With accurate field measurements, this model can be used as decision-making tool to apply site specific management of water resources.

Copyright © Javier Reyes 2018

Chapter 5 Spatial Variability of Clay Mineralogy in a Farmer's Field in Kentucky

5.1 Introduction

Soil minerals are important to provide physical support for plant growth, as they affect the formation of aggregates and therefore their air and water capacity. Through weathering processes, secondary minerals are formed which are mainly present in the clay fraction size (<2 μm). Minerals in the clay fraction are the most relevant ones participating in physical and chemical processes occurring in the soil (Schulze, 1989).

Several methods have been used to identify and characterize clay minerals, including x-ray diffraction, thermal analysis, scanning electron microscope (*SEM*), and Fourier Transform Infrared Spectroscopy. X-ray diffraction (XRD) is the most widely applied technique in the literature. It is a direct identification of crystalline soil minerals produced by bombarding a metal foil with electrons. In this process, some x-rays pass through a sample, some others are diffracted. The diffracted x-rays are associated to a specific crystallographic structure, allowing to identify specific minerals using different treatments (i.e. Mg, Mg, Glycerol, K). In the case of phyllosilicates, the peaks in the x-ray diffraction spectrogram are generated by spacing between layers (Essington, 2004). Other methods are the thermal analysis including thermogravimetry (TG), differential thermal analysis (DTA), and differential scanning calorimetry (DSC) (Karathanasis and Harris, 1994). Thermal analyses can be more useful than x-ray diffraction when the minerals present poor crystallinity. Another approach is the Fourier Transform Infrared Spectroscopy (White,

1971; Baes and Bloom, 1989). FTIR can be used complementary to x-ray diffraction, because different IR bands can be associated with clay minerals (Russel, 1987).

The dominant soil orders in Kentucky correspond to Alfisol and Ultisol, although Mollisols and Inceptisols can also be found (Soil Survey Staff, 1999). In general, soils in Kentucky are well developed and their soil mineralogy is widely found in the literature (Karathanasis, 1985; Karathanasis, 1991; Karathanasis et al., 1991; Zhang and Karathanasis, 1997; Karathanasis, and Macneal 1994; Karathanasis and Johnson, 2006). Minerals such as kaolinite and vermiculite are commonly dominant in these soils. Similarly, a significant presence of hydroxyl interlayered vermiculite (HIV) or smectite in case of fragipans (Karathanasis, 1987) has been identified.

Soil properties can vary drastically even within the same field (Beckett and Webster, 1971; Koestel et al., 2013), although the spatial variability of clay mineralogy has not been commonly studied at the field scale. By knowing spatial differences in clay mineralogy, we can obtain a better understanding about spatial variation of soils, and help to manage the field site-specifically. The purpose of this study was to determine if we can find spatial differences in soil mineralogy at the field scale in a silt loam soil located in Western Kentucky, and to evaluate these differences with other soil properties (i.e. soil texture, organic matter, total nitrogen, available nutrients). We hypothesize that spatial differences in clay mineralogy will be identified within the field and consequently, this differences will be observed in other soil properties as well.

5.2 Material and Methods

5.2.1 Site description and data sampling

The study was conducted at Hillview Farms located in Princeton KY, Caldwell County (37° 1'58.02"N, 87°51'33.06"W, 142 m asl). According to the Köppen system, the climate is classified as humid subtropical. The annual precipitation is around 1312 mm (US climate data, 2017), and annual mean temperature is 15 °C. The maximum and minimum mean temperatures occur in June and January, respectively.

The soil classification map is presented in Figure 5.1. The dominant soil series in the field is Crider, belonging to fine-silty, mixed, active, mesic Typic Paleudalfs; these soils are formed in a loess mantle and the underlying residuum from limestone. In some areas we found soils from the Nolin series, i.e., fine-silty, mixed, active, mesic Dystric Fluventic Eutrudepts; these soils are formed in alluvium derived from limestones, sandstones, siltstones, shales, and loess (Soil Survey Staff, 1999). The study area was approximately 27 ha. The field has been cultivated with corn (*Zea mays* L.), wheat (*Triticum aestivum* L) double crop soybean (*Glycine max* L), and tobacco (*Nicotiana tabacum* L) under no till soil management. To study the soil mineralogy, we took samples at the four locations indicated in Figure 5.1 at two depths: 0-20 cm and 20-40 cm. The locations are assigned as Nolin (map unit: Np), Crider I (map unit: CrA), Crider II (map unit: CrB2), and Crider III (map unit: CrC3).

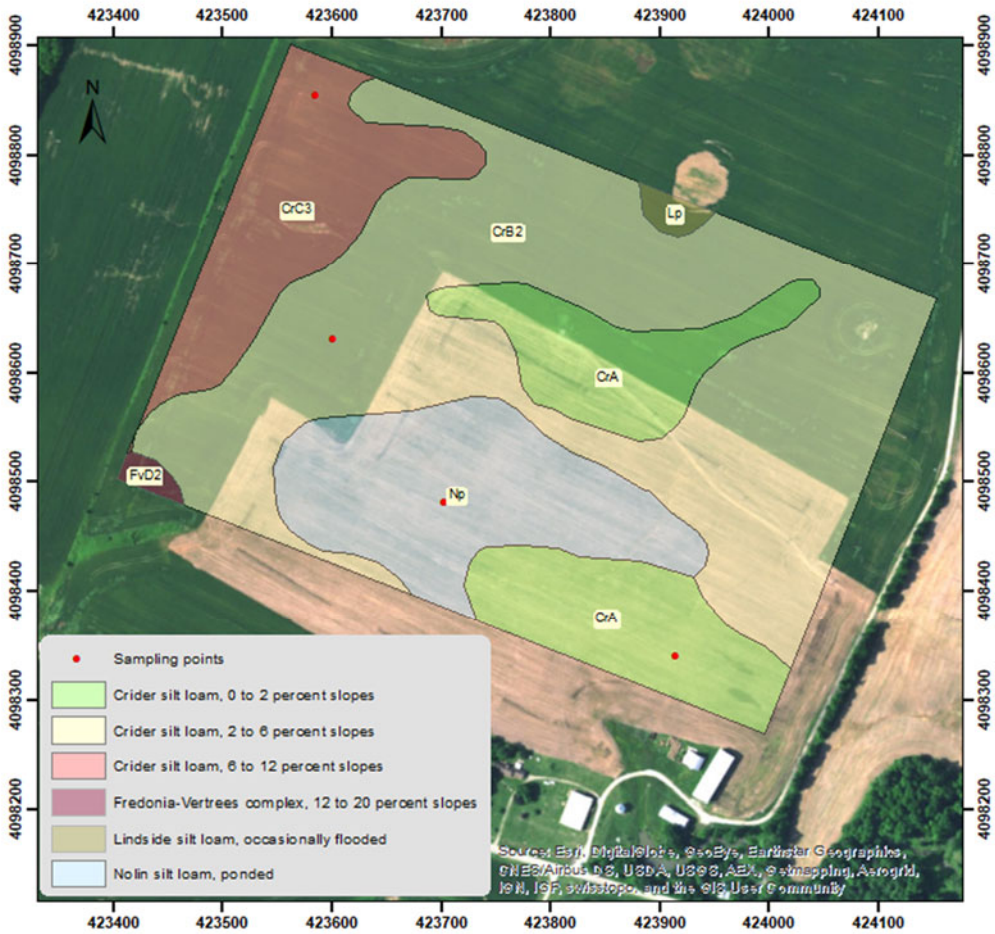

Figure 5.1. Study area and soil classification. Red bullets indicate the soil sampling location. The locations are assigned as Nolin (map unit: Np), Crider I (map unit: CrA), Crider II (map unit: CrB2), and Crider III (map unit: CrC3). Map units were obtained from Sol Survey Staff (2017).

5.2.2 Mineralogical characterization

For each location, we sampled 25 g of soil (< 2 mm). These samples were fractionated into particles of sand (50–2000 µm), silt (2–50 µm), and clay (< 2 µm) following the procedures described by Jackson (1974) and Karathanasis and Hajek (1982). To remove organic carbon, we applied continuous doses of 30% H_2O_2 under Na acetate buffer solution, until the sample stopped reacting. The removal of free iron oxide was omitted. The x-ray

diffraction analyses was applied to the clay fraction using PANalytical X'pert Pro as diffractometer and the anode material utilized was Cu. The step size was 0.07 2θ and the step time was 4 s. The samples were mounted on glass slides and saturated with Mg, Mg-glycerol, and K at 25 °C and 550 °C. PANalytical's XRD software suite was used for x-ray diffraction peak identification. A thermogravimetric analysis was applied to the clay fraction using a TGA Q50 (TA instruments) using glass slides saturated with Mg. The increasing temperature rate was 20 ºC per minute until reaching 1000 ºC.

Complementarily, an FTIR analysis was performed. Samples of 500 mg of spectroscopic grade KBr were mixed with 30 mg of clay and were analyzed using a Nicolet 6700 Fourier Transform Infrared (FTIR) spectrometer equipped with a Thermo Fisher Smart Collector Diffuse Reflectance accessory. The FTIR spectra were collected over a range of 4000 to 600 cm^{-1} with continuous nitrogen purge. Two hundred scans were co-added together at a spectral resolution of 4 cm^{-1}.

5.2.3 Soil properties

Soil texture and chemical properties were taken at each location and depth (0-20 cm and 20-40 cm), with five measurements for each location. The procedures used to quantify soil textural composition are described in Reyes et al. (2018). Soil organic matter and total nitrogen were determined by LECO combustion. Extractable P, K, Ca, Mg, and Zn were measured by Mehlich III extraction. For pH determination, a glass electrode was used in 1:1 soil:water and Sikora buffer for Buffer pH (Jones, 2000).

5.3 Results and Discussion

5.3.1 Clay Mineralogy

X-ray diffraction patterns of the clay fraction are presented in figures 5.2 and 5.3. In all cases, the appearance of an asymmetric 1.4 nm peak with the Mg treatment was observed which could reflect a combination of different minerals such as vermiculite, smectite and chloritized vermiculite or smectite (HIV or HISM). The XRD peak at 1.2 nm is indicative of mixed-layer minerals, perhaps illite interstratified with vermiculite. Peaks at 1.0, 0.49 and 0.33 nm could indicate the presence of illite. The Mg-glycerol treatment was employed to identify the presence of expanding smectitic minerals. This treatment resulted in a reduction in intensity of the 1.4 nm peak and some noisy peaks were observed in the range of 1.4-1.8 nm; specifically in the Crider III at both depths. The lower signal to noise ratio in glycerol-treated clay slides made it difficult to clearly identify a peak at 1.8 nm attributed to smectite. Thus, possible 2:1 expandable minerals are vermiculite, smectite, HIV/HISM, and mixed-layer minerals, although due to the noise in the signal it cannot be clearly stated what specific mineral is present in each area.

After applying the K at 25 °C and 550 °C treatments, we observe other differences among locations (Figure 5.3). In the K 25 °C treatment, a collapse of the 1.4 nm peak was evident. The 0.71 nm peak found with the Mg treatment which collapsed after the K 550 °C treatment is an indicator that kaolinite is present. It is interesting that there still were peaks between 1.0 and 1.4 nm, attributed to the resistant HIV/HISM minerals that cannot totally collapse to 1.0 nm. The TA analysis is presented in Figure 5.4. The differential weight loss causes peaks around 25 °C, 250 °C, 400 °C and 500 °C, which could be attributed to

smectite/vermiculite, gibbsite, goethite and kaolinite, respectively. Regarding the peak around 250 °C, it could be caused by the hydroxyl-Al layer of HIV/HISM minerals, considering that a characteristic peak for gibbsite was not detected with the x-ray diffraction analysis. A mineral quantification using TA (Karathanasis and Harris, 1994) is presented in Table 5.1. We found that the kaolinite and goethite percentage are higher in the eroded area (Crider III) compared with other locations. A similar trend is observed with smectite/vermiculite at the 20-40 cm depth. A reason for this behavior could be the fact that erosion has been occurring in this zone of the field, and a part of the original surface layer has been lost.

Table 5.1. Quantitative mineralogical composition of the clay fraction using Thermogravimetric analysis.

Location	Kaolinite	Smectite/Vermiculite/ HIV/HISM	Al-hydroxyl interlayer	Goethite
		%		
Nolin (0-20 cm)	29.3	21.9	3.0	6.7
Crider I (0-20 cm)	28.5	19.4	2.1	7.8
Crider II (0-20 cm)	31.2	19.5	3.2	5.0
Crider III (0-20 cm)	37.3	21.3	2.3	11.8
Nolin (20-40 cm)	29,1	18.1	1.9	5.2
Crider I (20-40 cm)	32.8	25.6	2.6	15.8
Crider II (20-40 cm)	42.6	25.3	3.9	11.2
Crider III (20-40 cm)	38.6	31.6	4.3	18.3

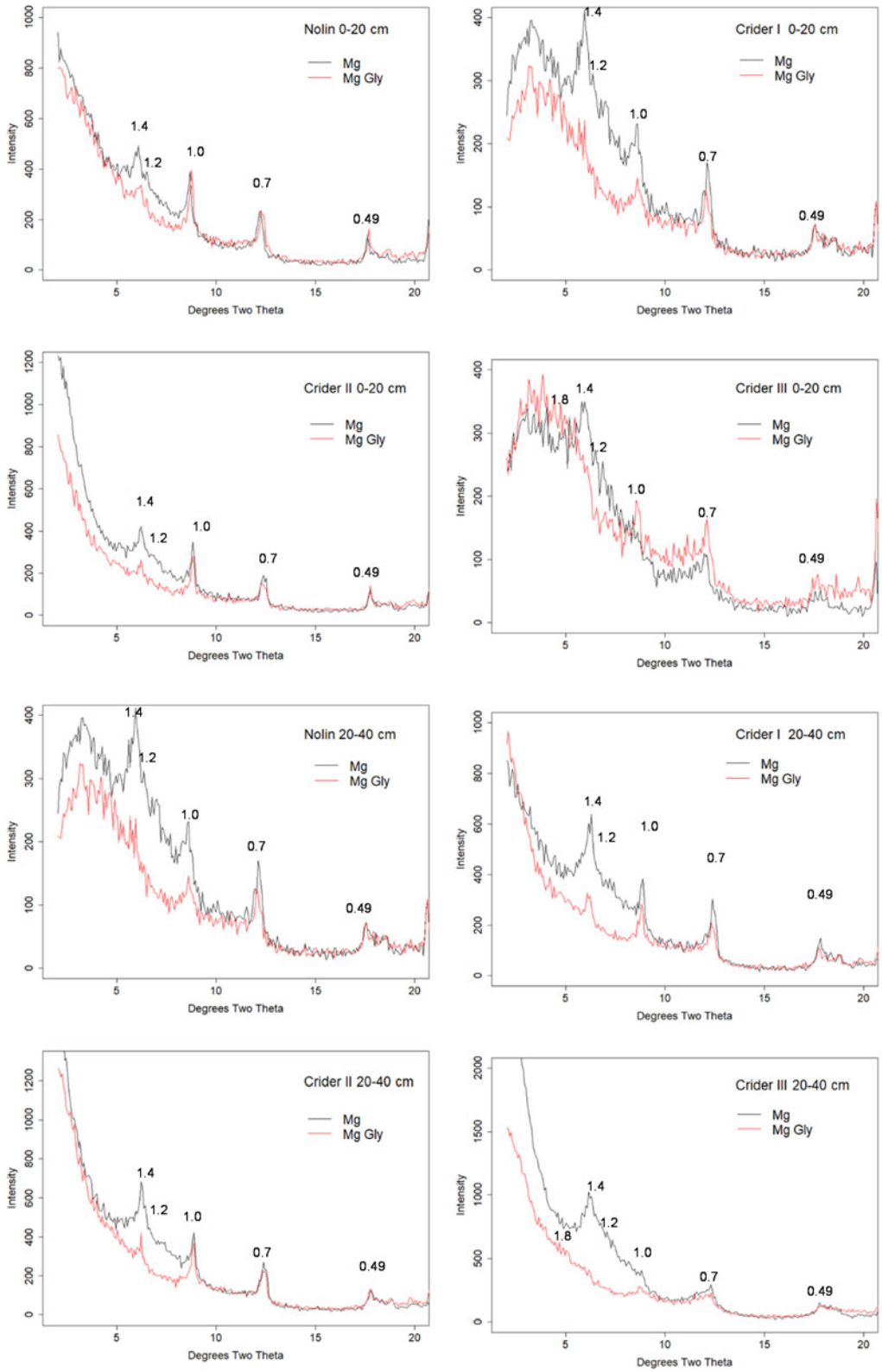

Figure 5.2. X-ray diffraction patterns of clay fractions for Mg and Mg glycerol treatments at different locations and depths.

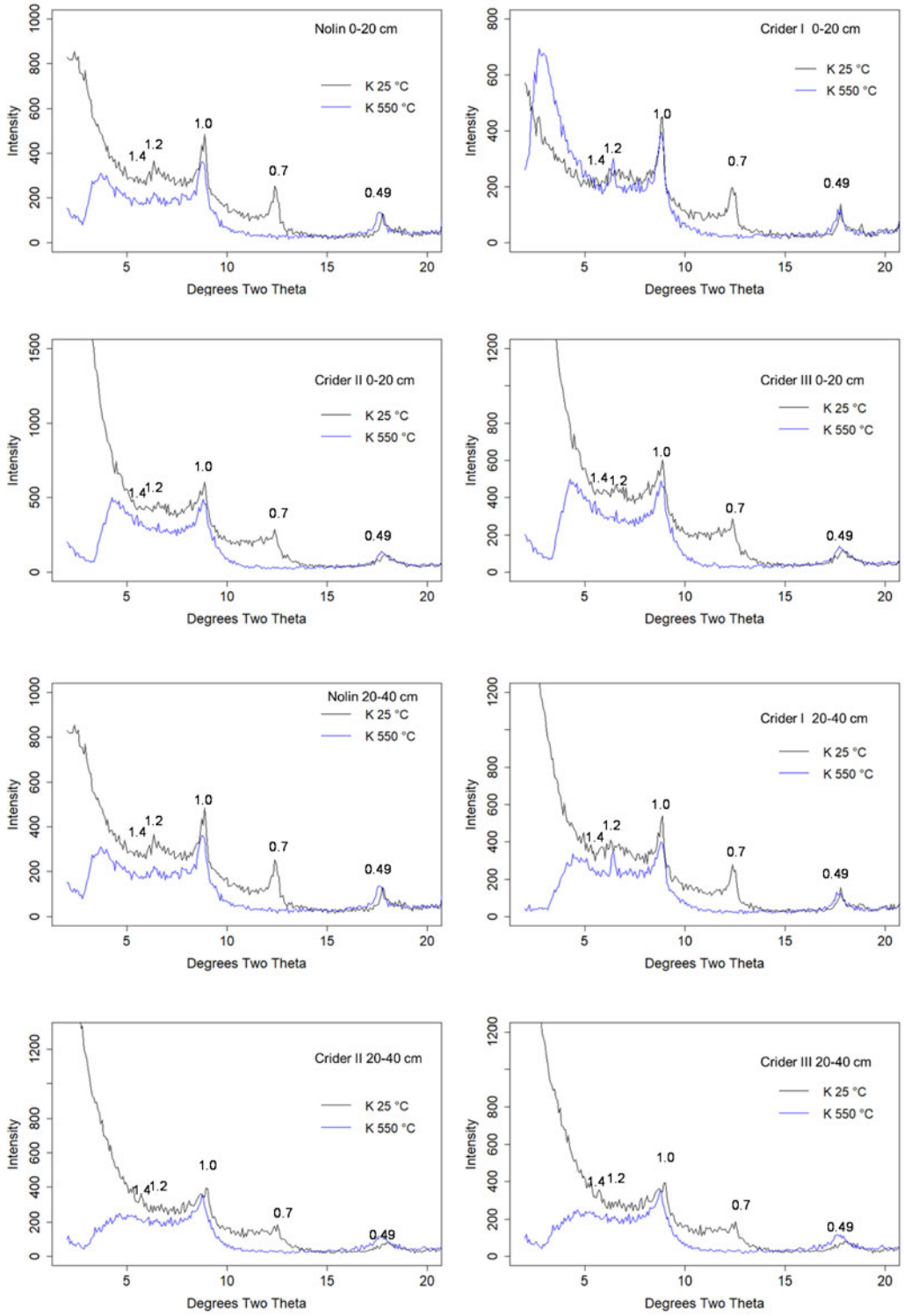

Figure 5.3. X-ray diffraction patterns of clay fractions for K 25 °C and K 550 °C treatments at different locations and depths.

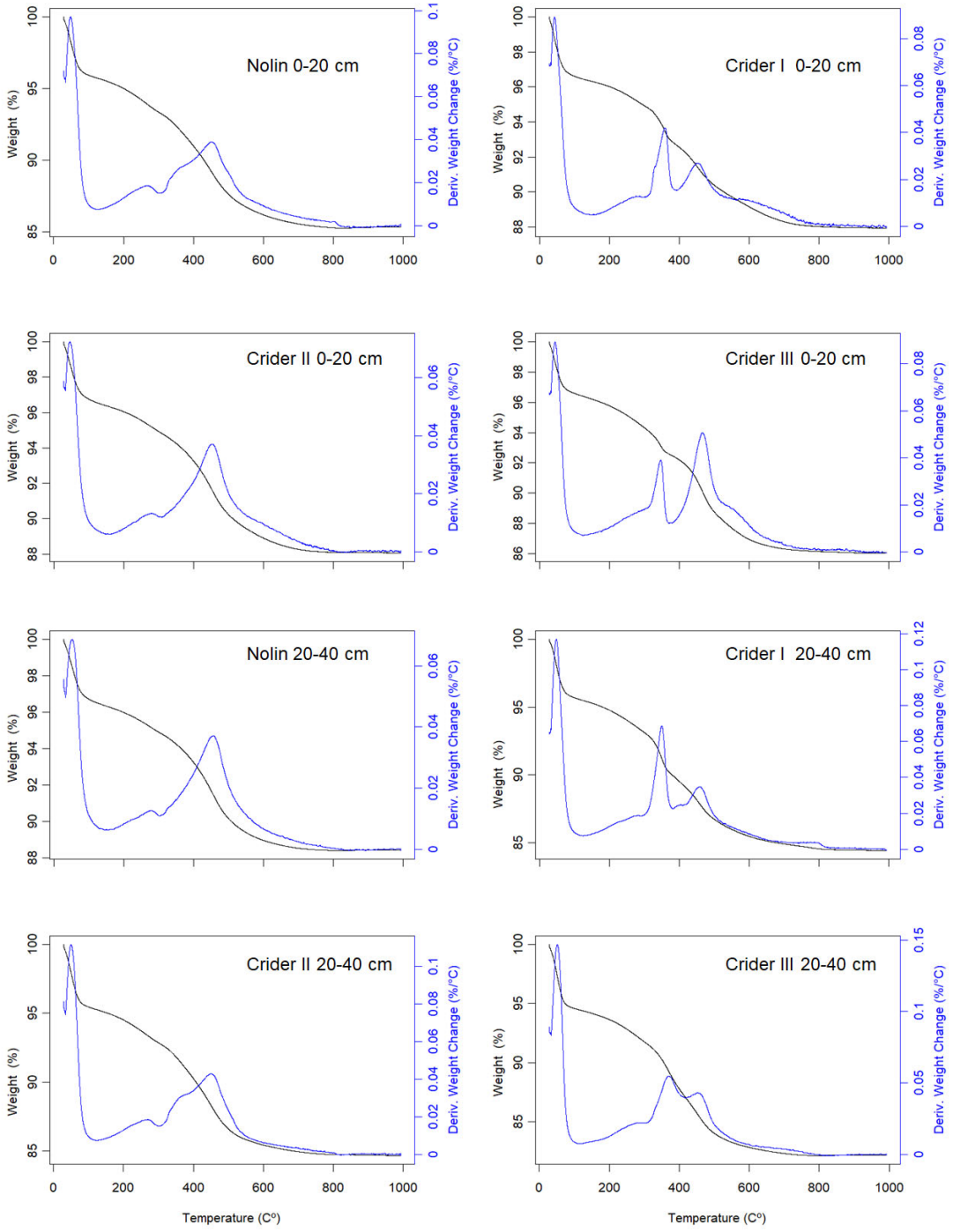

Figure 5.4. Thermal analysis of clay fractions at different locations and depths.

Results of the FTIR analysis are presented in Figure 5.5. The patterns obtained for the different locations share more similarity compared to the results that were obtained with the x-ray diffraction, while it helps to corroborate minerals identified with the x-ray diffraction. The IR band 3695 cm^{-1} is an indicator of Kaolinite, IR bands at 3620 cm^{-1} and 914 cm^{-1} could indicate the presence of vermiculite and illite as well as kaolinite (Russell, 1987, Matocha et al., 2016).

In addition, a peak near 1430 cm^{-1} was observed. It could be associated to the N-H bending mode of NH_4^+ in 2:1 phyllosilicates (Stone and Wild, 1978; Matocha et al., 2016). This peak increased in intensity at the 20-40 cm depth especially at the Crider II and Crider III locations. This peak has been assigned to NH_4^+ bound in either illite and/or vermiculite minerals. Matocha et al. (2016) observed this peak in a soil clay from an agroecosystem receiving nitrogen fertilizer, however, NH_4^+-illite can also occur naturally during weathering and diagenesis (Šucha et al., 2001). In our field, this particular peak was more marked in the eroded area and the subsurface (20-40 cm) than in other zones and depths, probably because the accessibility of plant roots to NH_4^+ and its oxidation to NO_3^- is more restricted here.

On the other hand, although organic matter was removed prior to the mineralogical characterization, peaks were observed in the range 1500-1700 cm^{-1} (i.e. C-H bend, Aromatic C=C stretch, Amide groups) and 2800-3000 cm^{-1} (i.e. CH_3 stretching mode) that can be associated with organic compounds; especially around 1570 cm^{-1} in Crider II and Crider III at 20-40 cm depth. This behavior could be due to tightly bound organic compounds in

the interlayer of 2:1 minerals (Skiba et al., 2011; Matocha et al., 2016) which can affect the observed x-ray diffraction peaks.

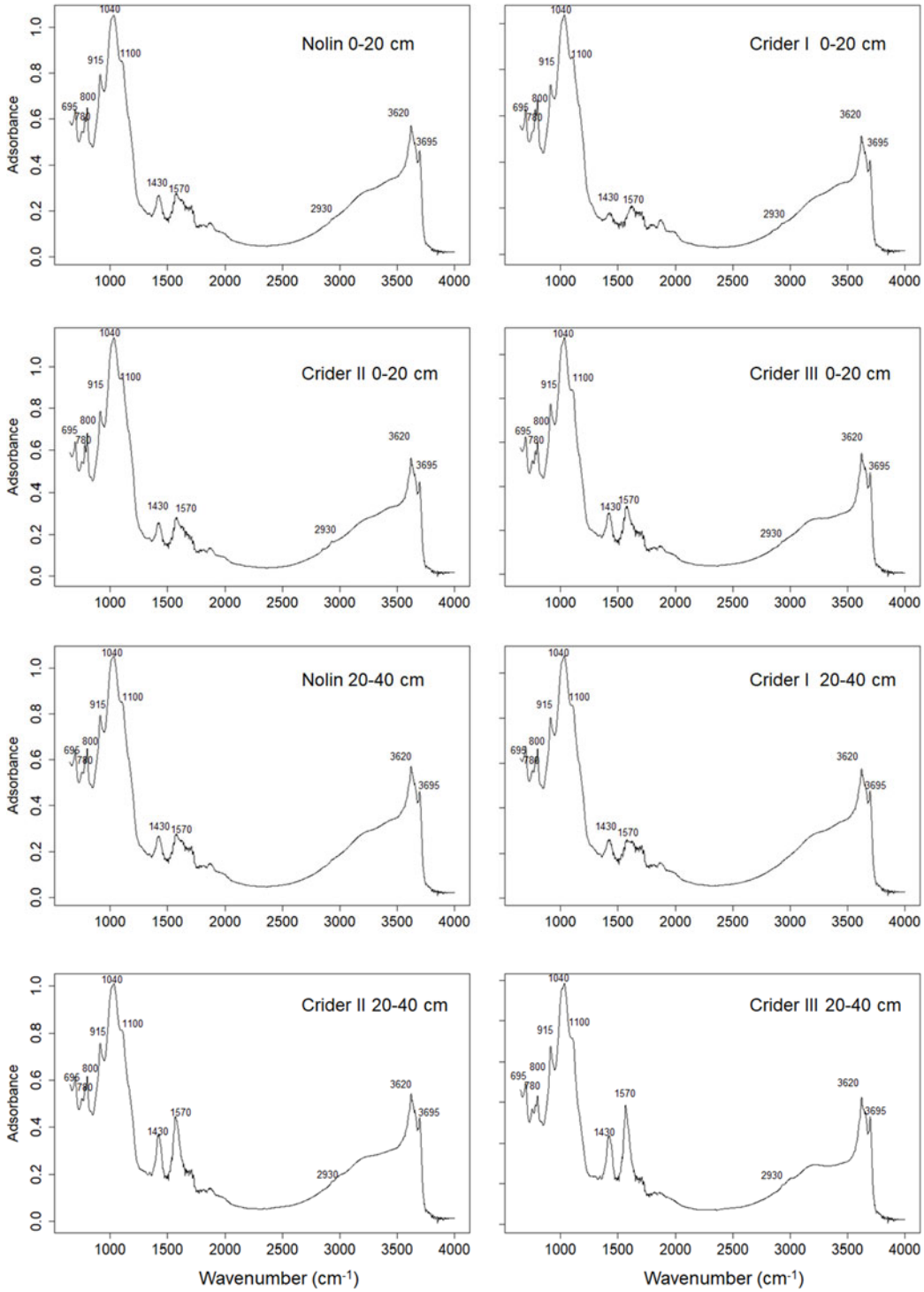

Figure 5.5. Fourier transform infrared (FTIR) spectra of clay fractions at different locations and depths.

5.3.2 Soil properties at each location

Soil properties measured at each of the selected locations are presented in Table 5.2. In general, the shallow soil presents more silt and soil nutrients compared with the 20-40 cm. In Crider III, the percentage of clay content is higher at 0-20 cm, with a texture corresponding to silty clay loam, although the soil surface is classified as silt loam across the entire field. Another characteristic in the Crider III area is the lower amount of exchangeable K and P. The larger amount of clay, including smectite, vermiculite and kaolinite minerals, could induce a higher fixation in this area. On the other hand, we observe that exchangeable C and Mg increase in the Crider III. The increase of Mg could be caused due to the weathering of vermiculite and HIV minerals (also increasing the presence of kaolinite). A lower C:Mg ratio (Haghnia and Pratt, 1988) in Crider III could cause a lower structural stability compared with other areas.

Table 5.2. Soil properties obtained at different locations and depths.

Location	Silt	Clay	OM	N	P	K	Ca	Mg	Zinc	pH
	%				kg ha^{-1}					
Nolin (0-20 cm)	77.3	20.9	1.3	0.07	122.6	261.9	3000.2	171.7	3.2	5.2
Crider I (0-20 cm)	77.1	19.1	1.2	0.07	194.5	281.6	3103.6	124.9	3.9	5.3
Crider II (0-20 cm)	74.5	23.1	1.8	0.10	89.0	432.4	4053.4	191.3	4.9	5.5
Crider III (0-20 cm)	68.3	27.8	1.5	0.08	21.7	259.4	5368.0	288.9	1.5	5.7
Nolin (20-40 cm)	69.7	25.4	0.7	0.06	36.8	175.0	3175.5	172.8	1.4	5.5
Crider I (20-40 cm)	69.6	27.7	0.9	0.06	102.7	211.8	3431.7	125.5	2.9	5.7
Crider II (20-40 cm)	68.2	29.1	0.9	0.07	32.8	293.7	3486.3	187.2	1.9	5.8
Crider III (20-40 cm)	64.8	29.5	0.6	0.05	3.5	204.2	4367.0	315.8	2.8	5.4

According to the official soil survey, a large percentage of the field is classified as an Alfisol (Crider series) and another section is classified as Inceptisol (Nolin). Nevertheless,

we found higher differences in mineralogy and soil properties in the eroded area compared with the rest of the field than between Nolin and Crider I-II areas. Soil classification maps are informative tools to obtain a general approach of the soil characteristics, but considering the scale resolution (generally around 1:12,000-1:25,000) it may not reveal a sufficient accuracy for various purposes at the field scale. Nevertheless, we found that soil properties vary in areas classified with different levels of erosion. Further mineralogy-based soil survey is required if the intention is to base site-specific management decisions on knowledge about mineralogy. In this study, the soil mineralogy varies at the field scale and it is related to other soil properties. Knowledge of field scale differences should be considered for soil management.

5.4 Summary

A clay mineralogical characterization was performed in a farmer's field. X-ray diffraction, thermogravimetric analysis and Fourier infrared spectroscopy (FTIR) were the methods applied. Observations were compared with soil physical and chemical properties. Kaolinite, vermiculite and HIV, were among the identified minerals over the entire field, and possibly, smectite was also observed within the most eroded zone (Crider III). Crider III also presents most distinct differences in soil properties, and the highest kaolinite and goethite quantity at both depths (0-20 cm and 20-40 cm). FTIR analysis shows a wavenumber (1430 cm^{-1}) that could be related with NH_4^+ fixation in some areas of the field. This information can help to have better understanding of spatial variability of other soil properties such as soil structure, CEC, nutrient fixation and soil water movement.

Copyright © Javier Reyes 2018

Chapter 6 Conclusions

A field scale investigation was performed to explore spatial and temporal relationships to improve irrigation management in a farmer's field located in Western Kentucky. Several methods were applied to characterize and map soil and crop variables. A study of mapping clay content coregionalized with apparent electrical conductivity was conducted. Soil sampling density was reduced from 96 to 48, 24, and 12 data points under different scenarios. Clay content maps estimated with cokriging utilizing high-density ancillary EC_a information were more precise than maps derived from ordinary univariate kriging and maintained a satisfactory precision when the sampling density was reduced to 1 sample per 2 hectares. This result shows that using apparent electrical conductivity as ancillary data is satisfactory to map clay content, even with low soil textural sampling density.

A set of direct and indirect measurements including soil clay content, apparent electrical conductivity, soil chemical properties (pH, organic matter, total nitrogen, P, K, Ca, Mg and Zn), satellite-based NDVI, topographic indices were used to delineated management zones. Cluster analyses revealed that 2 to 3 zones were the optimal number of classes when based on different criteria. Delineated zones were evaluated and revealed significant differences in corn yield and different patterns in temporal dynamics of soil moisture.

Soil water status was studied at different zones, based on the division presented on chapter 3. Root Zone Water Quality Model (RZWQM2) was used to predict temporal variation of soil water tension. The results indicated spatial differences of soil water tension at different depths and delineated zones. This behavior of soil water tension has concordances with the

spatial variation of other soil properties. Soil water tension predictions were better in the surface layer under both wheat and corn, while being more accurate under wheat. After model calibration, the estimation improved and satisfactory results were obtained in the surface layer. Our study demonstrates differences in soil water dynamics at the field scale that indicate the requirement for site-specific management. RZWQM2 shows to be an appropriate tool to identify differences in soil water status at different zones of the field. Predicted soil water tension could be utilized for irrigation management to decide when to turn on the irrigation water, and the amount of water to be applied could also be derived from model estimations.

A characterization of spatial differences in clay mineralogy was performed in the field. Sampling locations were based on the soil survey map divisions. Dominant minerals found were kaolinite, vermiculite and HIV, whereas smectite was also identified in the most eroded zone. Differences in mineral composition quantities were found when comparing areas. In the area severely eroded the presence of kaolinite was higher; also this sector presented low organic matter and high clay content. This result has concordance with the differences observed in soil water status in the eroded area in chapter 4, where the soil tended to dry faster between rainfall events. Results of the FTIR analysis were consistent with those obtained with the other methods. Moreover, a wavenumber peak that could be related with NH_4^+ fixation (1430 cm^{-1}) was found in some areas of the field. Spatial differences found in clay mineralogy could be considered as helpful guidance for precision agriculture management decisions.

The study shows the ability of the presented methods to identify and characterize field spatial variability, combining easily obtainable data to be applied for revealing soil and crop processes and their spatial variability under real-world farm conditions.

Copyright © Javier Reyes 2018

References

Adams, R.R., Berg, A.A., McNairn, H., 2013. Field level soil moisture variability at 6- and 3-cm sampling depths: implications for microwave sensor validation. Vadose Zone J. 12. http://dx.doi.org/10.2136/vzj2012.0070.

Ahuja, L. R., K. W. Rojas, J. D. Hanson, M. J. Shaffer, and L. Ma, eds. 2000. The Root Zone Water Quality Model. Highlands Ranch, Colo.: Water Resources Publications.

Allen, R. G., M. Tasumi, and R. Trezza. 2007. Satellite-based energy balance for mapping evapotranspiration with internalized calibration (METRIC) – Model. Journal of Irrigation and Drainage Engineering, vol. 133, p. 380.

Alperovitch, N, Shaiberg, I. and Keren, R. 1981 Specific effect of magnesium on the soil hydraulic conductivity of sodic soils. Journal of Soil Science, 32; 543-554

Anapalli, Saseendran S., L. Ma, D. C. Nielsen, M. F. Vigil, and L. R. Ahuja. 2005. Simulating planting date effects on corn production using RZWQM and CERES-maize models. Agronomy Journal 97, (1) (Jan): 58-71.

Baes, A.U., and P.R. Bloom. 1989. Diffuse reflectance and transmission Fourier transform infrared (DRIFT) spectroscopy of humic and fulvic acids. Soil Science Society of America Journal, 53(3): 695-700.

Beckett, P.H.T., and R. Webster. 1971. Soil variability: A review. Soils and Fertilizers 34:1–15.

Bell, K.R., B.J. Blanchard, T.J. Schmugge, M.W. Witczak. Analysis of surface moisture variations within large-field sites Water Resour. Res., 16 (4) (1980), pp. 796-810

Bishop, T.F.A, and A.B McBratney. 2001. A comparison of prediction methods for the creation of field-extent soil property maps. Geoderma 103:149–160. doi:10.1016/S0016-7061(01)00074-X

Biswas, A., and B.C. Si. 2011. Application of continuous wavelet transform in examining soil spatial variation: a review. Math. Geosci. 43: 379-396.

Biswas, A. 2014. Landscape characteristics influence the spatial pattern of soil water storage: similarity over times and at depths. Catena 116: 68-77

Blöschl, G., and M. Sivapalan. 1995. Scale issues in hydrological modeling-a review. Hydrol. Proc. 9: 251-290. doi: 10.1002/hyp.3360090305

Boyle, D.P., H.V. Gupta, and S. Sorooshian. 2000. Toward improved calibration of hydrologic models: Combining the strengths of manual and automatic methods. Water Resour. Res. 36:3663–3674

Boyer, C.N., J.A. Larson, R.K. Roberts, A.T. McClure, and D.D. Tyler. 2014. The impact of field size and energy cost on the profitability of supplemental corn irrigation, Agricultural Systems 127: 61-69.

Bronson, K.F., J.D. Booker, S.J. Officer, R.J. Lascano, S.J. Maas, S.W. Searcy, and J. Booker. 2005. Apparent electrical conductivity, soil properties and spatial covariance in the U.S. Southern high planes. Precis. Agric. 6: 297–311. doi:10.1007/s11119-005-1388-6

Brooks, R. H., and A. T. Corey. 1964. Hydraulic properties of porous media. Hydrology Paper No. 3. Fort Collins, Colo.: Colorado State University.

Brown, M.E., J.E. Pinzon, K. Didan, J.T. Morisette, and C.J. Tucker. 2006. Evaluation of the consistency of long-term NDVI time series derived from AVHRR, SPOT-

vegetation, SeaWiFS, MODIS, and Landsat ETM+ sensors. IEEE Trans. Geosci. Remote Sens. 44:1787–1793. doi:10.1109/TGRS.2005.860205

Burke I.C., C.M. Yonker, W.J. Parton, C.V. Cole, K. Flach, and Schimel D.S. 1989. Texture, climate, and cultivation effects on soil organic matter content in US grassland soils. Soil Sci. Soc. Am. J. 53:800–805. doi:10.2136/sssaj1989.03615995005300030029x

Cameira, M. R., R. M. Fernando, L. R. Ahuja, and L. S. Pereira. 2005. Simulating the fate of water in field soil-crop environment. J. Hydrol. 315(1-4): 1-24.

Carroll, Z.L., and M.A. Oliver. 2005. Exploring the spatial relations between soil physical properties and apparent electrical conductivity. Geoderma 128:354–374. doi:10.1016/j.geoderma.2005.03.008

Casa, R., F. Castaldi, S. Pascucci, B. Basso, and S. Pignatti. 2013. Geophysical and hyperspectral data fusion techniques for in-field estimation of soil properties. Vadose Zone J. 12. doi:10.2136/zj2012.0201. doi:10.2136/vzj2012.0201

Cohen, S., Y. Cohen, V. Alchanatis, and O. Levi. 2013. Combining spectral and spatial information from aerial hyperspectral images for delineating homogenous management zones. Biosyst. Eng.114:435–443. doi:10.1016/j.biosystemseng.2012.09.003

Conrad, O., B. Bechtel, M. Bock, H. Dietrich, E. Fischer, L. Gerlitz, J. Wehberg, V. Wichmann, and J. Böhner. 2015: System for Automated Geoscientific Analyses (SAGA) v. 2.1.4. Geosci. Model Dev. 8(7):1991-2007. doi:10.5194/gmd-8-1991-2015.

Corwin, D.L., and S.M. Lesch. 2003. Application of Soil Electrical Conductivity to Precision Agriculture: Theory, Principles, and Guidelines. Agron. J. 95:455–471. doi:10.2134/agronj2003.0455

Corwin, D.L., and E. Scudiero. 2016. Field-scale apparent soil electrical conductivity. Methods of Soil Analysis 1(1). doi:10.2136/methods-soil.2015.0038

Corwin, D.L., and S.M. Lesch. 2003. Application of Soil Electrical Conductivity to Precision Agriculture: Theory, Principles, and Guidelines. Agron. J. 95:455–471. doi:10.2134/agronj2003.0455

Dadfar, H., R.J. Heck, G.W. Parkin, and K. Barfoot-Kinsie. 2011. Evaluation of a Geonics EM31-3RT probe to delineate hydrologic regimes in a tile-drained field. Precis. Agric. 12(5) 623–638. doi:10.1007/s11119-010-9203-4

Deutsch, C.V., and A.G. Journel. 1992. GSLIB. Geostatistical software library and user's guide. Oxford University Press, New York.

Doolittle, J.A., and E.C. Brevik. 2014. The use of electromagnetic induction techniques in soils studies. Geoderma 223: 33–45. doi:10.1016/j.geoderma.2014.01.027

Downes, R.G., and R.S. Beckwith. 1951. Studies in the variation of soil reaction. I. Field variations at Barooga, N.S.W. Aust. J. Agric. Res. 2:60–72. doi:10.1071/AR9510060

Eghball, B., and G.E. Varvel. 1997. Fractal analysis of temporal yield variability of crop sequences: Implications for site-specific management. Agron. J. 89:851-855. doi:10.2134/agronj1995.00021962008700020003x

Essington, M.E. 2004. Soil and Water Chemistry: An integrative approach. CRC Press, Boca Raton, Florida.

Evans, R.G., and E.J. Sadler. 2008. Methods and technologies to improve efficiency of water use. Water Resour. Res., 44 (7): W00E04.

Fisher, D., and P. Gould. 2012. Open-Source Hardware Is a Low-Cost Alternative for Scientific Instrumentation and Research. Modern Instrumentation 1:8–20. doi:10.4236/mi.2012.12002

Fleming, K.L., D.F. Heermann, and D.G. Westfall. 2004. Evaluating Soil Color with Farmer Input and Apparent Soil Electrical Conductivity for Management Zone Delineation. Agron. J. 96:1581–1587. doi:10.2134/agronj2004.1581

Frogbrook, Z.L. 1999. The effect of sampling intensity on the reliability of predictions and maps of soil properties. In: J.V. Stafford, editor, Precision Agriculture '99, Proceedings of the Second European Conference on Precision Agriculture, Part 1, Odense Congress Centre, Sheffield Academic Press Limited, Sheffield, UK, 11–15 July 1999, p. 71–80.

Gee, G.W., and D. Orr. 2002. Particle-size analysis. In J.H. Dame, G.C. Topp, editors, Methods of Soil Analysis, Part 4 – Physical Methods, Soil Science Society of America, Madison, WI.

Goff, A., J. Huang, V.N.L. Wong, F.A. Monteiro Santos, R. Wege, and J. Triantafilis. 2014. Electromagnetic conductivity imaging of soil salinity in an estuarine–alluvial landscape. Soil Sci. Soc. Am. J. 78(5):1686–1693. doi:10.2136/sssaj2014.02.0078

Gouhier, T.C., A. Grinstead, and V. Simko. 2016. biwavelet: Conduct univariate and bivariate wavelet analyses (Version 0.20.10). http://github.com/tgouhier/biwavelet

Gupta, H., Sorooshian, S., & Yapo, P. 1999. Status of Automatic Calibration for Hydrologic Models: Comparison with Multilevel Expert Calibration. Journal of Hydrologic Engineering /, 4(2), 135-143.

Grant, L., Seyfried, M., and McNamara, J. 2004. Spatial variation and temporal stability of soil water in a snow-dominated, mountain catchment, Hydrol. Process., 18, 3493–3511.

Grinsted, A., J.C. Moore, and S. Jevrejeva. 2004. Application of the cross wavelet transform and wavelet coherence to geophysical time series. Nonlinear Process. G. 11:561–566. doi:10.5194/npg-11-561-2004

Haghnia, G.H. and Pratt, P.F 1988 Effect of exchangeable magnesium in soils. Soil Science 145: 432-436

Haghverdi, A., B.G. Leib, R.A. Washington-Allen, M.J. Buschermohle, and P.D. Ayers. 2016. Studying uniform and variable rate center pivot irrigation strategies with the aid of site specific water production functions. Comput. Electron. Agric. 123:327–340. doi:10.1016/j.compag.2016.03.010

Heil, K., and U. Schmidhalter. 2012. Characterisation of soil texture variability using the apparent soil electrical conductivity at a highly variable site. Comput. Geosci. 39:98–110. doi:10.1016/j.cageo.2011.06.017

Hijmans, R.J. 2016. raster: Geographic Data Analysis and Modeling. R package version 2.5-8. https://CRAN.R-project.org/package=raster

Hong, S., Shin, I., 2011. A physically-based inversion algorithm for retrieving soil moisture in passive microwave remote sensing. J. Hydrol. 405 (1–2), 24–30.

Hu, W., M. Shao, F. Han, K. Reichard, J. Tan. 2010. Watershed scale temporal stability of soil water content. Geoderma, 158:180-198

Husson, F., S. Le, and J. Pages. 2010. Exploratory Multivariate Analysis by Example Using R. Chapman and Hall.

Jackson, M.L. 1974. Soil Chemical Analysis—Advanced Course. University of Wisconsin Press, Madison, WI.

James, L.A., D.G. Watson, and W.F. Hansen. 2006. South Carolina, USA. Catena 71(1):132–144. doi:10.1016/j.catena.2006.10.010

Jiang J. Feng S. Huo Z. Zhao Z. Jia B. 2011. Application of the swap model to simulate water–salt transport under deficit irrigation with saline water Math. Comput. Model. 54:902–911. doi:10.1016/j.mcm.2010.11.014

Johnson, C.K., D.A. Mortensen, B.J. Wienhold, J.F. Shanahan, and J.W. Doran. 2003. Site-specific management zones based on soil electrical conductivity in a semiarid cropping system. Agron. J. 95(2):303–315. doi:10.2134/agronj2003.0303

Jones, J.B. 2000. Soil analysis handbook of reference methods. Soil and Plant Analysis Council, Inc., CRC Press, Boca Raton, FL.

Journel, A. G., and C. J. Huijbregts, 1978. Mining Geostatistics. Academic Press, London, UK.

Karathanasis, A. D. 1985. Mineralogical Variability within Clayey Soil Control Sections and Family Mineralogy Placement. Soil Sci. Soc. Am. J. 49:691-695. doi:10.2136/sssaj1985.03615995004900030033x

Karathanasis, A. D. 1987. Mineral Solubility Relationships in Fragiudalfs of Western Kentucky. Soil Sci. Soc. Am. J. 51:474-481. doi:10.2136/sssaj1987.03615995005100020041x

Karathanasis, A. D. 1991. Seasonal Variation in Solution Composition and Mineral Stability of Two Kentucky Alfisols. Soil Sci. Soc. Am. J. 55:881-890. doi:10.2136/sssaj1991.03615995005500030044x

Karathanasis, A.A., B.F. Hayek. 1982. Revised Methods for Rapid Quantitative Determination of Minerals in Soil Clays. Soil Science Society of America Journal, 46 (2): 419–425.

Karathanasis, A.A., W.G. Harris. 1994. Quantitative thermal analysis of soil minerals. In Ammonette, J., L.W. Zelazny (ed.). Quantitative methods in soil mineralogy. Soil Sci. Soc. Am. Miscellaneous Publication. Soil Sci. Soc. Am. Madison, WI.

Karathanasis, A.D. 1987. Mineral solubility relationships in Fragiudalfs of western Kentucky. Soil Sci. Soc. Am. J. 51(2):474–481. doi:10.2136/sssaj1987.03615995005100020041x

Karathanasis, A.D., and K.L. Wells. 1990. Conservation tillage effects on the potassium status of some Kentucky soils. Soil Sci. Soc. Am. J. 54:800–806

Karathanasis, A.D.; Golrick, P.A.; Barnhisel , R.I. 1991. Soil formation on loess/sandstone toposequences in west-central Kentucky. II. Mineralogical relationships. Soil science 152 (3): 151-161. doi: 10.1097/00010694-199109000-00002

Karathanasis, AD. B.R. Macneal. 1994. Evaluation of parent material uniformity criteria in loess influenced soils of west-central Kentucky, Geoderma 64(1-2):73-92. doi: 10.1016/0016-7061(94)90090-6.

Karathanasis, A.D., and D.M.C. Johnson. 2006. Stability and transportability of biosolid colloids through undisturbed soil monoliths. Geoderma 130(3–4): 334-345 doi: 10.1016/j.geoderma.2005.02.006.

Kaufman, L., and P.J. Rousseeuw. 1990. Finding Groups in Data: An Introduction to Cluster Analysis. Wiley, New York.

Kisekka, I., A. Schlegel, L. Ma, P.H. Gowda, P.V.V. Prasad. 2017. Optimizing preplant irrigation for maize under limited water in the High Plains. Agricultural Water Management 187:154-163.

Kitchen, N.R., K.A. Sudduth, D.B. Myers, S.T. Drummond, and S.Y. Hong. 2005. Delineating productivity zones on claypan soil fields using apparent soil electrical conductivity. Comput. Electron. Agric. 46(1):285–308. doi:10.1016/j.compag.2004.11.012.

Kitchen, N.R., S.T. Drummond, E.D. Lund, K.A. Sudduth, and G.W. Buchleiter. 2003. Soil electrical conductivity and topography related to yield for three contrasting soil-crop systems Agron. J. 95(3):483–495. doi: 10.2134/agronj2003.0483

Koestel, J.K., T. Norgaard, N.M. Luong, A.L. Vendelboe, P. Moldrup, N.J. Jarvis, M. Lamandé, B.V. Iversen, and L.Wollesen de Jonge. 2013. Links between soil properties and steady-state solute transport through cultivated topsoil at the field scale. Water Resour. Res 49(2):790–807. doi:10.1002/wrcr.20079

Kravchenko, A., G.A Bollero, R.A Omonode, and D.G. Bullock. 2002. Quantitative mapping of soil drainage classes using topographical data and soil electrical conductivity. Soil Sci. Soc. Am. J. 66: 235–243. doi:10.2136/sssaj2002.2350

Kravchenko, A.N. 2003. Influence of spatial structure on accuracy of interpolation methods. Soil Sci. Soc. Am. J. 67:1564–1571. doi:10.2136/sssaj2003.1564

Kühn, J., A. Brenning, M. Wehrhan, S. Koszinski, and M. Sommer. 2009. Interpretation of electrical conductivity patterns by soil properties and geological maps for precision agriculture. Precis. Agric. 10:490–507. doi: 10.1007/s11119-008-9103-z

Lambot, S. et al., 2006. Analysis of air-launched ground-penetrating radar techniques to measure the soil surface water content. Water Resour. Res. 42 (11).

Landrum, C., A. Castrignano, T. Mueller, D. Zourarakis, J. Zhu, and D. de Benedetto. 2014. An approach for delineating homogeneous within-field zones using proximal sensing and multivariate geostatistics. Agric. Water Manage. 147:144–153. doi:10.1016/j.agwat.2014.07.013

Lark, R.M. 2002. Robust estimation of the pseudo cross-variogram for cokriging soil properties. Eur. J. Soil Sci. 53:253–270. doi: 10.1046/j.1365-2389.2002.00456.x

Le, S., J. Josse, and F. Husson. 2008. FactoMineR: An R Package for Multivariate Analysis. J Stat. Softw. 25(1):1–18. doi:10.18637/jss.v025.i01

Lemon, J. 2006. Plotrix: a package in the red light district of R. R-News 6(4):8–12.

Li, Y., Z.Shi, F. Li, and H.Y. Li. 2007. Delineation of site-specific management zones using fuzzy clustering analysis in a coastal saline land. Comp. Electron. Agric. 56:174–186. doi:10.1016/j.compag.2007.01.013

Li, T., X. Hao, and S.Kang. Spatiotemporal Variability of Soil Moisture as Affected by Soil Properties during Irrigation Cycles. Soil Sci. Soc. Am. J. 78:598–608.

Liang, X., V. Liakos, O. Wendroth, and G. Vellidis. 2016. Scheduling irrigation using an approach based on the van Genuchten model. Agric. Water Manag. 176:170–179. doi:10.1016/j.agwat.2016.05.030.

Lin, L. 1989. A concordance correlation coefficient to evaluate reproducibility. Biometrics 45: 255–268. doi:10.2307/2532051

Liu, T.L., K.W. Juang, and D.Y. Lee. 2006. Interpolating soil properties using Kriging combined with categorial information of soil maps. Soil Sci. Soc. Am. J. 70:1200–1209. doi:10.2136/sssaj2005.0126

Luca, C., B.C. Si, and R.E. Farrell. 2007. Upslope length improves spatial estimation of soil organic carbon content. Can. J. Soil Sci. 87:291–300. doi:10.4141/CJSS06012

Ma, L., L.R. Ahuja, B.T. Nolan, R.W. Malone, T.J. Trout, and Z. Qi. 2012. Root Zone Water Quality Model (R ZWQM2): Model use, calibration, and validation. Trans. ASABE 55:1425–1446.

Ma, L., R.W. Malone, P. Heilman, L.R. Ahuja, T. Meade, S.A. Saseendran, J.C. Ascough II, R.S. Kanwar. 2007. 4 Sensitivity of tile drainage flow and crop yield on measured and calibrated soil hydraulic properties. Geoderma 140:284–296.

Ma, L., Hoogenboom, G., Saseendran, S., Bartling, P., Ahuja, L., & Green, T. 2009. Effects of Estimating Soil Hydraulic Properties and Root Growth Factor on Soil Water Balance and Crop Production. Agronomy Journal., 101(3), 572-583.

Ma, L., L. R. Ahuja, S. A. Saseendran, R. W. Malone, T. R. Green, B.T. Nolan, P. N. S. Bartling, G. N. Flerchinger, K. J. Boote, and G. Hoogenboom. 2011. A protocol for parameterization and calibration of RZWQM2 in field research. In Methods of

Introducing System Models into Agricultural Research, 1-64. L. R. Ahuja and L. Ma, eds. Madison, Wisc.: SSSA.

Ma, L., L.R. Ahuja, J.C. Ascough II, M.J. Shaffer, K.W. Rojas, R.W. Malone, and M.R. Cameira. 2000. Integrating system modeling with field research in agriculture: Applications of Root Zone Water Quality Model (RZWQM). Adv. Agron. 71, 233–292.

Mackown, C.T., S.J. Crafts-Brandner, and T.G. Sutton. 2000. Early-season plant nitrate test for leaf yield and nitrate concentration of air-cured burley tobacco. Crop Sci. 40(1):165–170. doi:10.2135/cropsci2000.401165x

Maechler, M., P. Rousseeuw, A. Struyf, M. Hubert, and K. Hornik. 2017. cluster: Cluster Analysis Basics and Extensions. R package version 2.0.4.

Malone, R.W., B.T. Nolan, L. Ma, R.S. Kanwar, C. Pederson, P. Heilman. 2014. Effects of tillage and application rate on atrazine transport to subsurface drainage: evaluation of RZWQM using a six-year field study. Agric. Water Manag., 132:10-22

Mann, L., V. Tolbert, and J. Cushman. 2002. Potential environmental effects of corn (Zea mays L.) stover removal with emphasis on soil organic matter and erosion. Agric. Ecosyst. Environ. 89(3):149–166. doi:10.1016/S0167-8809(01)00166-9

Matocha, C.J., J. Grove, A. Karathanasis, M. Vandiviere. 2016. Changes in soil mineralogy due to nitrogen fertilization in an agroecosystem. Geoderma 263: 176–184.

McBratney, A.B., M.L.M. Santos, and B. Minasny. 2003. On digital soil mapping. Geoderma 117:3–52. doi:10.1016/S0016-7061(03)00223-4

McCutcheon, M.C., H.J. Farahani, J.D. Stednick, G.W. Buchleiter, and T.R. Green. 2006. Effect of soil water on apparent soil electrical conductivity and texture relationships in a dryland field. Biosyst. Eng. 94(1):19–32. doi:10.1016/j.biosystemseng.2006.01.002

Mohanty, P.B. Soil Hydraulic Property Estimation Using Remote Sensing: A Review. Vadose Zone J. 12. doi:10.2136/vzj2013.06.0100

Moore, I.D., P.E. Gessler, G.A. Nielsen, and G.A. Peterson. 1993. Soil attribute prediction using terrain analysis. Soil Sci. Soc. Am. J. 57:443–452. doi:10.2136/sssaj1993.03615995005700020026x

Moral, F.J., J.M. Terrón, and J.R. Marques Da Silva. 2010. Delineation of management zones using mobile measurements of soil apparent electrical conductivity and multivariate geostatistical techniques. Soil Tillage Res. 106:335–34. doi:10.1016/j.still.2009.12.002

Mueller, T. G., F. J. Pierce. 2003. Soil carbon maps: Enhancing spatial estimates with simple terrain attributes at multiple scales. Soil Sci. Soc. Am. J. 67:258–267. doi:10.2136/sssaj2003.2580

Mueller, T. G., N. J. Hartsock, T. S. Stombaugh, S.A. Shearer, P. L. Cornelius and R. I. Barnhisel. 2003. Soil Electrical Conductivity Map Variability in Limestone Soils Overlain by Loess. Agron. J. 95(3):496-507. doi:10.2134/agronj2003.4960

Mueller, T.G., F.J. Pierce, O. Schabenberger, and D.D. Warncke. 2001. Map quality for site-specific fertility management. Soil Sci. Soc. Am. J. 65:1547–1558. doi:10.2136/sssaj2001.6551547x

Mueller, T.G., N.B. Pusuluri, K.K. Mathias, P.L. Cornelius, R.I. Barnhisel. 2014. Site-specific soil fertility management: a model for map quality. Soil Sci. Soc. Am. J., 68: 2031-2041.

Myers, D. E. 1991, Pseudo-cross variograms, positive-definiteness, and cokriging. Math Geol. 23(6): 805–816. doi:10.1007/BF02068776

Nash, J. E., and J. V. Sutcliffe. 1970. River flow forecasting through conceptual models: Part 1. A discussion of principles. J. Hydrol. 10(3): 282-290.

Nielsen, D.R., and O. Wendroth. 2003. Spatial and temporal statistics: sampling field soils and their vegetation. Catena Verlag, Reiskirchen, Germany.

Nielsen, D.R., J.W. Biggar, K.T. Erh. 1973. Spatial variability of field-measured soil-water properties. Hilgardia, 42 (7): 215-259

Ochsner, T.E., M.H. Cosh, R.H. Cuenca, W.A. Dorigo, C.S. Draper, Y. Hagimoto, Y.H. Kerr, E.G. Njoku, E.E. Small, and M. Zreda. 2013. State of the art in large-scale soil moisture monitoring. Soil Sci. Soc. Am. J., 77: 1888–1919.

Odeh, I.O., A.B. McBratney, and D.J. Chittleborough. 1992. Soil pattern recognition with fuzzy c-means: application to classification and soil-landform interrelatioship. Soil Sci Soc Am J. 56: 505–516. doi:10.2136/sssaj1992.03615995005600020027x

Odeh, I.O., and A.B. McBratney. 2000. Using AVHRR images for spatial prediction of clay content in the lower Namoi Valley of eastern Australia. Geoderma 97(3):237–254. doi:10.1016/S0016-7061(00)00041-0

Olmedo, G., S. Ortega-Farías, D. Fonseca-Luengo, D. de la Fuente-Sáiz, F. Fuentes, and M. Munafó. 2017. water:Actual Evapotranspiration with Energy Balance Models. R package version 0.7. https://CRAN.R-project.org/package=water

Pebesma, E.J. 2004. Multivariable geostatistics in S: the gstat package. Comput. Geosci.-UK 30:683–691. doi:10.1016/j.cageo.2004.03.012

Pebesma, E.J. 2004. Multivariable geostatistics in S: the gstat package. Comput. Geosci.-UK 30:683–691. doi:10.1016/j.cageo.2004.03.012

Peña J.M., J. Torres-Sánchez, A.I. de Castro, M. Kelly, F. López-Granados. 2013. Weed Mapping in Early-Season Maize Fields Using Object-Based Analysis of Unmanned Aerial Vehicle (UAV) Images. PLoS ONE 8(10):e77151. doi:10.1371/journal.pone.0077151

Peralta, N.R., J.L. Costa, M. Balzarini, H. Angelini. 2013. Delineation of management zones with measurements of soil apparent electrical conductivity in the southeastern pampas. Can. J. Soil Sci. 93:205–218. doi:10.4141/cjss2012-022

Peralta, N.R., J.L. Costa, M. Balzarini, M.C. Franco, M. Córdoba, and D. Bullock. 2015. Delineation of management zones to improve nitrogen management of wheat. Comput. Electron. Agric. 110:103–113. doi:10.1016/j.compag.2014.10.017

Qi, Z., L. Ma, M.J. Helmers, L.R. Ahuja, and R.W. Malone. 2012. Simulating nitrate-nitrogen concentration from a subsurface drainage system in response to nitrogen application rates using RZWQM2. J. Environ. Qual. 41:289–295. doi:10.2134/jeq2011.0195

Quinn, P.F., K. Beven, P. Chevallier, and O. Planchon. 1991. The prediction of hillslope flow paths for distributed hydrological modelling using digital terrain models. Hydrol. Process. 5(1):59–79. doi: 10.1002/hyp.3360050106

R Core Team. 2017. R: A language and environment for statistical computing. R Foundation for Statistical Computing, Vienna, Austria. URL https://www.R-project.org/.

Raun, W.R., J.B. Solie, G.V. Johnson, M.L. Stone, R.W. Mullen, K.W. Freeman, W.E. Thomason, and E.V. Lukina, 2002. Improving nitrogen use efficiency in cereal grain production with optical sensing and variable rate application. Agron. J. 94(4):815–820.

Reyes, J., O. Wendroth, C. Matocha, J. Zhu, W. Ren, and A.D. Karathanasis. 2018. Reliably Mapping Clay Content Coregionalized with Electrical Conductivity. Soil Science Society of America Journal, https:// doi:10.2136/sssaj2017.09.0327

Ribeiro Jr P., and P.J. Diggle. 2016. geoR: Analysis of Geostatistical Data. R package version 1.7-5.2. https://CRAN.R-project.org/package=geoR

Roger, S., E. Pebesma, and V. Gomez-Rubio. 2013. Applied spatial data analysis with R, Second edition. Springer, NY, USA.

Ruffo, M., G. Bollero, D.S. Bullock, D.G. Bullock. 2006. Site-specific production functions for variable rate corn nitrogen fertilization. Precis. Agric. 7:327–342. doi:10.1007/s11119-006-9016-7

Russell, J.D., 1987. Infrared methods. In: Wilson, M.J. (Ed.), A Handbook of Determinative Methods in Clay Mineralogy. Chapman and Hall, New York, pp. 133–173.

Sadler, E. J., R. G. Evans, K. C. Stone, and C. R. Camp. 2005. Opportunities for conservation with precision irrigation. Journal of Soil and Water Conservation 60, (6) (Nov): 371-379, http://ezproxy.uky.edu/login?url=https://search-proquest-

com.ezproxy.uky.edu/docview/220977725?accountid=11836 (accessed June 3, 2018).

Sarkar, D. 2008. Lattice: Multivariate Data Visualization with R. Springer, New York.

Saseendran, S.A., Ahuja, L.R., Ma, L., Trout, T.J., McMaster, G.S., Nielsen, D.C., Ham, J.M., Andales, A.A., Halvorson, A.D., Chávez, J.L., Fang, Q.X., 2014. Developing and normalizing average corn crop water production functions across years and locations using a system model. Agric. Water Manage. 157: 65–77.

Schepers, A.R., J.F. Shanahan, M.A. Liebig, J.S. Schepers, S.H. Johnson, and A. Luchiari. 2004. Appropriateness of management zones for characterizing spatial variability of soil properties and irrigated corn yields across years. Agron. J. 96:195–203. doi:10.2134/agronj2004.1950

Schulze, D.G. 1989. An introduction to soil mineralogy. Dixon, J.B., S.B. Weed (Eds.), Minerals in Soil Environments (2nd ed.), Soil Science Society of America, Madison, Wisc.

Šimůnek, J., M. Šejna, and M. Th. van Genuchten, New Features of the Version 3 of the HYDRUS (2D/3D). 2017. Computer Software Package, Journal of Hydrology and Hydromechanics, 66(2), 133-142, doi: 10.1515/johh-2017-0050, 2018.

Skiba, M., M. Szczerba, S. Skiba, D.L. Bish, M. Grybos. 2011. The nature of interlayering in clays from a podzol (Spodosol) from the Tatra Mountains, Poland. Geoderma 160: 425–433.

Soil Survey Staff. 1999. Soil Taxonomy. A basic system of soil classification for making and interpreting soil surveys, 2nd edition. Agricultural Handbook 436, Natural. Resources Conservation Service, USDA, Washington DC, USA.

Soil Survey Staff, Natural Resources Conservation Service, United States Department of Agriculture. 2017. Web Soil Survey. https://websoilsurvey.sc.egov.usda.gov/. Accessed January 10, 2017

Stevenson, M., T. Nunes, C. Heuser, J. Marshall, J. Sanchez, R. Thornton, J. Reiczigel, J. Robison-Cox, P. Sebastiani, and P. Solymos. 2017. epiR: Tools for the analysis of epidemiological data. R package version 0.9-87.

Stone, M.H., A. Wild. 1978. The reaction of ammonia with vermiculite and hydrobiotite. Clay Minerals 13: 337–350.

Sudduth K.A., N.R. Kitchen, W.J. Wiebold, W.D. Batchelor, G.A. Bollero, D.G. Bullock, D.E. Clay, H.L. Palm, F.J. Pierce, R.T. Schuler, and K.D. Thelen. 2005. Relating apparent electrical conductivity to soil properties across the north-central USA. Comput. Electron. Agr. 46: 263–283. doi: 10.1016/j.compag.2004.11.010

Sudduth, K.A., N.R. Kitchen, G.A. Bollero, D.G. Bullock, and W.J. Wiebold. 2003. Comparison of electromagnetic induction and direct sensing of soil electrical conductivity. Agron. J. 95:472–482. doi:10.2134/agronj2003.4720

Šucha, V., J. Środon, N. Clauer, F. Elsass, D.D. Eberl, I. Kraus, and J. Madejová. 2001. Weathering of smectite and illite-smectite under temperate climatic conditions. Clay Minerals 36, 403-419.

Taylor, K. 2001. Summarizing multiple aspects of model performance in a single diagram. J Geophys. Res. Atmos. 106.D7:7183–7192. doi:10.1029/2000JD900719

Teal, R., B. Tubana, K. Girma, K. Freeman, D. Arnall, O. Walsh, and W. Raun. 2006. In-season prediction of corn grain yield potential using normalized difference vegetation index. Agron. J. 98(6):1488-1494. doi:10.2134/agronj2006.0103

Tremblay, N., Y.M. Bouroubi, C. Bélec, R.W. Mullen, N.R. Kitchen, W.E. Thomason, S. Ebelhar, D.B. Mengel, W.R. Raun, D.D. Francis, and E.D. Vories. 2012. Corn response to nitrogen is influenced by soil texture and weather. Agron. J. 104(6):1658–1671. doi:10.2134/agronj2012.0184

Triantafilis, J., A.I. Huckel, and I.O. Odeh. 2001. Comparison of statistical prediction methods for estimating field-scale clay content using different combinations of ancillary variables. Soil Sci. 166 (6), 415–427. doi:10.1097/00010694-200106000-00007

Triantafilis, J., and S.M. Lesch. 2005. Mapping clay content variation using electromagnetic induction techniques. Comput. Electron. Agric. 46(1):203–237. doi:10.1016/j.compag.2004.11.006

Triantafilis, J., S.M. Lesch, K. La Lau, and S.M. Buchanan. 2009. Field level digital mapping of cation exchange capacity using electromagnetic induction and a hierarchical spatial regression model. Aust. J. Soil Res. 47, 651–663. doi:10.1071/SR08240

U.S. Geological Survey. 2016. Landsat-8 data user handbook. USGS. USA.

US climate data. 2017. Climate Princeton – Kentucky. http://www.usclimatedata.com/climate/princeton/kentucky/united-states/usky1255 (accessed 10 Apr. 2017)

Vachaud, G., A. Passerat de Silans, P. Balabanis, and M. Vauclin. 1985. Temporal stability of spatially measured soil water probability density function. Soil Sci. Soc. Am. J. 49:822–828. doi:10.2136/sssaj1985.03615995004900040006x

Van Genuchten, M. Th. 1980. A closed-form equation for predicting the hydraulic conductivity of unsaturated soils. Soil Sci. Soc. Am. J. 36:380-383.

Van Meirvenne, M., M. Islam, P. De Smedt, E. Meerschman, E. Van De Vijver, and T. Saey. 2013. Key variables for the identification of soil management classes in the aeolian landscapes of north–west Europe. Geoderma 199:99–105. doi:10.1016/j.geoderma.2012.07.017

Vereecken H., J.A. Huisman, Y. Pachepsky, C. Montzka, J. van der Kruk, H. Bogena, L. Weihermüller, M. Herbst, G. Martinez, J. Vanderborght. 2014. On the spatio-temporal dynamics of soil moisture at the field scale. Journal of Hydrology 516: 76-96.

Vereecken, H., A. Schnepf, J.W. Hopmans, M. Javaux, D. Or, T. Roose, J. Vanderborght, M.H. Young, W. Amelung, M. Aitkenhead, and S.D. Allison. 2016. Modeling soil processes: Review, key challenges, and new perspectives. Vadose Zone J. 15(5). doi: 10.2136/vzj2015.09.0131

Veris Technologies. 2017. Veris 3150. http://www.veristech.com (accessed 20 Jun. 2017)

Viscarra Rossel, R.A., V.I. Adamchuk, K.A. Sudduth, N.J. McKenzie, and C. Lobsey. 2011. Proximal soil sensing. An effective approach for soil measurements in space and time. Adv. Agron. 113:237–282.

Vitharana, U.W.A., M. Van Meirvenne, D. Simpson, L. Cockx, and J. De Baerdemaeker. 2008. Key soil and topographic properties to delineate potential management classes for precision agriculture in the European loess area. Geoderma 143: 206–215. doi:10.1016/j.geoderma.2007.11.003

Walsh, O.S., A.R. Klatt, J.B. Solie, C.B. Godsey, and W.R. Raun. 2012. Use of soil moisture data for refined GreenSeeker sensor based nitrogen recommendations in winter wheat (Triticum aestivum L.). Precis.Agric. 14 343–356. doi:10.1007/s11119-012-9299-9

Wang Z., Z. Qi, L. Xue, M. Bukovsky. 2016. RZWQM2 simulated management practices to mitigate climate change impacts on nitrogen losses and corn production. Environmental Modelling & Software 84: 99-111.

Wei, T., and V. Simko. 2016. corrplot: Visualization of a Correlation Matrix. R package version 0.77. https://CRAN.R-project.org/package=corrplot

Weihermuller, L., J.A. Huisman, S. Lambot, M. Herbst, H. Vereecken. 2007. Mapping the spatial variation of soil water content at the field scale with different ground penetrating radar techniques. J. Hydrol., 340 (3–4): 205-216.

Weller, U., M. Zipprich, M. Sommer, W.Z. Castell, and M. Wehrhan. 2007. Mapping clay content across boundaries at the landscape scale with electromagnetic induction. Soil Sci. Soc. Am. J. 71(6): 1740–1747. doi:10.2136/sssaj2006.0177

Wendroth, O., W. Paul, S. Koszinski, H. Rogasik, C.J. Ritsema, and D.R. Nielsen. 1999. Spatio-temporal patterns and covariance structures of soil water status in two Northeast-German field sites. J. Hydrol. 215:38– 58. doi:10.1016/S0022-1694(98)00260-1

Wendroth, O. K.C. Kersebaum, H.I. Reuter, A. Giebel, N. Wypler, M. Heisig, J. Schwarz, and D.R. Nielsen. 2003. MOSAIC: Crop Yield Prediction – Compiling Several Years' Soil and Remote Sensing Information. In: Stafford, J.V. and A. Werner

(Eds.). Precision Agriculture '03. Proc. 4th Europ. Conf. Prec. Agric., Berlin, Germany, pp. 723-729.

Wendroth, O., S. Koszinski, and E. Pena-Yewtukhiv. 2006. Spatial association between soil hydraulic properties, soil texture and geoelectric resistivity. Vadose Zone J. 5:341–355. doi:10.2136/vzj2005.0026

White, J.L. 1971. Interpretation of infrared spectra of soil minerals. Soil Sci. 112:22-31.

Wu, L., W. Chen, J. M. Baker, and J. A. Lamb. 1999. Evaluation of RZWQM field measured data from a sandy soil. Agro. J. 91:177-182.

Yang, Y., O. Wendroth, and R.J. Walton. 2016. Temporal dynamics and stability of spatial soil matric potential in two land use systems. Vadose Zone J. 15. doi:10.2136/vzj2015.12.015

Yao, R.J., J.S. Yang, T.J. Zhang, P. Gao, X.P. Wang, L.Z. Hong, and M.W. Wang. 2014. Determination of site-specific management zones using soil physico-chemical properties and crop yields in coastal reclaimed farmland. Geoderma 232:381–393. doi: 10.1016/j.geoderma.2014.06.006

Zhang, M., and A. Karathanasis. 1997. Characterization of iron-manganese concretions in Kentucky Alfisols with perched water tables. Clays and Clay Minerals, 45(3): 428-439.

Zhang, R., P. Shouse, and S. Yates. 1997. Use of pseudo-crossvariograms and cokriging to improve estimates of soil solute concentrations. Soil Sci. Soc. Am. J. 61(5): 1342–1347. doi:10.2136/sssaj1997.03615995006100050008x

Zhang, X., L. Shi, Xinhua J. George Seielstad, C. Helgason. 2010. Zone mapping application for precision-farming: a decision support tool for variable rate

application Precision Agric (2010) 11: 103. https://doi.org/10.1007/s11119-009-9130-4

Vita

Javier Andres Reyes Millalon

Education

Universidad Austral de Chile, Chile	Forest Resources	M.S., 2010-2012
Universidad Austral de Chile, Chile	Forestry Engineer	B.S., 2005-2009

Publications

Reyes, J., Wendroth, O., Matocha, C., Zhu, J., Ren, W., Karathanasis, A.D. 2018. Reliably Mapping Clay Content Coregionalized with Electrical Conductivity. Soil Science Society of America Journal, https:// doi:10.2136/sssaj2017.09.0327

Thiers, O., J. Reyes, V. Gerding, J.E. Schlatter. 2014. Suelos en Ecosistemas Forestales. Capítulo 3. In: Donoso C, M González, A Lara, P Donoso (Eds.). Ecología Forestal. Bases para el Manejo Sustentable de los Bosques Nativos. Editorial Marisa Cuneo Ediciones, Concepción, Chile. p. 133-178.

Reyes, J., O. Thiers, V. Gerding. 2014. Characterization of soil properties of Nothofagus spp. forest with and without scarification in the Andean region of southern Chile. Journal of Soil Science and Plant Nutrition 14(1): 115-127.

Reyes, J., O. Thiers, V. Gerding, P. Donoso. 2014. Effect of scarification on soil change and establishment of an artificial forest regeneration under Nothofagus spp. in southern chile. Journal of Soil Science and Plant Nutrition 14(1): 101-113.

Reyes, J., O. Thiers, V. Gerding, D.P. Soto. 2013. Recuperación de bosques con Nothofagus spp, en Los Andes del sur de Chile: uso de la escarificación del suelo como técnica facilitadora para la regeneración. Revista Bosque Nativo 52: 45-50.

Thiers, O., V. Gerding, J. Reyes, J. Gayoso. 2013. Bases edáficas para silvicultura en bosques nativos de Chile: Sistematización y validación de información sobre características y procesos de suelos (042/2010). In: Fondo de Investigación en Bosque Nativo-Departamento de Bosque Nativo. Corporación Nacional Forestal

(CONAF) (Ed.). Resúmenes proyectos financiados por el Fondo de Investigación del Bosque Nativo. Periodo 2010-2011. Vol 1:53-56.

Reyes, J., V. Gerding, O. Thiers. 2012. Controlled release fertilizers applied to Pinus radiata D. Don in Chile. Revista Chapingo Serie Ciencias Forestales y del Ambiente 18(3): 313-328.

Conference and Presentations

Wendroth O, Y Yang, J Reyes, X Zhang. New paradigms for Environmental and Agronomic Research and Education. ASA, CSSA, and SSSA Annual Meeting. Tampa, FL, USA. October 22-25, 2017.

Reyes J, O Wendroth. Temporal dynamics of soil water among delineated management zones. ASA, CSSA, and SSSA Annual Meeting. Tampa, FL, USA. October 22-25, 2017.

Zhang X, O Wendroth, J Reyes. Soil Water Movement As Affected By Hydraulic Conductivity, Initial Soil Moisture and Irrigation Intensity. ASA, CSSA, and SSSA Annual Meeting. Tampa, FL, USA. October 22-25, 2017.

Reyes J, O. Wendroth. Exploring soil and crop processes to improve irrigation. Meeting of W3188: Soil, Water, and Environmental Physics Across Scales. Las Vegas, NV, USA. January 03, 2017.

Reyes J, O Wendroth. Defining variables for site Specific Irrigation Management. Soybean Board Researcher Meeting. Lexington, KY, USA. December 12, 2017.

Reyes J, O Wendroth. Decomposing Soil Variability for Site-Specific Irrigation. KY Commodity Conference. Bowling Green, KY, USA. January 16, 2017.

Reyes J. Exploring spatio-temporal soil and crop processes to improve irrigation management. Meeting of W3188: Soil, Water, and Environmental Physics Across Scales. Las Vegas, NV, USA. January 03, 2017.

Reyes J, O Wendroth. Selecting variables for site Specific Irrigation Management. Soybean Board Researcher Meeting. Lexington, KY, USA. December 13, 2016.

Reyes J. Delineating zones for site specific management through soil and remote sensing variables. IPSS Graduate Student Research Symposium. Lexington, KY, USA. December 09, 2016.

Zhang X, Reyes J, O Wendroth. Measuring and Estimating Soil Hydraulic Property in a Farmer's Field, Western Kentucky. ASA, CSSA, and SSSA Annual Meeting. Phoenix, AZ, USA. November 7, 2016.

Wendroth O, Reyes J, X Zhang. Applying the RZWQM2 in a Spatial Variability Study of a 4-Year Crop Rotation. ASA, CSSA, and SSSA Annual Meeting. Phoenix, AZ, USA. November 7, 2016.

Reyes J, O Wendroth. Use of soil and remote sensing variables to explain spatial differences in corn yield. ASA, CSSA, and SSSA Annual Meeting. Phoenix, AZ, USA. November 7, 2016.

Reyes J, O Wendroth. Soil texture characterization using apparent electrical conductivity through kriging and cokriging analysis. ASA, CSSA, and SSSA Annual Meeting. Phoenix, AZ, USA. November 7, 2016.

Wendroth O, Y Yang, J Dorner, Q de Jong, R Armindo, M Ceddia, L Timm, J Reyes, X Zhang. Opportunities for Agro-Ecosystem Research: Lessons from Spatio-Temporal Field Observations. Invited keynote lecture. 21st Latin American Soil Science Congress, Quito, Ecuador. October 24-28, 2016. Oral.

Wendroth, O, J Reyes, Xi Zhang. Soil Water, Crop & Remote Sensing Measurements for Irrigation Management. UK 2016 Corn, Soybean & Tobacco Field Day. Princeton, KY, USA. July 28, 2016.

Reyes J. Kentucky Research Report. Meeting of Regional Research Committee S-1048. Oxford, MS, USA. June 02, 2016.

Reyes J, O Wendroth. Irrigation in Western Kentucky: Initial Results on Soil and Crop Spatial Variation to Improve Water Management. ASA, CSSA, and SSSA Annual Meeting. Minneapolis, MN, USA. November 17, 2015.

Reyes J. Irrigation in Kentucky: Exploring spatio-temporal soil and crop processes to improve water management. IPSS Graduate Student Research Symposium. Lexington, KY, USA. August 25, 2015.

Wendroth, O, R Walton, J Reyes. Irrigating the Soil to Maximize the Crop: An Approach for Corn, Wheat and Soybean to Efficient and Environmentally Sustainable Irrigation Water Management in Kentucky UK 2015 Corn, Soybean & Tobacco Field Day. Princeton, KY, USA. July 30, 2015.

Wendroth, O, J Reyes, Xi Zhang. Soil Water, Crop & Remote Sensing Measurements for Irrigation Management. UK 2016 Corn, Soybean & Tobacco Field Day. Princeton, KY, USA. July 28, 2016.

Reyes J. Kentucky Research Report. Meeting of Regional Research Committee S-1048. Oxford, MS, USA. June 02, 2016.

Reyes J, O Wendroth. Irrigation in Western Kentucky: Initial Results on Soil and Crop Spatial Variation to Improve Water Management. ASA, CSSA, and SSSA Annual Meeting. Minneapolis, MN, USA. November 17, 2015.

Reyes J. Irrigation in Kentucky: Exploring spatio-temporal soil and crop processes to improve water management. IPSS Graduate Student Research Symposium. Lexington, KY, USA. August 25, 2015.

Wendroth, O, R Walton, J Reyes. Irrigating the Soil to Maximize the Crop: An Approach for Corn, Wheat and Soybean to Efficient and Environmentally Sustainable Irrigation Water Management in Kentucky UK 2015 Corn, Soybean & Tobacco Field Day. Princeton, KY, USA. July 30, 2015.